

Doctoral Dissertation

博士論文

**Construction of Quantum Many-Body Scars in Spin Models
with Multibody Interactions**

(多体相互作用をもつスピン模型における量子多体傷跡状態の構成)

A Dissertation Submitted for the Degree of Doctor of Philosophy
December 2023

令和 5 年 12 月博士 (理学) 申請

Department of Physics, Graduate School of Science, The University of Tokyo
東京大学大学院理学系研究科物理学専攻

Kazuyuki Sanada

真田 兼行

ACKNOWLEDGMENTS

I would like to express my deepest appreciation to my supervisor, Prof. Hosho Katsura. He gives me constructive comments and warm encouragement. Without his kind support, I would not have completed my study. The most fortunate thing about my Ph.D. course is definitely having his guidance. My sincere thanks also go to Dr. Yuan Miao for offering valuable suggestions and feedback throughout this research. I am also particularly grateful to Prof. Eric Vernier for his advice on the exact eigenstates of the spin-1 scalar spin chirality term.

I would like to thank the members of the Katsura group for the interesting discussion and their studies. Particularly, I am grateful to Kensuke Tamura for his precise comments on my study.

I would also like to thank my family for their great moral support. Finally, I wish to express my gratitude to the Forefront Physics and Mathematics Program to Drive Transformation (FoPM) for their financial support and the valuable opportunities they provided for interaction with a wide variety of students and researchers. In particular, I would like to express my appreciation to my co-supervisor in FoPM, Prof. Masamitsu Hayashi for his advice and warm messages on research during our semi-annual meetings.

ABSTRACT

Nonthermal properties of quantum many-body systems have garnered significant attention in condensed matter physics in recent years. Latterly, the eigenstate thermalization hypothesis (ETH) is known as the framework of thermalization in typical quantum many-body systems. Roughly, strong ETH is a hypothesis assuming that all energy eigenstates are in thermal equilibrium. Although we do not have a rigorous proof of this hypothesis, there is substantial evidence that the strong ETH holds true in numerous quantum many-body systems. On the other hand, several classes of quantum many-body systems do not satisfy the strong ETH. Examples of systems violating the strong ETH include quantum integrable systems, many-body localized systems, and systems with Hilbert space fragmentation.

A recent experiment with Rydberg atoms has uncovered a new class of quantum many-body systems violating the strong ETH, and nonthermal states observed in the experiment are named quantum many-body scars (QMBS). Today, systems with QMBS are characterized by a small number of nonthermal energy eigenstates in the spectra of nonintegrable quantum systems. Theoretical studies of QMBS not only suggested the analysis of the PXP model, which is the effective model of the Rydberg atom experiment, but also introduced systematic methods to construct models with QMBS, including the Shiraishi-Mori embedding, the Onsager algebra, and the restricted spectrum generating algebra.

In this thesis, we introduce several classes of models with multibody interactions exhibiting QMBS. They can be divided into two categories based on differences in construction methods. The first approach uses the traditional restricted spectrum generating algebra, while the second employs integrable boundary states. Integrable boundary states are characterized as states that are annihilated by all parity-odd conserved charges of an integrable system. With the first method, we construct a large class of spin-1 models involving scalar spin chirality. By using the second method, we construct deformations of the Majumdar-Ghosh and Affleck-Kennedy-Lieb-Tasaki models, which are prototypes of frustration-free systems. The former is related to the spin-1/2 scalar spin chirality, which is the third conserved charge in the Heisenberg model. The latter adds the third conserved charge of the $SU(3)$ Sutherland model. In addition, we constructed models with QMBS by starting from the spin-1/2 scalar spin chirality or its deformation, where these

are the third conserved charges of the XXZ model and the XYZ model, respectively. Some of the models that we construct have multiple QMBS. For these models, we observe that a linear combination of these QMBS shows perfectly periodic behavior in the dynamics. In addition, we show that our methods can be applied to higher-dimensional lattices in some cases.

ACRONYMS

AKLT	Affleck-Kennedy-Lieb-Tasaki
ETH	Eigenstate Thermalization Hypothesis
GOE	Gaussian Orthogonal Ensemble
GUE	Gaussian Unitary Ensemble
IOM	Integral of Motion
MATE	Macroscopic Thermal Equilibrium
MBL	Many-Body Localization
MITE	Microscopic Thermal Equilibrium
MPS	Matrix Product State
QMBS	Quantum Many-Body Scars
RSGA	Restricted Spectrum Generating Algebra
VBS	Valence Bond Solid

TABLE OF CONTENTS

Acronyms	v
	Page
List of Tables	xi
List of Figures	xiii
1 Introduction	1
1.1 Thermalization in classical systems	1
1.2 Thermalization in quantum systems	4
1.3 Eigenstate Thermalization Hypothesis	8
1.4 Violation of ETH	10
1.4.1 Quantum Integrable Systems	10
1.4.2 Many Body Localization	11
1.4.3 Hilbert Space Fragmentation	13
1.5 Characterization of Thermal States and ETH Violation	16
1.5.1 Level-Spacing Statistics and r -value	16
1.5.2 Entanglement Entropy	17
1.6 Summary of This Chapter and Outline of the Thesis	18
2 Quantum Many-Body Scars	21
2.1 Rydberg Atom Simulator	22
2.2 PXP model	22
2.3 Construction of Exact Quantum Many-Body Scars	25
2.3.1 Shiraishi-Mori embedding	25
2.3.2 Onsager's Scar	27
2.3.3 Restricted Spectrum Generating Algebra	30
2.4 Summary of the Chapter	32
3 Construction of Scarred Models Related to the Spin-1 Scalar Spin Chirality	33
3.1 Spin-1 scalar spin chirality in one dimention	33

TABLE OF CONTENTS

3.2	Random single-ion anisotropy — scarred $ \bar{B}_n\rangle$	35
3.2.1	Dynamics	37
3.2.2	Extension for Higher Dimensional Lattices	40
3.3	Scarred $ \bar{A}_n\rangle$	43
3.3.1	Tower of eigenstates	43
3.3.2	Dynamics	44
3.4	Spin-1 AKLT model + scalar spin chirality	48
3.4.1	Hamiltonian	48
3.4.2	Scar state	49
4	Construction of Scarred Models Using Integrable Boundary States	51
4.1	Integrable Boundary States	51
4.1.1	Introduction for Integrable Boundary States	51
4.1.2	Method to Construct Models with QMBS from Integrable Boundary States	54
4.2	Spin-1/2 Majumdar-Ghosh Hamiltonian + Scalar Spin Chirality	55
4.3	AKLT Hamiltonian + Scalar Spin Chirality	59
4.3.1	AKLT Hamiltonian + SU(3) Scalar Spin Chirality	59
4.3.2	Inhomogeneous generalization	62
4.3.3	Further Generalizations	64
4.4	Scarred Models Related to XXZ Model and XYZ model	66
4.4.1	XXZ model	66
4.4.2	XYZ model	68
4.4.3	Extension for Higher Dimensional Lattices	72
5	Summary and Discussions	77
A	Supplemental Materials for Chapter 3	79
A.1	Zero energy states of C_{SC}	79
A.1.1	$C_{SC} \bar{A}_n\rangle = 0$	79
A.1.2	$C_{SC} \bar{B}_n\rangle = 0$	81
A.1.3	$C_{SC} K_{0,p}\rangle = 0$	82
A.1.4	Lower bound on the number of zero-energy states	82
A.2	Proof of $C_{SC} \Psi_{VBS}\rangle = 0$	84
B	Supplemental Materials for Chapter 4	87
B.1	Proof that $ \Psi_{VBS}\rangle$ is an integrable boundary state	87
B.2	SU(2) symmetry of H_3	89
B.3	Eigenenergy of ferromagnetic states	90
B.4	Proof that tilted-Néel states are integrable boundary states	91

Bibliography	95
---------------------	-----------

LIST OF TABLES

TABLE	Page
3.1 The explicit form of $(S_j^- - S_{j+1}^-)^n ++\rangle_{j,j+1}$ up to constant factors. The third and fourth columns indicate the eigenvalues of the corresponding operators for each state.	43
A.1 The number of zero-energy states (\mathcal{Z}_L) and the bound (\mathcal{N}_L) up to $L = 11$ sites. .	84

LIST OF FIGURES

FIGURE	Page
1.1 Illustration of classical ergodicity and integrability	3
1.2 Diagonal matrix elements of observables in an integrable system and a nonintegrable system	12
2.1 The time evolution of the fidelity in the PXP model	25
3.1 Level-spacing statistics in the middle half of the spectrum of $H_1(t)$ (Eq. (3.11))	36
3.2 Entanglement entropies in all eigenstates of $H_1(h, \{D_j\})$ in Eq. (3.11)	38
3.3 Entanglement entropies in all eigenstates of $H_1(h, \{D_j\})$ in Eq. (3.11)	39
3.4 The dynamics of the fidelity with the Hamiltonian (3.11)	40
3.5 Dynamics of the half-chain entanglement entropies with the same setup as Figure 3.4.	41
3.6 An example of the triangular lattice	42
3.7 Entanglement entropies in all eigenstates of $H_1^{2d}(h, \{D_j\})$ in Eq. (3.27)	43
3.8 Entanglement entropies in all eigenstates in Eq. (3.33) and Eq. (3.33)	45
3.9 The dynamics of the fidelity with the Hamiltonian (3.33)	46
3.10 The dynamics of the fidelity of the superposition of two coherent states $ \alpha\rangle$ and $ \beta\rangle$ driven by H_2 (Eq. (3.33))	48
3.11 Level-spacing statistics in the middle half of the spectrum of the model (3.43) .	49
3.12 Entanglement entropies in all eigenstates of $H(t)$ in Eq. (3.43)	50
4.1 Pictorial representation of two-dimensional Euclidean field theory with boundary on $x = 0$	52
4.2 Level-spacing statistics in the middle half of the spectrum of $H(t)$ in Eq. (4.12)	56
4.3 The mean level-spacing ratio $\langle r \rangle$ as a function of t for the Hamiltonian (4.12). .	57
4.4 Entanglement entropy S_A in all eigenstates of $H(t)$ in Eq. (4.12)	58
4.5 The expectation values of H_{st} in all eigenstates of $H(t)$ in Eq. (4.12)	59
4.6 Level spacing statistics in the middle half of the spectrum of $H(t)$ in (4.24) . .	61
4.7 Entanglement entropies in all eigenstates of $H(t)$ in Eq. (4.24)	63

4.8	Level-spacing statistics in the middle half of the spectrum of the inhomogeneous model $\tilde{H}(t)$ in Eq. (4.37)	64
4.9	Entanglement entropies in all eigenstates of the inhomogeneous model $\tilde{H}(t)$ in Eq. (4.37)	65
4.10	The expectation values of H_{AKLT} in all eigenstates of (4.37)	65
4.11	Level-spacing statistics in the middle half of the spectrum of $H_1(s, h_y)$ (Eq. (4.43))	67
4.12	The half-chain entanglement entropy and eigenenergy for all eigenstates of $H_1(t, h_y)$ in Eq. (4.43)	69
4.13	The half-chain entanglement entropy and eigenenergy of the all eigenstates of $H_2(t, h_y)$ in Eq. (4.54)	70
4.14	The time dependence of the fidelity of $ \mathbb{Z}_2\rangle$ and $ \mathbb{Z}_3\rangle$ driven by $H_2(s, h_y)$ in Eq. (4.54)	72
4.15	The time dependence of the correlation function $C_r^x(t)$	73
4.16	An example of the $L_x \times L_y$ square lattice.	74
4.17	The entanglement entropies and energies for all eigenstates of the Hamiltonian (4.67)	75
B.1	Graphical representation of the Yang-Baxter equation	92
B.2	Graphical representation of the boundary Yang-Baxter equation	93
B.3	Graphical representation of the reflection equation	93

INTRODUCTION

Thermalization of quantum systems has been discussed as one of the most essential topics of statistical physics for an extended period. In discussing the theory of thermalization in classical systems, it is impossible not to mention Boltzmann's contribution. For example, the Boltzmann H -theorem [1, 2] is the prototype of the second law of thermodynamics or the law of entropy increase, and the ergodic hypothesis [3] that he suggested remains a crucial hypothesis in explaining thermalization. Later, von Neumann suggested the theoretical formulation of quantum ergodicity in 1929 [4]. This formalization evolved into the eigenstate thermalization hypothesis (ETH), which has become the framework of the modern theory of thermalization in quantum many-body systems.

In this chapter, we provide the definition of thermalization, which is the starting point of our discussion, and an outline of the contents of ETH. In addition, we introduce various counterexamples of ETH and summarize features that characterize thermal or non-thermal states or systems. At the end of this chapter, we outline the organization of this thesis.

1.1 Thermalization in classical systems

Thermalization appears in terms of an ordinary assumption of statistical physics. It says that isolated systems reach thermal equilibrium in the long-time limit. In this thesis, we mainly focus on thermalization in isolated quantum systems. However, it is essential to consider classical thermalization because the quantum thermalization theories were developed as analogies to the classical ones. Therefore, we first formalize classical thermalization before considering thermalization in quantum systems.

The traditional concept to explain thermalization is called *ergodicity*. This concept was first suggested by Boltzmann [5, 6]:

“The great irregularity of thermal motion and the manifold forces affecting bodies from the outside make it probable that the atoms of the warm body, through the motion we call heat, runs through all positions and velocities compatible with the equation of kinetic energy so that we can use the equations developed above on the coordinates and component velocities of the atoms of warm bodies.”

In the language of modern physics, ergodicity is defined as follows. Let us consider the motion of N free particles in a closed space $\Lambda \subset \mathbb{R}^3$ with volume V . The information of the particles can then be expressed as a *micro-state* $x = \{\vec{q}, \vec{p}\}$ within the phase space $\Gamma = \Lambda^N \times \mathbb{R}^{3N}$. Let $H(x)$ be the classical Hamiltonian. By energy conservation, the motion of micro-state x is constrained on the energy shell $\Gamma_E := \{s \in \Gamma \mid |H(s) - E| < \Delta E\}$, with $E = H(x(t = 0))$. We assume that the half-width of energy window ΔE is extremely smaller than the typical energy scale. We introduce the *macrovariables* $\mathcal{M} = \{M_1(x), M_2(x), \dots, M_n(x)\}$. It is a set of functions of micro-states. We assume that each $M_\lambda(x)$ corresponds to a macroscopic quantity. Then, ergodicity states that the long-time limit of M_λ is equal to the average of M_λ on the energy shell Γ_E , that is,

$$\lim_{T \rightarrow \infty} \frac{1}{T} \int_0^T M_\lambda(x(t)) dt = \frac{\int_{\Gamma_E} M_\lambda(x) d\vec{q} d\vec{p}}{\text{vol}(\Gamma_E)}, \quad (1.1)$$

where $\text{vol}(\tilde{\Gamma}) := \int_{\tilde{\Gamma}} d\vec{q} d\vec{p}$ denotes the volume of $\tilde{\Gamma} \subset \Gamma$ in the phase space. Therefore, in ergodic systems, the long-time averages of macroscopic quantities depend only on the energy of the initial states. It means that the trajectory of the motion of any micro-state with the same energy E passes through every micro-state on the energy surface Γ_E with the same probability. As a result, after a certain amount of time, we cannot know which micro-state is the initial state from a given micro-state. Moreover, classical integrable systems do not show ergodicity because the motion of macro-state x is constrained in the small region of Γ_E due to the presence of other conserved quantities (Fig. 1.1).

We believe that thermal systems cannot be distinguished from each other in macroscopic observables. Therefore, ignoring the microscopic difference and using the coarse-grain method is natural. For each macrovariable M_i , we introduce a width ΔM_i such that it is sufficiently smaller than the magnitude of M_i but it is large enough to contain a sufficiently large number of micro-states. We then use the parameter ν to group each micro-state x into a larger category. A micro-state x labeled by ν must satisfy condition $M_i(x) \in \mathcal{M}_{\nu_i}^i$. Here, $\mathcal{M}_{\nu_i}^i$ is a semi-open interval with width ΔM_i , and we assume $\mathcal{M}_{\mu_i}^i \cap \mathcal{M}_{\nu_i}^i = \emptyset$ for $\mu_i \neq \nu_i$ and $\{\mathcal{M}_{\nu_i}^i\}_{\nu_i}$ is a cover of the range of $M_i(x)$. Finally, let Γ_ν denote the space of micro-states labeled by ν on the energy shell Γ_E , and we call the states

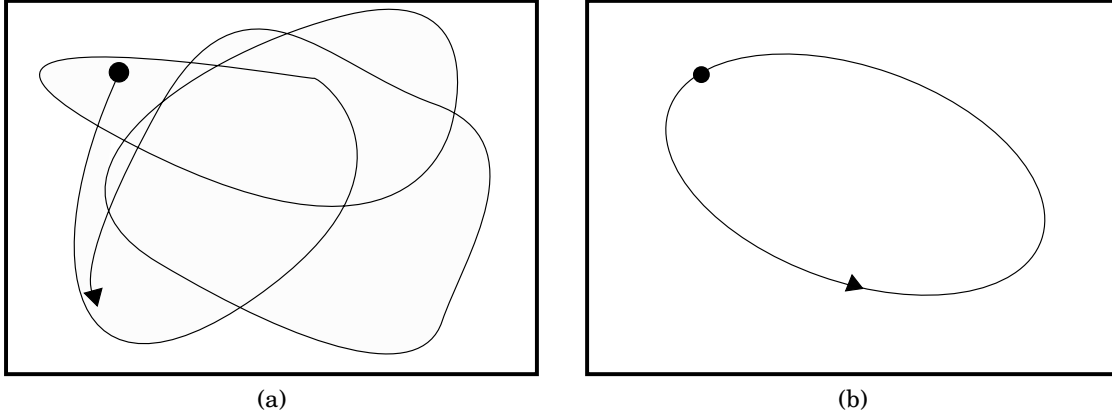


Figure 1.1: Illustration of classical ergodicity and integrability. The enclosing rectangles illustrate the energy shell Γ_E with fixed energy E . (a) Illustration of an ergodic trajectory. This trajectory passes through all the points in the energy shell Γ_E uniformly in the long-time limit. (b) Illustration of an orbit in an integrable system. Because many conserved quantities exist, the motion in the phase space is restricted to a very narrow range. Consequently, the orbit shows periodic behavior.

in the Γ_ν macro-state ν . Then we obtain

$$\Gamma_E = \bigcup_{\nu} \Gamma_\nu. \quad (1.2)$$

In this convention, the naive picture of thermalization is as follows: There exists a special macrostate ν^{eq} such that no matter what initial state we started, the trajectory of the microstate settles in $\Gamma_{\nu^{\text{eq}}}$ after a long enough time. As a natural consequence of this fact, we should introduce the assumption that the whole energy shell Γ_E is mostly occupied by the macrostate ν^{eq} , namely [7],

$$\frac{\text{vol}(\Gamma_{\nu^{\text{eq}}})}{\text{vol}(\Gamma_E)} \geq 1 - e^{-\alpha V}, \quad (1.3)$$

with a positive constant α . In this picture, a macroscopic feature of classical systems is mainly determined by only E , N , and V . It is called the *typicality of thermal equilibrium* [8, 9].

Note that both ergodicity and typicality are the theories developed to explain thermalization; however, these two theories have no relation to each other. When comparing the two theories, it can be said that the one more in line with reality is typicality [10]. The reasons are as follows. Firstly, in the ergodic hypothesis, thermalization needs a highly long time T_{evolve} ; typically it is longer than our lives because a microstate should pass through the whole phase space. However, we know empirically that thermalization does not need a very long time. In addition, T_{evolve} grows exponentially more significant as the

size of the system in the ergodic hypothesis increases. However, since statistical mechanics is an asymptotic theory, it becomes closer to thermodynamics in the thermodynamic limit. Therefore, we can conclude that typicality is closer to the essence of thermalization than ergodicity.

1.2 Thermalization in quantum systems

The theory of quantum thermalization was first suggested by von Neumann [4]. He called his theory “quantum ergodic theorem” [4, 11–13], but its contents are close to typicality rather than the ergodicity.

We start from the fundamental equation of quantum mechanics, namely, Schrödinger equation¹

$$i \frac{\partial}{\partial t} |\Psi\rangle = \hat{H} |\Psi\rangle, \quad (1.4)$$

where $|\Psi\rangle \in \mathcal{H}$ is a state vector with \mathcal{H} being the whole Hilbert space, and the operator $\hat{H} \in \text{End}(\mathcal{H})$ is called the quantum Hamiltonian. We can formally solve this equation and obtain the time evolution governed by \hat{H} with initial state $|\Psi\rangle$ as

$$|\Psi(t)\rangle = e^{-i\hat{H}t} |\Psi\rangle, \quad (1.5)$$

where $t \in \mathbb{R}$ is the elapsed time. To obtain the explicit form of $|\Psi(t)\rangle$, we need to consider the eigenvector of \hat{H} :

$$\hat{H} |E_\alpha\rangle = E_\alpha |E_\alpha\rangle. \quad (1.6)$$

We call $|E_\alpha\rangle$ an energy eigenstate and E_α an eigenenergy. We can take a set of energy eigenstates $\{|E_\alpha\rangle\}_\alpha$ as an orthonormal complete basis set of \mathcal{H} , namely, $\langle E_\alpha | E_\beta \rangle = \delta_{\alpha,\beta}$ and $\mathcal{H} = \text{Span}\{|E_\alpha\rangle\}_\alpha$. Then, any state $|\Psi\rangle$ can be expressed as a superposition of energy eigenstates as $|\Psi\rangle = \sum_\alpha c_\alpha |E_\alpha\rangle$ with $c_\alpha \in \mathbb{C}$. The time evolution of $|\Psi\rangle$ can be expressed as

$$|\Psi(t)\rangle = \sum_\alpha c_\alpha e^{-iE_\alpha t} |E_\alpha\rangle. \quad (1.7)$$

We focus on an energy interval $[E, E + \Delta E]$ and identify an *energy shell* $\mathcal{H}_{E,\Delta E} := \text{Span}\{|E_\alpha\rangle \in \mathcal{H} \mid E_\alpha \in [E, E + \Delta E]\}$. For simplicity, we drop the subscript and write $\mathcal{H}_{E,\Delta E}$ as \mathcal{H} in the following.

The quantum analogy of ergodicity (1.1) reads

$$\overline{|\Psi(t)\rangle\langle\Psi(t)|} = \hat{\rho}_{\text{MC}}, \quad (1.8)$$

where the overline means the long time average and the $\hat{\rho}_{\text{MC}}$ is the microcanonical ensemble

$$\hat{\rho}_{\text{MC}} = \frac{1}{D} \sum_\alpha |E_\alpha\rangle\langle E_\alpha|, \quad (1.9)$$

¹We use a system of units in which the reduced Plank constant $\hbar = 1$.

with $D = \dim \mathcal{H}$. However, von Neumann pointed out that the left-hand side of Eq. (1.8) can be evaluated as follows. We can directly calculate the expectation value of a macroscopic observable \hat{O} from Eq. (1.7) as

$$\begin{aligned} \langle \hat{O} \rangle_t &:= \langle \Psi(t) | \hat{O} | \Psi(t) \rangle = \langle \Psi | e^{i\hat{H}t} \hat{O} e^{-i\hat{H}t} | \Psi \rangle \\ &= \sum_{\alpha} |c_{\alpha}|^2 \langle E_{\alpha} | \hat{O} | E_{\alpha} \rangle + \sum_{\alpha \neq \beta} c_{\alpha}^* c_{\beta} e^{-i(E_{\beta} - E_{\alpha})t} \langle E_{\alpha} | \hat{O} | E_{\beta} \rangle. \end{aligned} \quad (1.10)$$

Since we are only interested in the behavior at long times, we take a long-time average. As a result, the phase factors cancel out and we obtain

$$\overline{\langle \hat{O} \rangle}_t := \lim_{T \rightarrow \infty} \frac{1}{T} \int_0^T dt \langle \hat{O} \rangle_t = \sum_{\alpha} |c_{\alpha}|^2 \langle E_{\alpha} | \hat{O} | E_{\alpha} \rangle. \quad (1.11)$$

It means that the initial state $|\Psi\rangle$ relaxes to a diagonal ensemble

$$|\overline{\Psi(t)}\rangle\langle\overline{\Psi(t)}| = \hat{\rho}_{\text{DE}} := \sum_{\alpha} |c_{\alpha}|^2 |E_{\alpha}\rangle\langle E_{\alpha}|. \quad (1.12)$$

To consider the relaxation to the diagonal ensemble, we have to discuss a long-time average and a long-time fluctuation. Let us define the fluctuation of the expectation value of the observable in the form of a long-time variance:

$$\mathbb{V}_t[\hat{O}] := \lim_{t \rightarrow \infty} \frac{1}{T} \int_0^T \left| \langle \hat{O} \rangle_t - \langle \hat{O} \rangle_{\text{DE}} \right|^2 dt, \quad (1.13)$$

with $\langle \hat{O} \rangle_{\text{DE}} := \text{Tr} \{ \hat{O} \rho_{\text{DE}} \}$. Under the nonresonance condition², we obtain [7, 14, 15]

$$\mathbb{V}_t[\hat{O}] \leq \frac{\|\hat{O}\|_{\text{op}}^2}{D_{\text{eff}}}, \quad (1.14)$$

where $\|\cdot\|_{\text{op}}$ is the operator norm defined by

$$\|A\|_{\text{op}} := \sup_{v \in \mathcal{H} \setminus \{0\}} \frac{\|Av\|}{\|v\|}, \quad (1.15)$$

and

$$D_{\text{eff}} = \frac{1}{\sum_{\alpha} |c_{\alpha}|^4} \quad (1.16)$$

is called the effective dimension. We can easily find $1 \leq D_{\text{eff}} \leq \dim \mathcal{H}$ and it reaches the maximum value if $|\Psi\rangle$ contains all eigenstates uniformly and it takes one if $|\Psi\rangle$ corresponds to an energy eigenstate.

²We say that a Hamiltonian H with eigenvalues $\{E_{\lambda}\}_{\lambda}$ is nonresonance if and only if

$E_{\alpha} - E_{\beta} \neq E_{\alpha'} - E_{\beta'}$ unless either $\{\alpha = \alpha' \wedge \beta = \beta'\}$ or $\{\alpha = \beta' \wedge \beta = \alpha'\}$.

Since the detail of the diagonal ensemble density matrix (Eq. (1.12)) depends highly on the initial state $|\Psi\rangle$, it is unsuitable for explaining quantum thermalization. Therefore, we have to loosen the definition of thermalization. Since we are interested in the macroscopic behavior, we consider that we distinguish quantum states by the macroscopic observables $\hat{\mathcal{M}} = \{\hat{M}_1, \hat{M}_2, \dots, \hat{M}_n\}$ as the classical case. However, each observable can be represented as a linear operator in quantum systems. This means that we cannot simultaneously measure all macroscopic observables if $[\hat{M}_i, \hat{M}_j] \neq 0$. Von Neumann suggested [4] that by allowing microscopic scale shifts $\Delta M_i \sim \mathcal{O}(\hbar)$, we can obtain the set of mutually commuting operators $\tilde{\mathcal{M}} = \{\hat{\mathcal{M}}_1, \hat{\mathcal{M}}_2, \dots, \hat{\mathcal{M}}_n\}$. Since this is macroscopically indistinguishable from $\hat{\mathcal{M}}$, the orthogonal decomposition of \mathcal{H} into the simultaneous eigenspaces of $\tilde{\mathcal{M}}$

$$\mathcal{H} = \bigoplus_{\nu} \mathcal{H}_{\nu}, \quad (1.17)$$

where $\nu = (m_1, m_2, \dots, m_n)$ are eigenvalues of $\tilde{\mathcal{M}}$, is an appropriate representation of the macroscopic structure of the whole Hilbert space \mathcal{H} ³. In the following, we use the notation $d_{\nu} = \dim \mathcal{H}_{\nu}$ and $D = \dim \mathcal{H}$.

If we discuss thermalization based on the macroscopic observation, we can relax the condition for thermalization (1.8) as

$$|\overline{\Psi(t)}\rangle\langle\overline{\Psi(t)}| \stackrel{\mathcal{Q}}{\sim} \hat{\rho}_{\text{MC}}, \quad (1.18)$$

where the symbol $\stackrel{\mathcal{Q}}{\sim}$ means *macroscopically equivalent* such that $\rho \stackrel{\mathcal{Q}}{\sim} \rho'$ holds if and only if $\text{Tr}\{\hat{\rho}\hat{P}_{\nu}\} \approx \text{Tr}\{\hat{\rho}'\hat{P}_{\nu}\}$, where the operator \hat{P}_{ν} is a projection operator onto the macrospace \mathcal{H}_{ν} , for all macrostates ν . Thus, $|\psi\rangle\langle\psi| \stackrel{\mathcal{Q}}{\sim} \hat{\rho}_{\text{MC}}$ means that

$$\|\hat{P}_{\nu}|\psi\rangle\| \approx \frac{d_{\nu}}{D}. \quad (1.19)$$

As a general description, the following theorem is known [13].

Theorem 1.1. *If \mathcal{H}_{ν} is any subspace with dimension d_{ν} and $|\varphi\rangle$ is drawn from the set of normalized states as $\mathbb{S} = \{|\psi\rangle \in \mathcal{H} \mid \langle\psi|\psi\rangle = 1\}$ uniform randomly, then*

$$\mathbb{E} \left[\|\hat{P}_{\nu}|\varphi\rangle\| \right] = \frac{d_{\nu}}{D}, \quad \mathbb{V} \left[\|\hat{P}_{\nu}|\varphi\rangle\| \right] = \mathbb{E} \left[\left(\|\hat{P}_{\nu}|\varphi\rangle\| - \frac{d_{\nu}}{D} \right)^2 \right] = \frac{1}{d_{\nu}} \left(\frac{d_{\nu}}{D} \right)^2 \frac{D - d_{\nu}}{D + 1}, \quad (1.20)$$

where \mathbb{E} and \mathbb{V} mean the expectation value and the variance taken with respect to the uniform measure on \mathbb{S} .

³In general, for given operators $\hat{A}_1, \dots, \hat{A}_k$ whose commutators are small, we cannot find approximate operators $\hat{M}_i \approx \hat{A}_i$ which commute with each other [13, 16]. However, we can redefine the macrospace \mathcal{H}_{ν} with $\nu = (m_1, m_2, \dots, m_n)$ as the intersection of an eigenspace of \hat{M}_i with eigenvalue m_i (for more details, see [17]).

Now, recalling the condition (1.18), we have

$$\left\| \hat{P}_\nu |\overline{\Psi(t)}\rangle \right\|^2 = \text{Tr} \left\{ \hat{P}_\nu \hat{\rho}_{\text{DE}} \right\} = \sum_\alpha |c_\alpha|^2 \langle E_\alpha | \hat{P}_\nu | E_\alpha \rangle \approx \frac{d_\nu}{D}, \quad (1.21)$$

for all ν . It holds if and only if

$$\langle E_\alpha | \hat{P}_\nu | E_\alpha \rangle \approx \frac{d_\nu}{D}, \quad (1.22)$$

for all α and ν . However, we know that we reach thermalization in finite time. It states that not only the time average (1.18) but also $|\Psi(t)\rangle$ itself for most t lies in thermal equilibrium, namely, for almost all time t and for all ν ,

$$\left\| \hat{P}_\nu |\Psi(t)\rangle \right\| \approx \frac{d_\nu}{D}. \quad (1.23)$$

This is only true when one macrostate covers most of the Hilbert space \mathcal{H} , that is, when the typicality picture is established. Thus, quantum thermalization can be described as classical typicality: There is a macrostate ν^{eq} such that

$$\frac{d_{\nu^{\text{eq}}}}{D} \simeq 1. \quad (1.24)$$

Therefore, we state the definition of quantum thermalization as follows [7, 8]:

Definition 1.2. *Let us denote P_ν a projection onto the macrospace \mathcal{H}_ν , which is a subspace of the whole Hilbert space \mathcal{H} , and α as a fixed positive number. Then, we call a normalized state $|\phi\rangle$ is thermalized if there is a special macrospace such that $\dim \mathcal{H}_{\nu^{\text{eq}}} / \dim \mathcal{H} \approx 1$ and*

$$1 - \langle \phi | \hat{P}_{\nu^{\text{eq}}} | \phi \rangle \leq e^{-\alpha V}. \quad (1.25)$$

This definition is called *macroscopic thermal equilibrium* (MATE) [18, 19]. There is another class of quantum thermalization called *microscopic thermal equilibrium* (MITE). It is inspired by the idea called *canonical typicality* [4, 20–22], which is the observation that for not too large subsystem S and most state $|\psi\rangle$ in the energy shell \mathcal{H} , the reduced density matrix is sufficiently close to the thermal equilibrium density matrix $\hat{\rho}^S \approx \hat{\rho}_{\text{MC}}^S$, where $\hat{\rho}^S = \text{Tr}_{S^c} [|\psi\rangle\langle\psi|]$ is the reduced density matrix of S obtained by tracing out the complementary subspace S^c . In addition, it is known that if S is small enough, $\hat{\rho}_{\text{MC}}^S \approx \hat{\rho}_{(\beta)}^S$ with appropriate $\beta > 0$, where $\hat{\rho}_{(\beta)}^S = \text{Tr}_{S^c} \hat{\rho}_{(\beta)}$ and

$$\hat{\rho}_{(\beta)} = \frac{e^{-\beta \hat{H}}}{\text{Tr} \left\{ e^{-\beta \hat{H}} \right\}}, \quad (1.26)$$

is the canonical ensemble (Gibbs ensemble) with respect to the Hamiltonian \hat{H} . Let $l_0 > 0$ be the longest length such that $\hat{\rho}_{\text{MC}}^S \approx \hat{\rho}_{(\beta)}^S$ holds for any S whose diameter⁴ is smaller than l_0 . Then, the definition of MITE is naturally led [18, 19]:

⁴the diameter of the subsystem S is defined by the supremum of the distance between two points in S .

Definition 1.3. Let $\hat{\rho} = \sum_{|\psi_i\rangle \in \mathbb{S}} p_i |\psi_i\rangle\langle\psi_i|$ be a density matrix of mixed state. We call $\hat{\rho}$ in MITE if

$$\hat{\rho}^S \approx \hat{\rho}_{\text{MC}}^S \quad (1.27)$$

holds for any subsystem S whose diameter is smaller than l_0 .

Generally, each state $|\psi\rangle \in \mathcal{H}$ is both in MATE and MITE. Thus, most of the mixed states in MATE also lie in MITE and vice versa. We can argue for a stronger statement, that is, the state in MITE must be in MATE [18]. More details will be given in a later section, but our discussion will now focus on MITE. Therefore, it should be noted that the implications are slightly different from those of classical thermalization.

1.3 Eigenstate Thermalization Hypothesis

As seen in the previous section, there are two types of quantum thermalization, namely, MATE and MITE. We need an ansatz arising from physical postulates. Eigenstate Thermalization Hypothesis (ETH) suggested by Deutsch [23] and Srednicki [24] has been the most plausible scenario up to the present time. Corresponding to MATE and MITE, there exist two versions of ETH, namely, MATE-ETH and MITE-ETH [7, 18, 19, 25].

MATE-ETH states that every state $|\psi\rangle \in \mathcal{H}$ lies in MATE [19]. In other words,

$$\langle\psi|\hat{P}_{\nu^{\text{eq}}}|\psi\rangle \approx 1, \quad (1.28)$$

holds for most of $|\psi\rangle \in \mathbb{S}$. In this situation, the long-time average of $|\psi(t)\rangle := e^{-i\hat{H}t}|\psi\rangle$ becomes

$$\begin{aligned} \overline{\langle\psi(t)|\hat{P}_{\nu^{\text{eq}}}|\psi(t)\rangle} &= \sum_{\alpha,\beta} \langle\psi|E_\alpha\rangle \overline{e^{iE_\alpha t} \langle E_\alpha|\hat{P}_{\nu^{\text{eq}}}^{\text{eq}}|E_\beta\rangle e^{-iE_\beta t} \langle E_\beta|\psi\rangle} \\ &= \sum_{\alpha} |\langle\psi|E_\alpha\rangle|^2 \langle E_\alpha|\hat{P}_{\nu^{\text{eq}}}^{\text{eq}}|E_\alpha\rangle \\ &\approx \sum_{\alpha} |\langle\psi|E_\alpha\rangle|^2 = 1. \end{aligned} \quad (1.29)$$

Thus, it guarantees that the long-time average is also in MATE. In contrast, if the system violates MATE, states outside MATE never reach MATE.

On the other hand, MITE-ETH corresponds to MITE. When we say simply ETH, it often refers to MITE-ETH. MITE-ETH states that every energy eigenstate in the energy shell $|E_\alpha\rangle \in \mathcal{H}_{E,\Delta E}$ shows represent MITE (Eq. (1.27)) [7], i.e.,

$$\langle E_\alpha|\hat{O}|E_\alpha\rangle = \left\langle \hat{O} \right\rangle_{\text{MC}}. \quad (1.30)$$

Combining it with the random matrix theory, Srednicki put forth a conjecture that the form of matrix elements of an observable \hat{O} in terms of the energy eigenbasis is [7, 12, 26]

$$O_{\alpha\beta} := \langle E_\alpha|\hat{O}|E_\beta\rangle = O(\bar{E})\delta_{\alpha\beta} + e^{-S(\bar{E})/2} f_O(\bar{E}, \omega) R_{\alpha\beta}, \quad (1.31)$$

where $\bar{E} = (E_\alpha + E_\beta)/2$, $\omega = E_\beta - E_\alpha$, $S(E)$ is the thermodynamic entropy at energy E , and $\{R_{\alpha\beta}\}$ is random variables with zero mean and unit variance. Moreover, we assume $O(E)$ and $f_O(E, \omega)$ are smooth functions of their arguments. Since we assume that the initial state $|\Psi\rangle$ contains energy eigenstates in only a narrow energy window $[E, E + \Delta E]$, the function $f_O(E, \omega)$ can be regarded as a constant [12]. Moreover, $S(E)$ scales linearly with system size. Thus, the off-diagonal part is sufficiently small. Note that there are two categories of MITE-ETH, distinguished by the strength of the statement; *strong* ETH and *weak* ETH. The former states that all energy eigenstates satisfy Eq. (1.31). In contrast, the latter states that *almost* all eigenstates satisfy it [27, 28]. From here, we use a given state is *thermal* in the sense that the state is a superposition of eigenstates that satisfy ETH. By plugging Eq. (1.31) into Eq. (1.11), we obtain

$$\overline{\langle \hat{O} \rangle}_t = \sum_{\alpha} |c_{\alpha}|^2 \left[O(E_{\alpha}) + e^{-S(E_{\alpha})/2} f_O(E_{\alpha}, \omega = 0) R_{\alpha\alpha} \right] \simeq \sum_{\alpha} |c_{\alpha}|^2 O(E_{\alpha}). \quad (1.32)$$

On the other hand, the microcanonical ensemble average of \hat{O} reads

$$\langle \hat{O} \rangle_{\text{MC}} := \text{Tr} \{ \hat{O} \rho_{\text{MC}} \} \simeq \frac{1}{D} \sum_{\alpha} O(E_{\alpha}). \quad (1.33)$$

Since we only consider in the narrow energy window $[E, E + \Delta E]$ and $O(E)$ is a smooth function of E ,

$$\overline{\langle \hat{O} \rangle}_t \approx O(E_{\alpha}) \approx O(E). \quad (1.34)$$

Therefore, we can conclude

$$|\overline{\Psi(t)}\langle\Psi(t)| \approx \hat{\rho}_{\text{MC}}, \quad (1.35)$$

which means that the whole system relaxes to thermal equilibrium.

Furthermore, to evaluate the difference between these two ensembles, we consider the Taylor expansion of $O(E)$ and $\langle \hat{O} \rangle_{\text{MC}}$ around $\langle E \rangle := \langle \Psi | \hat{H} | \Psi \rangle$:

$$O(E_{\alpha}) \simeq O(\langle E \rangle) + (E_{\alpha} - \langle E \rangle) \frac{dO}{dE} \bigg|_{\langle E \rangle} + \frac{1}{2} (E_{\alpha} - \langle E \rangle)^2 \frac{d^2 O}{dE^2} \bigg|_{\langle E \rangle}. \quad (1.36)$$

Substituting it into (1.32) leads to

$$\overline{\langle \hat{O} \rangle}_t \simeq O(\langle E \rangle) + \frac{1}{2} (\Delta E)^2 O''(\langle E \rangle). \quad (1.37)$$

Using the ETH ansatz, we can estimate the variance of the long-time average, namely,

$$\begin{aligned} \mathbb{V}_t[\hat{O}] &= \lim_{T \rightarrow \infty} \frac{1}{T} \int_0^T \left(\langle \hat{O} \rangle_t^2 - \langle \hat{O} \rangle_{\text{DE}}^2 \right) dt \\ &= \lim_{T \rightarrow \infty} \frac{1}{T} \int_0^T dt \sum_{\alpha, \beta, \gamma, \delta} e^{i(E_{\alpha} - E_{\beta} + E_{\gamma} - E_{\delta})t} O_{\alpha\beta} O_{\gamma\delta} c_{\alpha}^* c_{\beta} c_{\gamma}^* c_{\delta} - \langle \hat{O} \rangle_{\text{DE}}^2 \\ &= \sum_{\alpha \neq \beta} |O_{\alpha\beta}|^2 |c_{\alpha}|^2 |c_{\beta}|^2 \leq \max_{\alpha \neq \beta} |O_{\alpha\beta}|^2 \sum_{\alpha \neq \beta} |c_{\alpha}|^2 |c_{\beta}|^2 \leq \max_{\alpha \neq \beta} |O_{\alpha\beta}|^2 \propto \exp\{-S(E)\}. \end{aligned} \quad (1.38)$$

Since $S(E)$ is linear in system size, the fluctuation is exponentially suppressed. It implies that the expectation values of observables stay near the thermal value.

1.4 Violation of ETH

As we have seen in the previous section, quantum systems satisfying ETH show thermalization. However, there are many systems that do not satisfy strong ETH. We introduce several classes of systems with a lack of ETH.

1.4.1 Quantum Integrable Systems

The most famous counterexample of strong ETH is a quantum integrable system. As opposed to classical integrability, we do not have a proper definition of quantum integrability, and several definitions are suggested [29]. In this thesis, we adopt the following formalism [30]: If we have a system with n degrees of freedom whose Hamiltonian is \hat{H} , it is called integrable if it has n independent conserved quantities $\hat{I}_1, \hat{I}_2, \dots, \hat{I}_n$ that are commuting to the Hamiltonian \hat{H} and are mutually commuting, namely, $[\hat{I}_i, \hat{I}_j] = 0$. In our formalism, we assume that the number of independent conserved charges n is equal to the dimension of the Hilbert space [29, 30]. We can give an intuitive explanation for why quantum integrable systems violate strong ETH as follows: The time evolutions under integrable Hamiltonians keep track of the integrals of motion (IOMs). Thus, although a long time has passed, time-evolved states that started from initial states with different values of conserved charges cannot be identical. It is contradictory to the description of ETH that states belonging to the same energy shell have approximately the same expectation values for observables.

Reference [31] shows the result that supports this intuition, that is, ETH assumption fails to be true in integrable systems. We start from the spin-1/2 XXZ spin chain with open boundary conditions:

$$H_{\text{XXZ}} = \sum_{j=1}^{N-1} (\sigma_j^x \sigma_{j+1}^x + \sigma_j^y \sigma_{j+1}^y + \Delta \sigma_j^z \sigma_{j+1}^z). \quad (1.39)$$

We take the number of sites N to be even. The anisotropy parameter Δ governs the feature of the system, that is, in $|\Delta| \leq 1$, the system is in the gapless phase and spin transport is ballistic, and in $\Delta > 1$, it is in the gapped antiferromagnetic phase and spin transport is diffusive [32]. Here, we consider $\Delta = 0.55$ case, for which spin transport is ballistic. This model is known as a typical integrable system [33, 34]. On the other hand, we can prepare a non-integrable system by adding a perturbation. We add a single impurity to H_{XXZ} , such as

$$H_{\text{SI}} = H_{\text{XXZ}} + h \sigma_{N/2}^z, \quad (1.40)$$

where h is the strength of magnetic impurity. Henceforth, we fix $h = 1$. Both of these Hamiltonians have $U(1)$ symmetry: $[H_{\text{XXZ}}, \sum_j \sigma_j^z] = [H_{\text{SI}}, \sum_j \sigma_j^z] = 0$. Thus, we consider the zero magnetization sector where $\sum_j \sigma_j^z = 0$. We denote the dimension of the zero-magnetization sector as $\mathcal{D} = \frac{N!}{(N/2)!}$.

To see the breakdown of ETH, it is effective to calculate the expectation values of observables for all eigenstates. As an observable, we choose the local kinetic energy at $j = N/4$,

$$K := \sigma_{\frac{N}{4}}^x \sigma_{\frac{N}{4}+1}^x + \sigma_{\frac{N}{4}}^y \sigma_{\frac{N}{4}+1}^y, \quad (1.41)$$

and the average of local kinetic energy

$$T := \frac{1}{N} \sum_{j=1}^{N-1} (\sigma_j^x \sigma_{j+1}^x + \sigma_j^y \sigma_{j+1}^y). \quad (1.42)$$

Figure 1.2 shows the diagonal matrix elements of K and T in the basis of energy eigenstates. It implies that the distributions of expectation values in the integrable Hamiltonian (1.39) are wider than those in the nonintegrable Hamiltonian (1.40). Furthermore, in the nonintegrable case, fluctuations decay with a power of \mathcal{D} (inset of Figure 1.2 (b), (d)). On the other hand, the fluctuation of the integrable systems does not seem to depend on the system size. It is concrete evidence that integrable systems do not obey strong ETH because Eq. (1.31) implies that the diagonal elements are given as $O_{mm} \simeq O(E) + e^{-O(N)}$. Reference [31] also studies off-diagonal elements and gives the same result.

1.4.2 Many Body Localization

The second class of systems violating the strong ETH is called many-body localized systems. The concept of localization was first suggested by Anderson [35]. He pointed out that a single-particle eigenfunction may be spatially localized as a result of impurity potential. Later, it was extended to many-body systems [36–40] and is called *many-body localization* (MBL). The numerical calculations [36, 41, 42] show that the MBL systems fail to reach thermal equilibrium. Actually, MBL systems violate not only the strong ETH but also the weak ETH [28].

A typical example of a system showing MBL is the spin-1/2 Heisenberg XXZ model with a random magnetic field [36, 41, 42]:

$$H_{\text{rfm}} = \sum_j \left\{ \frac{J_{\perp}}{2} (\sigma_j^x \sigma_{j+1}^x + \sigma_j^y \sigma_{j+1}^y) + \frac{J_z}{2} \sigma_j^z \sigma_{j+1}^z \right\} - \sum_j h_j \sigma_j^z, \quad (1.43)$$

where the strength of field h_j is uniformly chosen from $[-h, h]$ and h is a disorder strength. This model shows the phase transition between the MBL phase and the thermal phase, where the system obeys strong ETH, at the transition point $h = h^*$. In the strong disorder region, namely $h > h^*$, this model shows MBL. As we will discuss in follows, in MBL

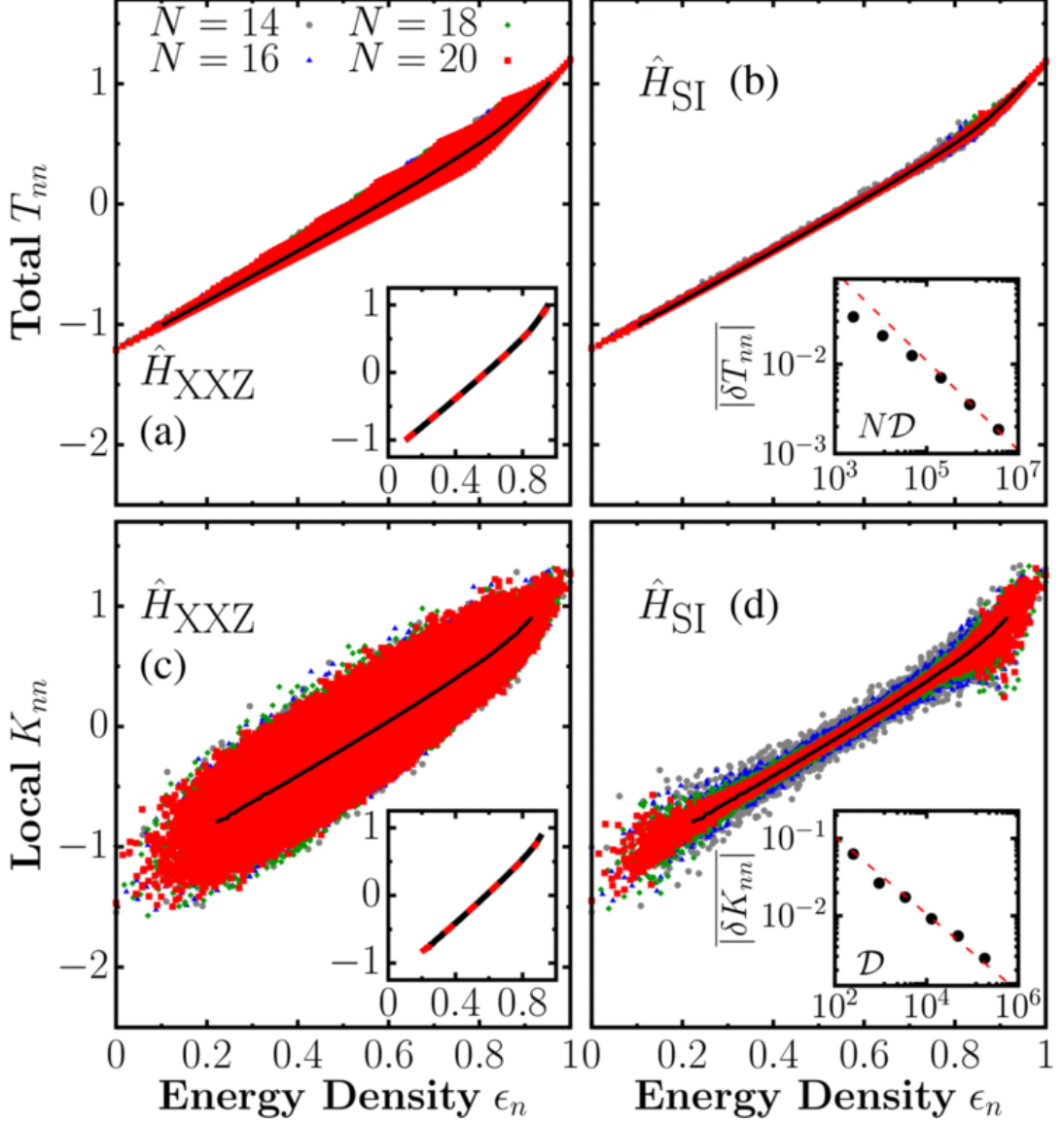


Figure 1.2: The diagonal matrix elements of T [(a), (b)] and K [(c), (d)] in the basis of all eigenstates of H_{XXZ} [(a), (c)] and H_{SI} [(b), (d)], respectively. The energy density represents normalized eigenenergy such that $\epsilon_n = (E_n - E_{\min})/(E_{\max} - E_{\min})$. The black line represents the microcanonical average for $N = 20$. The inset in (a) and (c) show the equivalence of the microcanonical predictions in both models for each observable. On the other hand, the insets in (b) and (d) show that the fluctuation of T and K in the middle of spectrum show the scaling $(ND)^{-\frac{1}{2}}$ and $D^{-\frac{1}{2}}$, respectively. This figure is reprinted with permission from Ref. [31], Copyright (2023) by the American Physical Society.

phases, energy eigenstates are connected to simple product states by quasi-local unitary transformations, and do not satisfy ETH due to the strong disorder potential.

In this model, when we take the limit $J_\perp \rightarrow 0$, since $[H_{\text{rfm}}, \sigma_i^z] = 0$ for all i , the Hamiltonian (1.43) is diagonal in the σ^z -basis. Then, in the region of weak J_\perp , we can define quasi-local integrals of motion (localized-bits; l-bits [37]) $\tau_j^z := U^\dagger \sigma_j^z U$ such that $[H_{\text{rfm}}, \tau_j^z] = 0$. Specifically, τ_j^z can be expanded as

$$\tau_j^z = Z \sigma_j^z + \sum_{n=1}^{\infty} V_j^{(n)} \hat{O}_j^{(n)}, \quad (1.44)$$

where the operator $\hat{O}_j^{(n)}$ can be written down by up to $(2n+1)$ -body operators acting on sites whose distances from site j are equal to or less than n . We presumptively normalize $\hat{O}_j^{(n)}$ by the Frobenius norm (trace norm) $\|\hat{O}_j^{(n)}\|_F := \sqrt{\text{Tr}\{\hat{O}_j^{(n)}(\hat{O}_j^{(n)})^\dagger\}} = 1$. The magnitude of the long-range interaction $V_j^{(n)}$ decays exponentially as $V_j^{(n)} \sim e^{-\frac{n}{\xi}}$, where $\xi > 0$ is the length scale that determines the locality of τ_j^z . The local IOM τ_j^z and the spin operator σ_j^z are related to a quasi-local unitary transformation U such that $U = \prod_i \cdots U_{i,i+1,i+2}^{(3)} U_{i,i+1}^{(2)}$, where $U_{i,i+1,\dots,i+n-1}^{(n)}$ is an n -body unitary operator acting on sites $i, i+1, \dots, i+n-1$. In this expansion, long-range unitary rotation becomes exponentially small such that $\|1 - U_{i,i+1,\dots,i+n-1}^{(n)}\|_F^2 \sim e^{-\frac{n}{\xi}}$. Moreover, MBL Hamiltonians are generally expressed as the quasi-local integrals of motion τ_j^z such that

$$H_{\text{MBL}} = E_0 + \sum_j J_j \tau_j^z + \sum_{i>j} J_{ij} \tau_i^z \tau_j^z + \sum_{i>j>k} J_{ijk} \tau_i^z \tau_j^z \tau_k^z \cdots \quad (1.45)$$

Typically, the magnitudes of the interaction J_{ij}, J_{ijk}, \dots are exponentially decaying through the distance of interaction:

$$J_{ij} \propto J_0 e^{-\frac{|i-j|}{\kappa}}, \quad J_{ijk} \propto J_0 e^{-\frac{|i-k|}{\kappa}}, \dots, \quad (1.46)$$

with the length scale $\kappa > 0$. We can show $\kappa^{-1} \geq (\xi^{-1} + \ln 2)/2$ [40], which implies that κ remains finite even if the length scale ξ diverges.

In this situation, since τ^x or τ^y do not appear in the Hamiltonian H_{MBL} , this Hamiltonian can be regarded as classical in the sense that all eigenstates can be expressed as simple product states of the l-bit basis. The existence of l-bits conservation tells us that the mechanism of violation of ETH is the same as in integrable systems. Moreover, MBL systems keep the information of initial l-bits $\{\tau_j^z\}$ in the dynamics, which is applicable to memory devices that store quantum information [37].

1.4.3 Hilbert Space Fragmentation

The third class of systems that do not show thermalization is systems with Hilbert space fragmentation [28, 43, 44]. It refers to the phenomenon in which the system has an exponentially large number of dynamically disconnected subspaces. That is, the whole Hilbert

space is decomposed into an exponential number of Krylov subspaces:

$$\mathcal{H} = \bigoplus_j \mathcal{K}_j, \quad \mathcal{K}_j = \text{Span}\{|\psi_j\rangle, H|\psi_j\rangle, H^2|\psi_j\rangle, \dots\}. \quad (1.47)$$

Since the dynamics of states are restricted to corresponding fragmented subspaces, these states may not show thermalization. Of course, by choosing the basis as the eigenstates of the Hamiltonian H , the Hilbert space can be decomposed into $\dim \mathcal{H}$ disconnected Krylov subspaces in any system. However, when we think about the Hilbert space fragmentation, we consider the case that the initial states $|\psi_j\rangle$ can be taken as “simple” states such as product states. Moreover, these distinct subspaces are not labeled by quantum numbers of any local symmetry and the number of these subspaces scales exponentially with the system size. In this case, whether the weak ETH holds or not depends on the structure of the fragmented Hilbert spaces. The Hilbert space fragmentation is classified according to whether the Hilbert space has a dominant Krylov subspace. Let $D := \dim \mathcal{H}$ be a dimension of the whole Hilbert space and let $d_{\max} := \max_j (\dim \mathcal{K}_j)$ be the largest dimension of the Krylov subspaces. Then, if $d_{\max}/D \rightarrow 0$ in the thermodynamic limit, each subspace is sufficiently fragmentized and the weak ETH does not hold. On the other hand, the situation is quite different when $d_{\max}/D \rightarrow 1$. In this case, there exists a dominant subspace that occupies almost all of the Hilbert space, and almost all states belong to it. Since there is little difference between this large subspace and a system without Hilbert space fragmentation, states in this dominant subspace are considered to obey ETH. Thus, the weak ETH holds.

A canonical example of a fragmented model is the one-dimensional $t - J_z$ model [45, 46]. The following discussion considers open boundary conditions, but Ref. [47] shows that this model exhibits Hilbert space fragmentation with both open and periodic boundary conditions. The Hamiltonian of the $t - J_z$ model is

$$H_{t-J_z} = - \sum_{j=1}^{L-1} \left[t_j \sum_{\sigma \in \{\uparrow, \downarrow\}} (\tilde{c}_{j,\sigma} \tilde{c}_{j+1,\sigma}^\dagger + \text{H.c.}) + J_j^z S_j^z S_{j+1}^z \right] + \sum_{j=1}^L (h_j S_j^z + g_j (S_j^z)^2), \quad (1.48)$$

where $t_j, J_j^z, h_j, g_j \in \mathbb{R}$ are random constants and

$$S_j^z := \tilde{c}_{j,\uparrow}^\dagger \tilde{c}_{j,\uparrow} - \tilde{c}_{j,\downarrow}^\dagger \tilde{c}_{j,\downarrow}, \quad (1.49)$$

$$\tilde{c}_{j,\sigma} := c_{j,\sigma} (1 - c_{j,-\sigma}^\dagger c_{j,-\sigma}). \quad (1.50)$$

The symbol $-\sigma$ denotes the spin opposite to σ , i.e. $(-\uparrow) = \downarrow$ and vice versa. The operators $c_{j,\sigma}$ and $c_{j,\sigma}^\dagger$ are ordinary fermionic annihilation and creation operators with canonical anticommutation relations $\{c_{i,\sigma}, c_{j,\sigma'}^\dagger\} = \delta_{ij} \delta_{\sigma\sigma'}$ and $\{c_{i,\sigma}, c_{j,\sigma'}\} = \{c_{i,\sigma}^\dagger, c_{j,\sigma'}^\dagger\} = 0$. Each site can accommodate at most one fermion and we can map fermionic creation/annihilation operators to spin-1 operators by a generalized Jordan-Wigner transformation [48]. As

obvious symmetries, there exist the particle number conservations of both \uparrow and \downarrow spins:

$$N^\uparrow := \sum_{j=1}^L N_j^\uparrow, \quad N^\downarrow := \sum_{j=1}^L N_j^\downarrow, \quad (1.51)$$

where

$$N_j^\sigma = \tilde{c}_{j,\sigma}^\dagger \tilde{c}_{j,\sigma}. \quad (1.52)$$

It is worth to mention that the Hamiltonian (1.48) permits only the following transitions:

$$|\uparrow 0\rangle \leftrightarrow |0 \uparrow\rangle, \quad |\downarrow 0\rangle \leftrightarrow |0 \downarrow\rangle, \quad (1.53)$$

where the two sites are adjacent, and $|\uparrow\rangle$, $|\downarrow\rangle$, and $|0\rangle$ denote a site occupied by spin \uparrow , \downarrow , and an empty site, respectively. In this situation, the sequence with all $|0\rangle$ removed from the spin configuration does not change by this Hamiltonian. For example, in $L = 6$ case, the state $|\uparrow 0 \downarrow \downarrow 0 \uparrow\rangle$ has a transition to $|00 \uparrow \downarrow \downarrow \uparrow\rangle$, but it has no transition to $|00 \downarrow \uparrow \downarrow \uparrow\rangle$ because the sequence $\downarrow \uparrow \downarrow \uparrow$ is not equal to $\uparrow \downarrow \downarrow \uparrow$. As a result, the Hilbert space is divided into dynamically disconnected subspaces, and the number of the subspaces is

$$\sum_{i=1}^L 2^i = 2^{L+1} - 1. \quad (1.54)$$

It implies that Hilbert space fragmentation occurs in this model.

We follow the argument in Ref. [43], where the authors give an explanation for this phenomenon from a more algebraic point of view. We introduce symbols that refer to local terms of the Hamiltonian, such as

$$T_j = \sum_{\sigma \in \{\uparrow, \downarrow\}} (\tilde{c}_{j,\sigma} \tilde{c}_{j+1,\sigma}^\dagger + \text{H.c.}), \quad (1.55)$$

$$V_j = S_j^z S_{j+1}^z. \quad (1.56)$$

Obviously, these operators satisfy a commutation relation

$$[N_j^\sigma + N_{j+1}^\sigma, T_j] = [N_j^\sigma + N_{j+1}^\sigma, V_j] = 0 \quad (\sigma \in \{\uparrow, \downarrow\}). \quad (1.57)$$

Moreover, we can find another relation

$$[N_j^{\sigma_1} N_{j+1}^{\sigma_2}, T_j] = [N_j^{\sigma_1} N_{j+1}^{\sigma_2}, V_j] = 0 \quad (\sigma_1, \sigma_2 \in \{\uparrow, \downarrow\}). \quad (1.58)$$

From these relations, we can construct a quadratic integral of motion:

$$N^{\sigma_1 \sigma_2} = \sum_{j_1 < j_2} N_{j_1}^{\sigma_1} N_{j_2}^{\sigma_2} \quad (\sigma_1, \sigma_2 \in \{\uparrow, \downarrow\}). \quad (1.59)$$

These are independent integrals of motion in the sense that they cannot be expressed as the product of N^\uparrow and N^\downarrow when $\sigma_1 \neq \sigma_2$. Similarly, we can construct families of the integral of motions

$$N^{\sigma_1 \sigma_2 \dots \sigma_k} = \sum_{j_1 < j_2 < \dots < j_k} N_{j_1}^{\sigma_1} N_{j_2}^{\sigma_2} \dots N_{j_k}^{\sigma_k} \quad (\sigma_j \in \{\uparrow, \downarrow\}), \quad (1.60)$$

for $0 \leq k \leq L$. Some of the quantities written as Eq. (1.60) with $k \geq 2$ are independent integrals of motion that cannot be written as a polynomial of N^\uparrow and N^\downarrow . Furthermore, Ref. [43] shows that the quantities in Eq. (1.60) are linearly independent and form the complete basis of the commutant algebra for the $t - J_z$ model. These integrals of motion are diagonal in the product state basis. Hence, Hilbert space fragmentation occurs.

Some numerical calculations show that this system is prevented from reaching thermalization by fragmentation. For example, Ref. [47] shows that the autocorrelation function $\langle S_j^z(t) S_i^z \rangle$ in the $t - J_z$ model (Eq. (1.48)) scales $\sim L^{-\frac{1}{2}}$ in the thermodynamic limit, whereas in one of the thermal systems, it spreads out over the whole system and behaves like $\mathcal{O}(L^{-1})$.

1.5 Characterization of Thermal States and ETH Violation

In the previous discussions, we argued the definition of thermalization, ETH, and the process of violation of ETH in some special cases. As seen in the previous sections, whether a given non-thermal initial state reaches thermalization depends on whether the state can vary in an efficiently large subspace of the whole Hilbert space. In this section, we focus on the features of thermal and nonthermal systems, and we give standard methods to verify whether a given state or system is thermal or nonthermal.

1.5.1 Level-Spacing Statistics and r -value

When we consider typical quantum many-body systems, they exhibit similar behaviors. Hence, they must behave as a system whose Hamiltonian matrix is chosen randomly, and we can use the results of the random matrix theory. This theory is often mentioned in the context of quantum chaos [49], but it can be applied to distinguish whether a given system is thermal or not. We consider the Hamiltonian H with the energy spectrum $\{E_n\}_{n=1}^N$, and we assume that the energy levels are arranged in ascending order such that $E_1 \leq E_2 \leq \dots \leq E_N$. Then, the j -th normalized level spacing (s_j) is defined as

$$s_j = \frac{E_{j+1} - E_j}{E_N - E_1} \quad (1.61)$$

for $j = 1, 2, \dots, N - 1$. It is known that $\{s_j\}$ in nonintegrable systems obeys the Wigner-Dyson distribution [49–52]. Moreover, we consider two types of the Wigner-Dyson distri-

bution corresponding to the time-reversal (complex-conjugate) symmetry: If the Hamiltonian is time-reversal invariant (real), the normalized level spacing statistics obey the Gaussian orthogonal ensemble (GOE) defined by

$$P_{\text{GOE}}(s) := \frac{\pi}{2} s e^{-\frac{\pi s^2}{4}}. \quad (1.62)$$

In contrast, if the Hamiltonian does not have time-reversal invariance (complex), the normalized level spacing obeys the Gaussian unitary ensemble (GUE)

$$P_{\text{GUE}}(s) := \frac{32}{\pi^2} s^2 e^{-\frac{4}{\pi} s^2}. \quad (1.63)$$

However, in integrable systems and MBL systems, the distribution of $\{s_j\}$ obeys a different distribution, namely the Poisson distribution [51]:

$$P_{\text{Poisson}}(s) := e^{-s}. \quad (1.64)$$

In addition, the r -value $\langle r \rangle$ is useful to discuss the level-spacing statistics. It is based on the gap ratio for consecutive levels

$$r_n = \frac{\min(s_n, s_{n+1})}{\max(s_n, s_{n+1})}. \quad (1.65)$$

The r -value is given as the average of r_n :

$$\langle r \rangle = \frac{1}{N-2} \sum_{j=1}^{N-2} r_j. \quad (1.66)$$

By calculating the r -value for each of the distributions, we get $\langle r_{\text{Poisson}} \rangle = 2 \ln 2 - 1 \approx 0.386$ for Poisson, $\langle r_{\text{GOE}} \rangle = 4 - 2\sqrt{3} \approx 0.536$ for GOE, and $\langle r_{\text{GUE}} \rangle = \frac{2\sqrt{3}}{\pi} - \frac{1}{2} \approx 0.603$ for GUE [53].

1.5.2 Entanglement Entropy

The entanglement entropy is not an observable⁵. However, it is useful to characterize thermal or nonthermal states [55]. The definition of the entanglement entropy in lattice systems is given as follows: We assume that the lattice can be divided into two parts, A and B . Then the reduced density matrix of a given pure state $|\psi\rangle$ is $\rho_A = \text{Tr}_B(|\psi\rangle\langle\psi|)$, where Tr_B is the partial trace over the subsystem B . Then, the entanglement entropy for the subsystem A is given as

$$S_A = -\text{Tr}\{\rho_A \ln \rho_A\}. \quad (1.67)$$

Its values for thermal states can be predicted as the value for the microcanonical density matrix $\hat{\rho}_{\text{MC}}$ [56, 57]. For highly excited states, ETH predicts the volume law of the

⁵Recently, Rényi entropy

$$S_A^n = \frac{1}{1-n} \ln \text{Tr} \rho_A^n,$$

a generalization of the entanglement entropy, has been measured experimentally for $n = 2$ [54].

entanglement entropy [28]. In the middle of the spectrum, it becomes closer to the mean value of states in the Hilbert space, which is also known as the Page entropy [58]. For one-dimensional chains with L sites, the half-chain entanglement entropy becomes

$$S_A \sim \frac{L}{2} \ln \delta, \quad (1.68)$$

where δ is the number of possible states per site.

In contrast, entanglement entropy of nonthermal states usually obeys the area law [40] (in one-dimensional systems, S_A is suppressed by a constant irrelevant to L) or sub-volume law [59] (in one-dimensional systems, $S_A/L \rightarrow 0$ in the thermodynamic limit) rather than the volume law.

1.6 Summary of This Chapter and Outline of the Thesis

In this section, we briefly reviewed the definitions of thermalization and ETH, and we argued that there exist some exceptions to ETH. In quantum many-body systems, we can consider microscopic thermalization equilibrium (MITE), and it becomes a central topic to discuss the quantum version of thermalization. ETH, which says that all energy eigenstates in thermal systems are inherently thermal, emerges as a foundational theory for understanding thermalization in these systems. Nonetheless, there are notable exceptions that violate ETH, including quantum integrable systems, many-body localized systems, and systems experiencing Hilbert space fragmentation. These exceptions are characterized by an abundance of integrals of motion (IOMs) or similar structures that disrupt typical thermalization patterns.

The organization of the thesis is as follows: In Chapter 2, we introduce another class of exceptions to ETH, called Quantum Many-Body Scars (QMBS), and review several studies on QMBS. First, we describe a recent experiment on Rydberg atom arrays which marked the beginning of QMBS research [60] and review it from a theoretical perspective. We also discuss some theoretical ways to construct models with QMBS, including the Shiraishi-Mori embedding method [61], the method using Onsager algebra [62], and the restricted spectrum generating algebra. We also mention how to diagnose whether a given system or state is thermal or not.

In Chapters 3 and 4, we propose new examples of quantum many-body models with QMBS. In Chapter 3, we focus on the spin-1 scalar spin chirality and apply the method using the restricted spectrum generating algebra. We propose three classes of models with QMBS. The first and second classes of models are obtained by perturbing the spin-1 scalar spin chirality by tailored disorder. In the first model, we choose the random single-ion anisotropy as a perturbation. The second model considers a slightly more complex form of perturbation. This model can be extended to higher-dimensional lattices. We introduce the case of the two-dimensional triangular lattice. These models provide us with

towers of scar states generated by restricted spectrum generating algebra. It allows us to demonstrate that a superposition of these scar states shows perfectly periodic revivals in the dynamics. Interestingly, in the second model, two different kinds of QMBS towers coexist, and we observe that their combined state exhibits complex but periodic dynamics. The third class is the combination of the Affleck-Lieb-Kennedy-Tasaki (AKLT) Hamiltonian and the scalar spin chirality. It is a deformation of the system constructed in Chapter 4.

In Chapter 4, we propose another method to construct models with QMBS. In our method, we use integrable boundary states [63], which are defined as states that are annihilated by all of parity-odd conserved charges of some integrable system. This method allows us to construct deformations of the Majumdar-Ghosh and AKLT models—prototypes of frustration-free systems. The former is related to the spin-1/2 scalar spin chirality, which is the third conserved charge of the Heisenberg model, and the latter is related to the third conserved charge of the SU(3) Sutherland model, respectively. In addition, we construct models starting from the spin-1/2 scalar spin chirality and its deformation. The scalar spin chirality and its deformation are the third conserved charges of the XXZ model or the XYZ model, respectively. In these models, the tilted Néel (q -Néel) states serve as integrable boundary states. Unlike the two previous models, i.e., the Majumdar-Ghosh and AKLT-based models, these models contain towers consisting of multiple independent QMBS. We observe that the Néel state, which is a combination of these QMBS, shows perfectly periodic revivals in its dynamics. In addition, we discuss the extension of these models to any bipartite lattice. As an example, we provide the case of the two-dimensional square lattice. Finally, we summarize this thesis in Chapter 5. Some supplemental materials related to Chapter 3 and 4 are provided in Appendices A and B, respectively.

QUANTUM MANY-BODY SCARS

We reviewed some classes of models that show the violation of the strong ETH in the previous chapter. However, the recent experimental research revealed another class of systems with the ETH violation [64]. We call nonthermal states that appear in these systems Quantum Many-Body Scars. In the context of quantum physics, the word “scar” was first used in Ref. [65], which argued for unstable periodic orbits that appear in a quantum version of systems of billiards in a Bunimovich stadium. The classical billiard problem considers the motion of a single particle in a stadium potential. Thus, kinetic energy is conserved. Reference [66] shows that for a large class of stadium shapes, including Bunimovich stadiums, most of the particle motions are ergodic. However, there are a few periodic orbits in such a system. Correspondingly, in the quantum version of the model, there are a few exceptional eigenfunctions that congregate along these periodic orbits.

A few decades later, Ref. [64] reported that several states in a Rydberg atom array show robust periodic dynamics while almost all states rapidly saturate to thermal equilibrium. Theoretical studies later gave these states the name *quantum many-body scars* (QMBS) because they looked a lot like single-particle quantum scars [67]. Today, it is agreed that QMBS are nonthermal eigenstates embedded in the spectra of nonintegrable quantum systems [68], but actually, it implies that their nonthermal behavior is explained by neither many-body localization nor Hilbert space fragmentation. Recently, several studies suggest the application of QMBS to quantum information processing [69–71]. In this section, we introduce the Rydberg Atom Simulator experiment, the dawn of QMBS research, and some previous theoretical research.

2.1 Rydberg Atom Simulator

The recent development of experimental technology allows us to examine the behavior of some lattice models. Bernien et al. discovered a strange behavior of a non-integrable system with the 51-atom Rydberg simulator [64]. The system has some peculiar states that show slow relaxation and persistent oscillations.

This experiment was realized by trapping individual ^{87}Rb atoms with the optical tweezer technique [72–74] and the van der Waals interaction generated by the dipole trap arrays with two different lasers [75]. In this setup, the quantum state living in each atom can be regarded as a two-level system: the ground state $|g\rangle$ and the Rydberg state $|r\rangle$. The Hamiltonian of the entire system is given by

$$H = \sum_i \frac{\Omega_i}{2} \sigma_i^x - \sum_i \Delta_i n_i + \sum_{i < j} V_{ij} n_i n_j, \quad (2.1)$$

where $\sigma_i^x = |r\rangle_i \langle g| + |g\rangle_i \langle r|$ corresponds to the coupling between the ground state $|g\rangle_i$ and the Rydberg state $|r\rangle_i$ at position i , Ω_i is the corresponding Rabi frequency, Δ_i is the detuning, $n_i = |r\rangle_i \langle r|$, and V_{ij} is the strength of the van der Waals interaction between the Rydberg state at position i and j . They focused on the homogeneous case such that $\Omega_i = \Omega$ and $\Delta_i = \Delta$ for all i .

In such a setting, three particular initial states are stabilized by tuning the intensity of detuning Δ ; $|\mathbb{Z}_2\rangle := |rgrgrg \cdots\rangle$, $|\mathbb{Z}_3\rangle := |rggrgg \cdots\rangle$, and $|\mathbb{Z}_4\rangle := |rgggrggg \cdots\rangle$. Then, they observed the processes of thermalization of these states after the detuning Δ is suddenly changed to the single atom resonance ($\Delta \rightarrow 0$).

Now that the Hamiltonian (2.1) is non-integrable, we expect that any initial state equilibrates into a thermal state whose energy is the same as the initial state at a later time. However, they found that the number of domain walls, which are identified as two neighboring atoms in the same state, developed from $|\mathbb{Z}_2\rangle$ oscillates for a long time.

2.2 PXP model

In this section, we discuss the phenomena argued in the previous section from a theoretical point of view. Here, we introduce the model discussed by Turner et al. [60, 67].

We first derive the effective Hamiltonian to analyze the phenomena. We consider the post-quench Hamiltonian such that $\Delta \rightarrow 0$. Since the intensity of the van der Waals interaction $V_{i,j}$ is proportional to $|i - j|^{-6}$, we only take into account the nearest-neighbor interaction $V_{i,i+1} \equiv V$ and ignore long-range interactions. Taking the limit of strong interaction $V \gg \Omega$ yields

$$H \sim \sum_i n_i n_{i+1} + \epsilon \sum_i \sigma_i^x, \quad (2.2)$$

where $\epsilon = \Omega/2V \ll 1$ is a small parameter. Here, the first term of the Hamiltonian (2.2) is much larger than the second term. Therefore, the first term works effectively as the constraint on the Hilbert space such that two neighboring atoms cannot be in the Rydberg state simultaneously. Thus, the effective Hamiltonian can be written down only by the contribution from the second term of Eq. (2.2). By introducing the projection onto the restricted Hilbert space $\mathcal{P} = \prod_i (1 - n_i n_{i+1})$, we can write the effective Hamiltonian as

$$\begin{aligned}
H_{\text{eff}} &= \mathcal{P} \sum_i \sigma_i^x \mathcal{P} \\
&= \prod_j (1 - n_j n_{j+1}) \left(\sum_i \sigma_i^x \right) \prod_k (1 - n_k n_{k+1}) \\
&= \sum_i \left(\prod_j (1 - n_j n_{j+1}) \prod_{k \neq i-1, i} (1 - n_k n_{k+1}) \sigma_i^x (1 - n_{i-1} n_i) (1 - n_i n_{i+1}) \right) \\
&= \sum_i \left(\left[\prod_{j \neq i-1, i} (1 - n_j n_{j+1}) \right] (1 - n_{i-1} n_i) (1 - n_i n_{i+1}) \sigma_i^x (1 - n_{i-1} n_i) (1 - n_i n_{i+1}) \right) \\
&= \sum_i \left(\left[\prod_{j \neq i-1, i} (1 - n_j n_{j+1}) \right] (\sigma_i^x - n_{i-1} \sigma_i^x - \sigma_i^x n_{i+1} + n_{i-1} \sigma_i^x n_{i+1}) \right). \tag{2.3}
\end{aligned}$$

By introducing the projection onto the ground state $P_i = 1 - n_i = |g_i\rangle\langle g_i|$, it can be simplified as

$$H_{\text{eff}} = \sum_i \left(\left[\prod_{j \neq i-1, i} (1 - n_j n_{j+1}) \right] (P_{i-1} \sigma_i^x P_{i+1}) \right). \tag{2.4}$$

On the restricted Hilbert space, $1 - n_j n_{j+1}$ acts as the identity operator. Thus, we arrive at the effective Hamiltonian

$$H_{\text{eff}} = \sum_{i=1}^L P_{i-1} \sigma_i^x P_{i+1}. \tag{2.5}$$

Since we consider it under open boundary conditions, we assume P_0 and P_{L+1} are equivalent to the identity operator. For simplicity, we use the notation $|\uparrow\rangle := |r\rangle$, $|\downarrow\rangle := |g\rangle$ in the following discussion.

Figure 2.1 shows the development of the fidelity $\mathcal{F}(t) = |\langle \phi(t) | \phi \rangle| = |\langle \phi | e^{-iH_{\text{eff}}t} | \phi \rangle|$ for the Néel state $|\mathbb{Z}_2\rangle = |\uparrow\downarrow\uparrow\downarrow \cdots\rangle$, period-3 state $|\mathbb{Z}_3\rangle = |\uparrow\downarrow\downarrow\uparrow\downarrow \cdots\rangle$, and the period-4 state $|\mathbb{Z}_4\rangle = |\uparrow\downarrow\downarrow\downarrow\uparrow\downarrow\downarrow \cdots\rangle$ ¹. We can see that $|\mathbb{Z}_2\rangle$ and $|\mathbb{Z}_3\rangle$ show a periodical behavior whereas the fidelity of $|\mathbb{Z}_4\rangle$ rapidly decreases.

The violation of ETH of $|\mathbb{Z}_2\rangle$ can be understood by the method called forward scattering approximation. First, we consider the paramagnetic model $H_{\text{PM}} = \sum_j \sigma_j^x$. It can be

¹Throughout this thesis, including this figure, we used the QuSpin package for numerical calculation [76, 77].

decomposed into $H_{\text{PM}} = \tilde{H}^+ + \tilde{H}^-$, where

$$\tilde{H}^+ = \sum_{j:\text{even}} \sigma_j^+ + \sum_{j:\text{odd}} \sigma_j^-, \quad (2.6)$$

$$\tilde{H}^- = \sum_{j:\text{odd}} \sigma_j^+ + \sum_{j:\text{even}} \sigma_j^-. \quad (2.7)$$

These operators act on $|\mathbb{Z}_2\rangle$ as ladder operators. That is, let us denote $|\tilde{0}\rangle = |\mathbb{Z}_2\rangle$ and $|\tilde{n}\rangle = (\tilde{H}^+)^n |\tilde{0}\rangle / \|(\tilde{H}^+)^n |\tilde{0}\rangle\|$, we obtain

$$\tilde{H}^- |\tilde{n}\rangle = \beta_n |\widetilde{n-1}\rangle, \quad (2.8)$$

$$\tilde{H}^+ |\tilde{n}\rangle = \beta_{n+1} |\widetilde{n+1}\rangle, \quad (2.9)$$

where $\beta_n = \sqrt{n(L-n+1)}$. Therefore, the subspace $S = \text{Span}\{|\tilde{0}\rangle, |\tilde{1}\rangle, \dots, |\tilde{L}\rangle\}$ is an invariant subspace of H_{PM} and the matrix form of the restricted Hamiltonian of H_{PM} in S is tridiagonal

$$H_{\text{PM}}|_S = \begin{pmatrix} 0 & \beta_1 & 0 & & \\ \beta_1 & 0 & \beta_2 & & \\ 0 & \beta_2 & 0 & \ddots & \\ & & \ddots & \ddots & \beta_L \\ & & & \beta_L & 0 \end{pmatrix}. \quad (2.10)$$

Now, we come back to the PXP Hamiltonian. We can decompose the Hamiltonian (2.5) as $H_{\text{eff}} = H^+ + H^-$, where

$$H^+ = \sum_{j:\text{even}} P_{j-1} \sigma_j^+ P_{j+1} + \sum_{j:\text{odd}} P_{j-1} \sigma_j^- P_{j+1}, \quad (2.11)$$

$$H^- = \sum_{j:\text{odd}} P_{j-1} \sigma_j^+ P_{j+1} + \sum_{j:\text{even}} P_{j-1} \sigma_j^- P_{j+1}. \quad (2.12)$$

These operators act as pseudo-ladder operators. That is, let us denote $|n\rangle = (H^+)^n |\mathbb{Z}_2\rangle / \|(H^+)^n |\mathbb{Z}_2\rangle\|$. In this situation, the recursive relation like Eq. (2.8) holds only for $n = 1, 2$. Here, we introduce the error vectors $|\delta w_n\rangle$ such that

$$H^- |n-1\rangle = \beta_{n-1} |n-2\rangle + |\delta w_n\rangle. \quad (2.13)$$

Then, we can evaluate the squared norm of $|\delta w_n\rangle$ as

$$\langle \delta w_n | \delta w_n \rangle = \langle n-1 | [H^+, H^-] | n-1 \rangle + \beta_n^2 - \beta_{n-1}^2. \quad (2.14)$$

The numerical calculation evaluated the norm of the normalized error vector $|\delta v_n\rangle = |\delta w_n\rangle / \beta_n$ as $\| |\delta v_n\rangle \|^2 = \mathcal{O}(n^2/L^3)$. It guarantees that the fidelity of $|\mathbb{Z}_2\rangle$ shows persistent oscillation for a long time because the error $|\delta w_n\rangle$ is sufficiently small for small n .

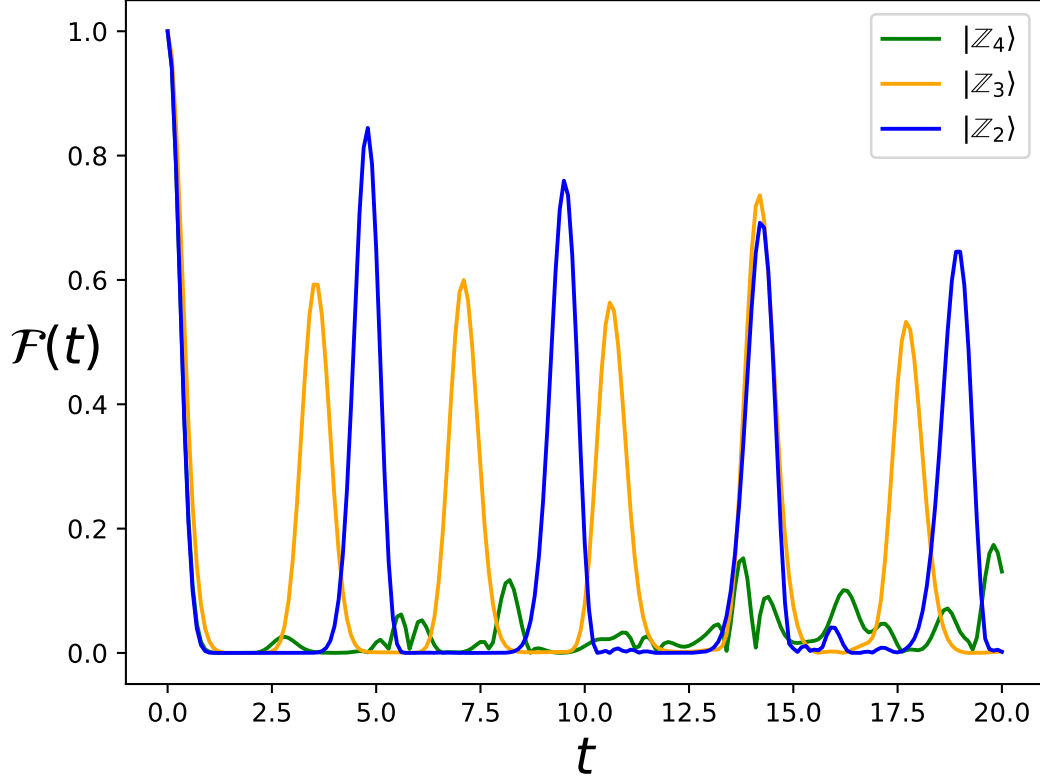


Figure 2.1: The time evolution of the fidelity starting from $|\mathbb{Z}_2\rangle$, $|\mathbb{Z}_3\rangle$, and $|\mathbb{Z}_4\rangle$. We can see that $|\mathbb{Z}_2\rangle$ and $|\mathbb{Z}_3\rangle$ show persistent oscillation while $|\mathbb{Z}_4\rangle$ rapidly decreases and crawls around $\mathcal{F}(t) = 0$. This calculation was done for $L = 24$.

In addition, there have been in-depth studies on QMBS that appear in the PXP model. For example, Choi et al. suggested that adding a perturbation makes the stability of QMBS $|\mathbb{Z}_2\rangle$ robust [78]. Lin and Motrunich showed the existence of exact QMBS in the PXP model [79]. Ho et al. revealed the dynamics of $|\mathbb{Z}_2\rangle$ state at finite temperature by using a matrix-product-state approach [80]. Omiya and Müller expanded their result to the PXP model in general bipartite lattices and showed the similarity between exact scars and $|\mathbb{Z}_2\rangle$ [81].

2.3 Construction of Exact Quantum Many-Body Scars

2.3.1 Shiraishi-Mori embedding

The first formalism of “embedding” nonthermal eigenstates to the thermal Hamiltonian is introduced by Shiraishi and Mori [61]. The Shiraishi-Mori (SM) method is given as

follows. We first prepare a set of local projection operators $\{P_i\}_{i=1}^N$ ². Let $\mathcal{T} = \bigcap_{i=1}^L \ker P_i$ and we assume $\dim \mathcal{T} > 0$, that is, there exists a nonzero state $|\Psi\rangle$ such that $P_j |\Psi\rangle = 0$ for all $j = 1, 2, \dots, N$. Then, the target states are in \mathcal{T} .

Next, we consider the following Hamiltonian

$$H_{\text{SM}} = \sum_{j=1}^L P_j h_j P_j + H', \quad (2.15)$$

where each h_j is an arbitrary local Hamiltonian and the operator H' satisfies $[H', P_j] = 0$ for any j . Then, for any $|\psi\rangle \in \mathcal{T}$, we obtain

$$\begin{aligned} P_j H_{\text{SM}} |\psi\rangle &= P_j \left(\sum_{i=1}^L P_i h_i P_i \right) |\psi\rangle + P_j H' |\psi\rangle \\ &= P_j H' |\psi\rangle \\ &= H' P_j |\psi\rangle \\ &= 0, \end{aligned} \quad (2.16)$$

for any $j = 1, 2, \dots, N$. Therefore, \mathcal{T} is invariant under the operation H_{SM} . In general, the energy eigenstates in \mathcal{T} are in the middle of the energy spectrum. However, the expectation value of P_j in these eigenstates is exactly zero without fluctuations. It contradicts ETH since the expectation value of P_j in thermal states will be finite. Thus, we can conclude that the states in \mathcal{T} are QMBS.

Here, we introduce an example of a model obtained by the Shiraishi-Mori method. We consider an even-site spin-1/2 chain with periodic boundary conditions. We use Pauli matrices σ_j^μ ($\mu = x, y, z$) as spin operators on the site j and introduce a spin operator of three neighboring sites as

$$S_j^{\text{tot},3} = \frac{1}{2}(\sigma_{j-1} + \sigma_j + \sigma_{j+1}). \quad (2.17)$$

Let us denote the eigenvalues of $(S_j^{\text{tot},3})^2$ by $S(S+1)$. Then, it is known that S takes $S = 1/2$ or $3/2$. We denote by $P_j^{S=3/2}$ the projection operator onto the subspace with $S = 3/2$. It is explicitly given as

$$P_j^{S=3/2} = \frac{1}{6}(\sigma_{j-1} \cdot \sigma_j + \sigma_j \cdot \sigma_{j+1} + \sigma_{j-1} \cdot \sigma_{j+1}) + \frac{1}{3}. \quad (2.18)$$

This operator is known as the local Hamiltonian of the Majumdar-Ghosh (MG) model [82, 83] whose Hamiltonian is given by $H_{\text{MG}} = \sum_j P_j^{S=3/2}$. It is known that the MG model has twofold degenerate ground states

$$|\Psi_1\rangle = |\text{sing}\rangle_{1,2} \otimes |\text{sing}\rangle_{3,4} \otimes \cdots \otimes |\text{sing}\rangle_{L-1,L}, \quad (2.19)$$

$$|\Psi_2\rangle = |\text{sing}\rangle_{2,3} \otimes |\text{sing}\rangle_{4,5} \otimes \cdots \otimes |\text{sing}\rangle_{L,1}, \quad (2.20)$$

²These subspaces must not be orthogonal complement to each other, i.e., $P_i P_j$ ($i \neq j$) is not always 0.

where

$$|\text{sing}\rangle_{i,j} = \frac{1}{\sqrt{2}}(|\uparrow\downarrow\rangle_{i,j} - |\downarrow\uparrow\rangle_{i,j}), \quad (2.21)$$

is the spin singlet state for site i and j . Note that these states have area-law entanglement because they are represented by two-site product states. We will discuss the entanglement entropy of $|\Psi_{1,2}\rangle$ in Chapter 4.

We can embed these states into the spectrum of the Hamiltonian

$$H_1 = \sum_{j=1}^L P_j^{S=3/2} h_j P_j^{S=3/2}, \quad (2.22)$$

where

$$h_j = \sum_{\mu=x,y,z} [J_\alpha (S_{j-1}^\alpha S_j^\alpha + S_j^\alpha S_{j+1}^\alpha) + J'_\alpha (S_{j-2}^\alpha S_j^\alpha + S_j^\alpha S_{j+2}^\alpha)]. \quad (2.23)$$

In this situation, $|\Psi_1\rangle$ and $|\Psi_2\rangle$ become exact QMBS of H_1 .

2.3.2 Onsager's Scar

Shibata et al. [62] have introduced another class of systems with QMBS. Their method relies on the Onsager algebra [84], which was originally introduced to solve the two-dimensional classical Ising model. The Onsager algebra is generated by $\{A_n, G_n\}$, which obeys

$$\begin{aligned} [A_m, A_n] &= 4G_{m-n}, \\ [A_m, G_n] &= 2A_{m-n} - 2A_{m+n} \\ [G_m, G_n] &= 0. \end{aligned} \quad (2.24)$$

Furthermore, there exists an equivalent expression known as the Dolan-Grady relations [85–87]

$$\begin{aligned} [Q, [Q, [Q, \hat{Q}]]] &= n^2 [Q, \hat{Q}], \\ [\hat{Q}, [\hat{Q}, [\hat{Q}, Q]]] &= n^2 [\hat{Q}, Q], \end{aligned} \quad (2.25)$$

with $Q = (4/n)A_0$ and $\hat{Q} = (4/n)A_1$. The authors of Ref. [62] pointed out that if the given Hamiltonian H is invariant under the action of the Onsager algebra, i.e. if there exist operators Q, \hat{Q} that satisfy the Dolan-Grady relation (2.25) and $[H, Q] = [H, \hat{Q}] = 0$, we can construct a scarred model.

Let us review this fact through a concrete example. We consider the following Hamiltonian under the periodic boundary conditions:

$$H_n := - \sum_{j=1}^L \sum_{a=1}^{n-1} \frac{1}{2 \sin(\pi a/n)} \left\{ n(-1)^a [(S_j^+ S_{j+1}^-)^a + (S_j^- S_{j+1}^+)^a] + (n-2a) \omega^{\frac{a}{2}} \tau_j^a \right\}, \quad (2.26)$$

where $\omega := e^{\frac{2\pi i}{n}}$ is the n -th root of unity and the operators S_j^\pm are $n \times n$ matrices that are defined as

$$S_j^+ = \begin{pmatrix} 0 & 1 & & \\ & \ddots & \ddots & \\ & & 0 & 1 \\ 0 & & & 0 \end{pmatrix}_j, \quad S_j^- = (S_j^+)^\dagger, \quad (2.27)$$

and $\tau_j = \text{diag}(1, \omega, \omega^2, \dots, \omega^{n-1})_j$. We assume that the number of sites L is even. In the $n = 2$ case, this model is reduced to the spin-1/2 XX model

$$H_{\text{XX}} = \sum_{j=1}^L (S_j^+ S_{j+1}^- + S_j^- S_{j+1}^+). \quad (2.28)$$

Moreover, the $n = 3$ case is known as the Fateev-Zamolodchikov model [88–91]. We can see that the Hamiltonian (2.26) is $U(1)$ invariant and the corresponding charge is

$$Q = \sum_{j=1}^L S_j^z = \sum_{j=1}^L \sum_{a=1}^{n-1} \frac{1}{1 - \omega^{-a}} (\tau_j)^a, \quad (2.29)$$

where $S_j^z = \text{diag}(\frac{n-1}{2}, \frac{n-3}{2}, \dots, -\frac{n-1}{2})_j$. Note that the set of operators $\{S_j^+, S_j^-, S_j^z\}$ does not form an $\mathfrak{sl}(2)$ triple (except for the $n = 2$ or 3 case) because $[S^+, S^-] \not\propto S^z$ for $n \geq 4$. Furthermore, we can verify that H_n commutes with Q^r ($r = 0, +, -$) defined by

$$Q^0 = \sum_{j=1}^L \sum_{a=1}^{n-1} \frac{(-1)^a}{\sin(\pi a/n)} [(S_j^- S_{j+1}^+)^a - (S_j^+ S_{j+1}^-)^a], \quad (2.30)$$

$$Q^\pm = \sum_{j=1}^L \sum_{a=1}^{n-1} \frac{(-1)^{(n+1)j+a}}{\sin(\pi a/n)} (S_j^\pm)^a (S_{j+1}^\pm)^{n-a}. \quad (2.31)$$

We can find that Q and $\hat{Q} := Q^+ + Q^0 + Q^-$ satisfy the Dolan-Grady relations (2.25). Therefore, the given Hamiltonian is invariant under the action of the Onsager algebra.

Finally, the Hamiltonian of scarred model is formed as

$$H_{S,n} := H_n + H_{\text{pert}} + h \sum_{j=1}^L S_j^z. \quad (2.32)$$

Here, we aim to determine the perturbation term H_{pert} that disturbs all eigenstates of H_n other than states belonging to a Krylov subspace generated by Q^+ . To avoid complexity, in the following discussion, we consider the $n = 2$ case. We focus on a subspace

$$V = \text{Span}\{|\Downarrow\rangle, Q^+ |\Downarrow\rangle, \dots, (Q^+)^{L/2} |\Downarrow\rangle\}, \quad (2.33)$$

where $|\Downarrow\rangle = |\Downarrow\rangle^{\otimes L}$. We can easily see $V \subset \ker H_2$ since $[H, Q^+] = 0$, and $|\Downarrow\rangle$ is annihilated by $H_2 \equiv H_{\text{XX}}$. Instead of considering each basis vector, we consider the coherent state

that is given as

$$|\phi(\beta)\rangle := \exp\{\beta^2 Q^+\} |\Downarrow\rangle = \sum_{n=0}^{L/2} \frac{\beta^{2n}}{n!} (Q^+)^n |\Downarrow\rangle, \quad (2.34)$$

with an arbitrary constant $\beta \in \mathbb{C}$. Then one can obtain the matrix product operator (MPO) form of $\exp\{\beta^2 Q^+\}$ as follows:

$$\begin{aligned} \exp\{\beta^2 Q^+\} &= \prod_{j=1}^L \exp\left[(-1)^{j+1} \beta^2 S_j^+ S_{j+1}^+\right] \\ &= \prod_{j=1}^L \left[1 + (-1)^j \beta^2 S_j^+ S_{j+1}^+\right] \\ &= \prod_{j=1}^L \begin{pmatrix} 1 & (-1)^{j+1} \beta S_j^+ \\ \beta S_{j+1}^+ & 0 \end{pmatrix} \begin{pmatrix} 1 \\ \beta S_{j+1}^+ \end{pmatrix} \\ &= \text{Tr}_{\mathcal{A}}\{C_1 C_2 \cdots C_L\}, \end{aligned} \quad (2.35)$$

where

$$C_j = \begin{pmatrix} 1 & (-1)^{j+1} \beta S_j^+ \\ \beta S_j^+ & 0 \end{pmatrix} \in \text{End } \mathcal{A} \otimes \text{End } \mathcal{H}_j \quad (2.36)$$

is a 2×2 matrix with local operator entries. The symbols \mathcal{A} and \mathcal{H}_j denote an auxiliary space ($\simeq \mathbb{C}^2$) and the local Hilbert space at the site j , respectively. The action of this operator is given as the Kronecker product such that

$$X \otimes_K |v\rangle = \begin{pmatrix} X_{11} |v\rangle & X_{12} |v\rangle \\ X_{21} |v\rangle & X_{22} |v\rangle \end{pmatrix}, \quad (2.37)$$

where X_{ij} is the (i, j) -component of X . Therefore, we obtain the matrix product states (MPS) form of the coherent state:

$$\begin{aligned} |\phi(\beta)\rangle &= \text{Tr}\{(C_1 C_2 \cdots C_L) \otimes_K |\Downarrow \cdots \Downarrow\rangle\} \\ &= \text{Tr}\left\{\prod_{j=1}^L C_j \otimes_K |\Downarrow\rangle\right\} \\ &=: \text{Tr}\{A_1 A_2 \cdots A_L\}, \end{aligned} \quad (2.38)$$

where

$$A_j = \begin{pmatrix} |\Downarrow\rangle & (-1)^{j+1} \beta |\Uparrow\rangle \\ \beta |\Uparrow\rangle & 0 \end{pmatrix}_j. \quad (2.39)$$

Then, by focusing on three consecutive sites, we obtain

$$A_{2j-1} A_{2j} A_{2j+1} = \begin{pmatrix} |\Downarrow\Downarrow\Downarrow\rangle - \beta^2(|\Downarrow\Uparrow\Uparrow\rangle - |\Uparrow\Uparrow\Downarrow\rangle) & \beta|\Downarrow\Downarrow\Uparrow\rangle + \beta^3|\Uparrow\Uparrow\Uparrow\rangle \\ \beta|\Uparrow\Downarrow\Downarrow\rangle - \beta^3|\Uparrow\Uparrow\Uparrow\rangle & \beta^2|\Uparrow\Downarrow\Uparrow\rangle \end{pmatrix}_{2j-1, 2j, 2j+1}. \quad (2.40)$$

This matrix form implies that the coherent states are orthogonal to $|\downarrow\uparrow\downarrow\rangle$ and $(|\downarrow\uparrow\uparrow\rangle + |\uparrow\uparrow\downarrow\rangle)/\sqrt{2}$. Therefore, the perturbation term

$$\begin{aligned}
 H_{\text{pert}} = \sum_{j=1}^L \Big\{ & c_j^{(1)} |\downarrow\uparrow\downarrow\rangle\langle\downarrow\uparrow\downarrow| \\
 & + \frac{c_j^{(2)}}{2} (|\downarrow\uparrow\uparrow\rangle + |\uparrow\uparrow\downarrow\rangle)(\langle\downarrow\uparrow\uparrow| + \langle\uparrow\uparrow\downarrow|) \\
 & + c_j^{(3)} [|\downarrow\uparrow\downarrow\rangle (\langle\downarrow\uparrow\uparrow| + \langle\uparrow\uparrow\downarrow|) + (|\downarrow\uparrow\uparrow\rangle + |\uparrow\uparrow\downarrow\rangle) \langle\downarrow\uparrow\downarrow|] \Big\}_{j-1, j+1}
 \end{aligned} \tag{2.41}$$

is suitable for (2.32) in the sense that it keeps the states $(Q^+)^n |\downarrow\rangle$ as eigenstates of the given Hamiltonian. In addition, we can verify that its level-spacing statistics in the middle of the spectrum obey the Wigner-Dyson GOE distribution, which implies that this model is nonintegrable. Therefore, the states $(Q^+)^n |\downarrow\rangle$ are left behind as nonthermal eigenstates, that is, these states become QMBS.

2.3.3 Restricted Spectrum Generating Algebra

Restricted spectrum generating algebra (RSGA) [92, 93] is regarded as one of the standard methods to construct systems with QMBS³. It allows for the construction of many systems with QMBS, such as spin-chain models [96–98], η -pairing scars in the Hubbard-type models [93, 99, 100], the Affleck-Kennedy-Lieb-Tasaki (AKLT)-based models [101, 102]. RSGA is a natural extension of the concept called *spectrum generating algebra* or *dynamical symmetry* [103–106], and it is formalized as follows: Suppose that we have a Hamiltonian H and an operator Q^\dagger . In addition, we assume that there exists a nontrivial invariant subspace of Q^\dagger , denoting W , such that $Q^\dagger W \subset W$ and it satisfies

$$([H, Q^\dagger] - \omega Q^\dagger)W = 0. \tag{2.42}$$

Then, when we pick an eigenstate of H with eigenenergy E from W , denoting $|\Psi_0\rangle \in W$, $(Q^\dagger)^n |\Psi_0\rangle$ is also an eigenstate of H with eigenenergy $E + n\omega$. In this situation, the operator Q^\dagger is not associated with any symmetry of H . Hence, the states $(Q^\dagger)^n |\Psi_0\rangle$ will be good candidates for QMBS.

As an example, we consider the spin-1 Affleck-Lieb-Kennedy-Tasaki (AKLT) Hamiltonian [107–109]:

$$H_{\text{AKLT}} = \sum_{j=1}^L \left[\frac{1}{2} \mathbf{S}_j \cdot \mathbf{S}_{j+1} + \frac{1}{6} (\mathbf{S}_j \cdot \mathbf{S}_{j+1})^2 + \frac{1}{3} \right]. \tag{2.43}$$

³Remarkably, the concept of RSGA was introduced in the context of ground states [94, 95] before used in the construction of QMBS.

The AKLT Hamiltonian can be regarded as the sum of the projection operators onto the spin 2 states of neighboring spins, namely,

$$H_{\text{AKLT}} = \sum_{j=1}^L P_{j,j+1}^{S=2} = \sum_{j=1}^L \left(\sum_{M=-2}^2 |T_{2,M}\rangle \langle T_{2,M}| \right)_{j,j+1}, \quad (2.44)$$

where $P_{j,j+1}^{S=2}$ denotes the projection operator of two spin-1 spins living on site j and $j+1$ onto the subspace with total spin 2, and $|T_{J,M}\rangle$ denotes a two-site state with total spin J and z component M . The ground state of H_{AKLT} is known as the valence bond solid (VBS) state [108]. It takes the form of a matrix product state (MPS) [110, 111]:

$$|\Psi_{\text{VBS}}\rangle = \sum_{\{s\}} \text{Tr}[A^{s_1} A^{s_2} \cdots A^{s_L}] |s_1, s_2, \dots, s_L\rangle, \quad (2.45)$$

where $s_j \in \{+, 0, -\}$ denotes the spin state at site j and

$$A^+ = \sqrt{\frac{2}{3}}\sigma^+, A^0 = -\sqrt{\frac{1}{3}}\sigma^z, A^- = -\sqrt{\frac{2}{3}}\sigma^-, \quad (2.46)$$

with $\sigma^\pm = (\sigma^x \pm i\sigma^y)/2$ and σ^z being the Pauli matrices. The summation is taken over all possible spin configurations.

In this setup, the low-entanglement scar states $|\mathcal{S}_{2n}\rangle$ can be found as

$$|\mathcal{S}_{2n}\rangle = (\mathcal{Q}_\pi^+)^n |\Psi_{\text{VBS}}\rangle, \quad (2.47)$$

where

$$\mathcal{Q}_\pi^+ = \sum_{j=1}^L (-1)^j (S_j^+)^2. \quad (2.48)$$

Here, the subscript π means the momentum carried by the operator (\rightarrow see Chapter 3). This operator satisfies the following relation [92]:

$$[H_{\text{AKLT}}, \mathcal{Q}_\pi^+] |\mathcal{S}_{2n}\rangle = 2\mathcal{Q}_\pi^+ |\mathcal{S}_{2n}\rangle, \quad (2.49)$$

which implies that $|\mathcal{S}_{2n}\rangle$ is an eigenstate of H_{AKLT} with eigenenergy $2n$. To verify this formula, we have to show the following:

$$[H_{\text{AKLT}}, \mathcal{Q}_\pi^+] = 2\mathcal{Q}_\pi^+ + A, \quad A |\mathcal{S}_{2n}\rangle = 0. \quad (2.50)$$

We first note that

$$[H_{\text{AKLT}}, \mathcal{Q}_\pi^+] = \sum_{j=1}^L (-1)^j [P_{j,j+1}^{S=2}, (S_j^+)^2 - (S_{j+1}^+)^2]. \quad (2.51)$$

We express the factors appearing on the right-hand side in terms of the basis states $|T_{J,M}\rangle$:

$$\begin{aligned} [P_{j,j+1}^{S=2}, (S_j^+)^2 - (S_{j+1}^+)^2] &= -2(|T_{2,1}\rangle \langle T_{1,-1}| + \sqrt{2}|T_{2,2}\rangle \langle T_{1,0}| + |T_{1,1}\rangle \langle T_{2,-1}| + \sqrt{2}|T_{1,1}\rangle \langle T_{2,-2}|)_{j,j+1} \\ &= (S_j^+)^2 - (S_{j+1}^+)^2 - 4(|T_{1,1}\rangle \langle T_{2,-1}| - \sqrt{2}|T_{1,0}\rangle \langle T_{2,-2}|)_{j,j+1}. \end{aligned} \quad (2.52)$$

To show Eq. (2.50), it is sufficient to check $\langle T_{2,-1} | \mathcal{S}_{2n} \rangle_{j,j+1} = \langle T_{2,-2} | \mathcal{S}_{2n} \rangle_{j,j+1} = 0$. It can be obtained as follows: Since the VBS state is a zero-energy eigenstate of $H_{\text{AKLT}} = \sum_j P_{j,j+1}^{S=2}$, $|\Psi_{\text{VBS}}\rangle_{j,j+1}$ can be expressed as a superposition of $|T_{1,1}\rangle_{j,j+1}$, $|T_{1,0}\rangle_{j,j+1}$, $|T_{1,-1}\rangle_{j,j+1}$ and $|T_{0,0}\rangle_{j,j+1}$. Thus, since $|\mathcal{S}_{2n}\rangle_{j,j+1}$ can be expressed using a polynomial $f_n(\cdot)$ as $f_n((S_j^+)^2 - (S_{j+1}^+)^2) |\Psi_{\text{VBS}}\rangle_{j,j+1}$, the only component with $S_j^z + S_{j+1}^z \leq -1$ in $|\mathcal{S}_{2n}\rangle$ is $|T_{1,-1}\rangle_{j,j+1}$. Therefore, $\langle T_{2,-1} | \mathcal{S}_{2n} \rangle_{j,j+1} = \langle T_{2,-2} | \mathcal{S}_{2n} \rangle_{j,j+1} = 0$ and the states $|\mathcal{S}_{2n}\rangle$ are eigenstates of the AKLT Hamiltonian with eigenenergy $2n$. Moreover, these states have sub-volume entanglement entropy [101], which implies that these states are QMBS in this system.

We can generalize this discussion to the following Hamiltonian [92]

$$H_{\text{new}} = \sum_{j=1}^L P_{j,j+1}^{S=2} + (a |T_{2,-2}\rangle\langle T_{2,-2}| + b |T_{2,-1}\rangle\langle T_{2,-2}| + c |T_{2,0}\rangle\langle T_{2,-2}| + d |T_{2,-1}\rangle\langle T_{2,-1}| + e |T_{2,0}\rangle\langle T_{2,-1}| + f |T_{2,0}\rangle\langle T_{2,0}| + \text{H.c.})_{j,j+1}, \quad (2.53)$$

where $a, d, f \in \mathbb{R}$ and $b, c, e \in \mathbb{C}$ are arbitrary constants. The states $|\mathcal{S}_{2n}\rangle$ are also eigenstates of this Hamiltonian. In addition, Ref. [111] shows that the level-spacing of the AKLT Hamiltonian obeys the Wigner-Dyson distribution, which implies it is nonintegrable. It means that $|\mathcal{S}_{2n}\rangle$ are QMBS in the Hamiltonian H_{new} . In addition, it can be extended to general integer spin- s AKLT models. References [92, 101] provide detailed calculations for the case $s = 2$ as an example.

2.4 Summary of the Chapter

In this chapter, we have introduced another class of systems that violate ETH, and we call their nonthermal states Quantum Many-Body Scars (QMBS). QMBS was first discovered in an experiment using the Rydberg atom simulator. Its effective Hamiltonian, that is, the PXP model, exhibits persistent oscillations for the Néel initial state for a long time. Theoretical and numerical analysis has shown that there exists a structure that effectively holds several states, including the Néel state, within the subspace spanned by these states under time evolution.

We also introduced several methods to construct models with QMBS, namely, the Shiraishi-Mori embedding, the Onsager algebra, and restricted spectrum generating algebra. These methods reproduce the characteristic features of QMBS, a few specific non-thermal states isolated from the rest of the states in the Hilbert space.

CONSTRUCTION OF SCARRED MODELS RELATED TO THE SPIN-1 SCALAR SPIN CHIRALITY

In this chapter, based on our work [112], we discuss the construction of QMBS with the existing method using restricted spectrum generating algebra (RSGA) in spin systems with multibody interactions. Specifically, we construct scarred models from a three-body interaction called spin-1 scalar spin chirality.

3.1 Spin-1 scalar spin chirality in one dimension

The scalar spin chirality corresponds to a solid angle subtended by the three neighboring spins [113–115]. The explicit form of spin-1 scalar spin chirality term in one dimension is

$$C_{\text{SC}} = \sum_{j=1}^L \mathbf{S}_j \cdot (\mathbf{S}_{j+1} \times \mathbf{S}_{j+2}), \quad (3.1)$$

where $\mathbf{S}_j := (S_j^x, S_j^y, S_j^z)$ is the spin-1 operators acting on site j . In components, they read

$$S_j^x = \frac{1}{\sqrt{2}} \begin{pmatrix} 0 & 1 & 0 \\ 1 & 0 & 1 \\ 0 & 1 & 0 \end{pmatrix}_j, \quad S_j^y = \frac{1}{\sqrt{2}} \begin{pmatrix} 0 & -i & 0 \\ i & 0 & -i \\ 0 & i & 0 \end{pmatrix}_j, \quad S_j^z = \begin{pmatrix} 1 & 0 & 0 \\ 0 & 0 & 0 \\ 0 & 0 & -1 \end{pmatrix}_j. \quad (3.2)$$

The quantity C_{SC} is not integrable, but it has a number of symmetries, like SU(2), translation, and parity-reflection (\mathcal{PT}) symmetries. Therefore, a large number of degeneracies remain. We label the following zero-energy eigenstates of C_{SC} : Let us introduce the reference states $|\uparrow\rangle := |++\cdots+\rangle$, $|0\rangle := |00\cdots 0\rangle$, and $|\downarrow\rangle := |--\cdots-\rangle$, where $|+\rangle$, $|0\rangle$, and $|-\rangle$ are the S^z basis states such that $S^z |\mu\rangle = \mu |\mu\rangle$ ($\mu = +, 0, \text{ or } -$). Then, we introduce two

kinds of ladder operators

$$\mathcal{O}_k^- = \sum_{j=1}^L e^{ikj} S_j^-, \quad \mathcal{Q}_k^- = \sum_{j=1}^L e^{ikj} (S_j^-)^2, \quad (3.3)$$

where k denotes the momentum they carry. Fortunately, we can find several series of zero-energy eigenstates of C_{SC} by acting with ladder operators \mathcal{O}_k^- or \mathcal{Q}_k^- on $|\uparrow\rangle$ and $|0\rangle$. We found that the following states are the zero-energy states of C_{SC} :

$$|A_{m,n}\rangle := (\mathcal{O}_0^-)^m (\mathcal{O}_\pi^-)^n |\uparrow\rangle \quad (0 \leq m+n \leq 2L), \quad (3.4)$$

$$|B_{m,n}\rangle := (\mathcal{O}_0^-)^m (\mathcal{Q}_0^-)^n |\uparrow\rangle \quad (n \geq 1, 1 \leq m \leq 2L-2n). \quad (3.5)$$

Note that $|A_{m,n}\rangle$ are well defined only for even length of the lattice L . To see that the above states are zero-energy states of C_{SC} , it is sufficient to consider the case $m=0$. This is because the operator \mathcal{O}_0^- is exactly the spin-lowering operator $\mathcal{S}^- = \sum_{j=1}^L S_j^-$ commuting with C_{SC} due to the $\text{SU}(2)$ symmetry. For convenience, we introduce the notation $|\bar{A}_n\rangle := |A_{0,n}\rangle$, $|\bar{B}_n\rangle := |B_{0,n}\rangle$ to denote the above states with $m=0$. One can prove that $|\bar{A}_n\rangle$ and $|\bar{B}_n\rangle$ are zero-energy eigenstates of C_{SC} by noting that C_{SC} and \mathcal{O}_π^- or \mathcal{Q}_0^- satisfy a restricted spectrum generating algebra of order 2 [93].

The towers of states $|A_{m,n}\rangle$ and $|B_{m,n}\rangle$ do not exhaust the zero-energy manifold of C_{SC} . In fact, there are other towers of zero-energy states generated by \mathcal{O}_p^- :

$$|+_m\rangle := (\mathcal{O}_0^+)^m |0\rangle, \quad (3.6)$$

$$|-_m\rangle := (\mathcal{O}_0^-)^m |0\rangle, \quad (3.7)$$

$$|K_{m,p}\rangle := (\mathcal{O}_0^-)^m \mathcal{O}_p^- \mathcal{O}_{-p}^- |\uparrow\rangle, \quad (3.8)$$

where $0 \leq m \leq 2L-2$ and $p = \frac{2\pi}{L}, \frac{4\pi}{L}, \dots, \frac{2\pi}{L}(\lfloor \frac{L}{2} \rfloor - 1)$. Again since \mathcal{O}_0^- commutes with C_{SC} , it suffices to consider the case $m=0$. It is easy to see that $|+_0\rangle = |-_0\rangle = |0\rangle$ is annihilated by each local term in C_{SC} , and hence $C_{\text{SC}} |\pm_m\rangle = 0$. To see that $C_{\text{SC}} |K_{m,p}\rangle = 0$, it is convenient to rewrite the state $|K_{0,p}\rangle$ as

$$|K_{0,p}\rangle = \sum_{n=1}^L e^{inp} |\Phi_n\rangle \quad (3.9)$$

where

$$|\Phi_n\rangle = \sum_{j=1}^L S_j^- S_{j+n}^- |\uparrow\rangle. \quad (3.10)$$

One can show that each $|\Phi_n\rangle$ is annihilated by C_{SC} . Therefore, it follows that $C_{\text{SC}} |K_{m,p}\rangle = 0$. See Appendix A.1 for a detailed proof.

In this way, we have constructed a number of exact zero-energy states of C_{SC} . It should be noted that they are exact eigenstates of $H_0(h) = C_{\text{SC}} + hS^z$ as well because each of them

is a superposition of states with fixed S^z . We also remark that the obtained states in Eqs. (3.4)-(3.8) are not orthogonal to each other. In fact, they are not even linearly independent. This can be seen by considering, for example, the $L = 3$ site chain. In this case, $|B_{1,1}\rangle$, $|B_{3,0}\rangle$, and $|+_0\rangle$ satisfy $3|B_{1,1}\rangle - |B_{3,0}\rangle + 12\sqrt{2}|+_0\rangle = 0$, and hence linearly dependent. In Appendix A.1, we derive a lower bound on the number of zero-energy states of C_{SC} , which proves that the number grows exponentially with the system size. Such an exponentially large degeneracy can be a source of QMBS and Hilbert space fragmentation, as discussed in the context of geometrically frustrated systems [116, 117].

In the following, we will consider $H_0(h) = C_{\text{SC}} + h \sum_{j=1}^L S_j^z$ under tailored disorder, which is designed such that some of the obtained zero-energy states of C_{SC} remain intact. In other words, we consider the scalar spin chirality C_{SC} as the unperturbed Hamiltonian, and we look for QMBS in the spectra of the Hamiltonian with anisotropic perturbation terms.

3.2 Random single-ion anisotropy — scarred $|\bar{B}_n\rangle$

In this section, we focus on the model in which $|\bar{B}_n\rangle$ become scars. We consider the Hamiltonian

$$H_1(h, \{D_j\}_j) = C_{\text{SC}} + h \sum_{j=1}^L S_j^z + \sum_{j=1}^L D_j (S_j^z)^2, \quad (3.11)$$

with the intensity of the magnetic field h and random real variables $\{D_j\}$. We imply periodic boundary conditions hence $S_{j+L} \equiv S_j$. In a later discussion, we omit the dependency of h and D_j unless we need to.

As we mentioned in Section 1.5.1, the level-spacing statistics is useful to determine whether the given Hamiltonian is non-integrable or not. Due to the randomness of D_j , the Hamiltonian H_1 has only two conserved quantities, that is, the total magnetization S^z and the spin-flip \mathcal{F} . Therefore, since this model does not have (pseudo-)time reversal symmetry, we expect that its level-spacing in each fixed $S^z = \sum_{j=1}^L S_j^z$ sector obeys the GUE Wigner-Dyson distribution if the model (3.11) is nonintegrable. Figure 3.1 shows the level spacing in the sector with $S^z = 0$ and $\mathcal{F} = 1$. We can see the level-spacing statistics is similar to the GUE Wigner-Dyson distribution rather than the Poisson distribution. In addition, its r -value $\langle r \rangle \simeq 0.593$ also supports that it belongs to the GUE class with $\langle r_{\text{GUE}} \rangle \simeq 0.603$.

On the other hand, we can show that each $|\bar{B}_n\rangle$ is an eigenstate of H_1 as follows. We already see that $|\bar{B}_n\rangle$ are simultaneous eigenstates of C_{SC} and S^z . To check $|\bar{B}_n\rangle$ are

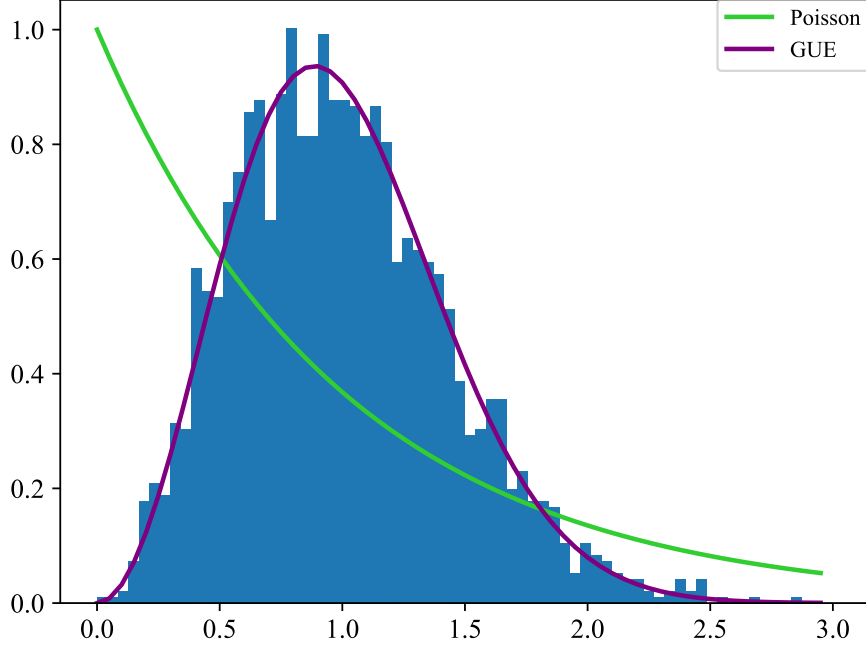


Figure 3.1: Level-spacing statistics in the middle half of the spectrum of $H_1(h, \{D_j\})$ (Eq. (3.11)) with $L = 10, h = 1$ in the sector $(S^z, \mathcal{F}) = (0, 1)$. The random constants D_j are chosen from $[-5, 5]$. The green and purple lines indicate the Poisson distribution $P_{\text{Poisson}}(s)$ and the GUE Wigner-Dyson distribution $P_{\text{GUE}}(s)$, respectively.

eigenstates of the D term, we expand it in the terms of the basis of S_j^z eigenstates:

$$|\bar{B}_0\rangle = |\uparrow\rangle = |++\cdots+\rangle, \quad (3.12)$$

\vdots

$$|\bar{B}_n\rangle = (\mathcal{Q}_0^-)^n |\uparrow\rangle = 2^n \times n! \sum_{1 \leq j_1 < j_2 < \cdots < j_n \leq L} |++\cdots-j_1 \cdots -j_2 \cdots -j_n \cdots+\rangle, \quad (3.13)$$

\vdots

$$|\bar{B}_L\rangle = 2^L \times L! |--\cdots-\rangle. \quad (3.14)$$

We can see that the basis vectors that appear in the summation consist of $|+\rangle$ or $|-\rangle$, and they do not contain $|0\rangle$. Thus, all of these basis vectors are eigenstates of $\sum_j D_j (S_j^z)^2$ with eigenvalue $\sum_j D_j$, hence it follows that $|\bar{B}_n\rangle$ are eigenstates of $\sum_j D_j (S_j^z)^2$ with eigenvalue $\sum_j D_j$. Therefore, we can conclude that each $|\bar{B}_n\rangle$ is an eigenstate of H_1 with eigenenergy $h(L - 2n) + \sum_j D_j$.

We can see these states are exceptions of ETH by calculating the half-chain entanglement entropy of each eigenstate of $H_1(h, \{D_j\})$. One can calculate the half-chain entanglement entropy of $|\bar{B}_n\rangle$ in the same way as the ferromagnetic states with spin-1/2. The

result reads

$$S_A(|\bar{B}_n\rangle) = - \sum_{k=0}^n \frac{\binom{L/2}{k} \binom{L/2}{n-k}}{\binom{L}{n}} \ln \frac{\binom{L/2}{k} \binom{L/2}{n-k}}{\binom{L}{n}}. \quad (3.15)$$

The state $|\bar{B}_{L/2}\rangle$ has the largest entanglement entropy in $\{|\bar{B}_n\rangle\}_{n=0,1,\dots,L}$, and the asymptotic form of $S_A(|\bar{B}_{L/2}\rangle)$ for $L \gg 1$ is given by

$$S_A(|\bar{B}_{L/2}\rangle) \approx \frac{1}{2} \left(\ln \frac{\pi L}{8} + 1 \right), \quad (3.16)$$

which obeys a sub-volume law. As seen in Figure 3.2, $|\bar{B}_n\rangle$ make a tower of low-entanglement states. However, we cannot perfectly separate low-entanglement states due to the degeneracies, especially, near $E = 0$. By checking the entanglement entropy with respect to each symmetry sector, we can clearly determine low-entanglement states. Figure 3.3 shows that $|\bar{B}_{L/2}\rangle$ has low-entanglement entropy in the sector with fixed quantum numbers $(S^z, \mathcal{F}) = (0, 1)$. We can regard this state as QMBS. Moreover, there are two other low-entanglement states, namely, $|0\rangle = |000 \cdots 0\rangle$ and $|\psi_s\rangle = \frac{1}{\sqrt{2}}(|+-+ - \cdots\rangle + |-+-+ \cdots\rangle)$. Whether these states are QMBS or not should be carefully considered. We consider that it is highly likely that $|\psi_s\rangle$ is a QMBS, while $|0\rangle$ is not. Because the projection on $|0\rangle$ is given as $\mathcal{P} = \prod_j (1 - (S_j^z)^2)$, and \mathcal{P} commutes to the Hamiltonian $H_1(t)$, it is natural to regard the state $|0\rangle$ as the state which is separated by symmetries rather than QMBS. Therefore, only $|\bar{B}_{L/2}\rangle$ and $|\psi_s\rangle$ are identified as QMBS.

3.2.1 Dynamics

To illustrate the nonthermal features of scarred states, we study the quench dynamics of the system. The initial states we consider are coherent states of \mathcal{Q}_0^- , namely superpositions of $|\bar{B}_n\rangle$ defined as

$$|\beta\rangle := C_L^{-1} \exp(\beta \mathcal{Q}_0^-) |\uparrow\rangle = C_L^{-1} \sum_{n=0}^L \frac{\beta^n}{n!} |\bar{B}_n\rangle, \quad (3.17)$$

where $\beta \in \mathbb{C}$ and $C_L := (1 + 4|\beta|^2)^{\frac{L}{2}}$ is a normalization factor such that $\langle\beta|\beta\rangle = 1$. Under time evolution by the Hamiltonian (3.11), the initial state $|\beta\rangle$ evolves into

$$|\beta(t)\rangle := e^{-iH_1 t} |\beta\rangle \quad (3.18)$$

at time t . Since the states $|\bar{B}_n\rangle$ are common eigenstates of the D term with eigenvalue $D = \sum_j D_j$, we can rewrite it as

$$|\beta(t)\rangle = e^{-iD t} e^{-i\mathcal{H} S^z t} |\beta\rangle. \quad (3.19)$$

We first consider the fidelity between initial and time-evolved states. For an arbitrary initial state $|\phi(0)\rangle$, it is defined by

$$\mathcal{F}(t) = |\langle\phi(0)|\phi(t)\rangle|, \quad (3.20)$$

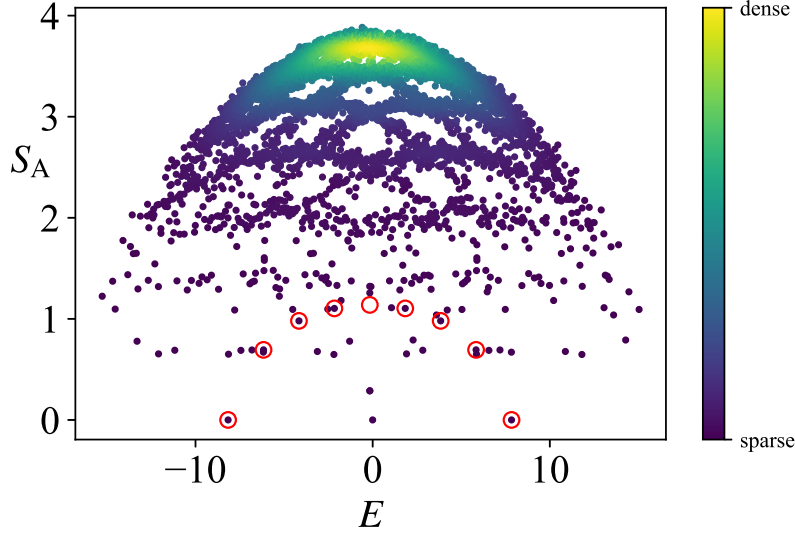


Figure 3.2: Entanglement entropies in all eigenstates of $H_1(h, \{D_j\})$ in Eq. (3.11) for $L = 8$ and $h = 1$. Each D_j is randomly chosen from $[-1, 1]$. The density of data points is color coded. The red circle corresponds to $|\bar{B}_n\rangle$ ($n = 0, 1, \dots, L$). We can see each $|\bar{B}_n\rangle$ is lying on the low-entanglement area. However, because of the existence of degeneracies, we cannot determine these are only

where $|\phi(t)\rangle = e^{-iH_1 t} |\phi(0)\rangle$. For the coherent states $|\beta\rangle$, we can calculate the fidelity as

$$\begin{aligned}
 \mathcal{F}(t) &= C_L^{-2} \left| \sum_{m,n=0}^L \frac{(\beta^*)^m \beta^n}{m!n!} \langle \bar{B}_m | e^{-ihS^z t} | \bar{B}_n \rangle \right| \\
 &= C_L^{-2} \left| \sum_{n=0}^L \frac{|\beta|^{2n}}{(n!)^2} e^{2ihnt} \langle \bar{B}_n | \bar{B}_n \rangle \right| \\
 &= C_L^{-2} \left| \sum_{n=0}^L (4|\beta|^2 e^{2iht})^n \binom{L}{n} \right| \\
 &= \left| \frac{1 + 4|\beta|^2 e^{2iht}}{1 + 4|\beta|^2} \right|^L.
 \end{aligned} \tag{3.21}$$

Clearly, it is a periodic function with period $T = \pi/h$, exhibiting perfect revivals, that is, $\mathcal{F}(t) = 1$ at $t = nT$ ($n \in \mathbb{N}$), irrespective of the system size. We show in Figure 3.4 the numerical results of the fidelity dynamics with several initial states. As we can see, the coherent states show perfectly periodic revivals, indicating that they never thermalize. This is in stark contrast to the fidelity of a generic state, which decays rapidly to zero. We note that a perfect revival of the initial state after a time of at most $\mathcal{O}(\text{poly}(L))$, in general, implies the existence of QMBS [118].

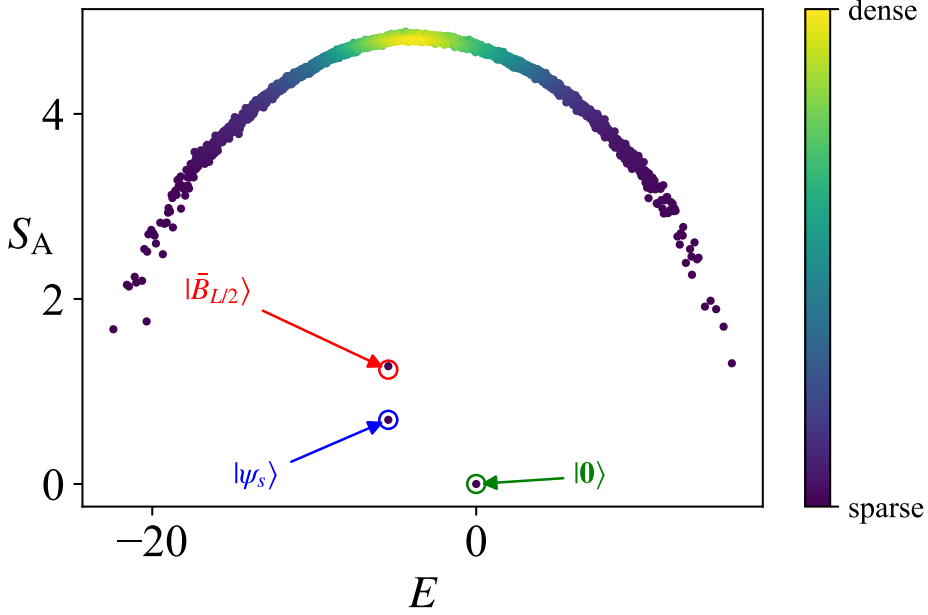


Figure 3.3: Entanglement entropies in all eigenstates of $H_1(h, \{D_j\})$ in Eq. (3.11) for $L = 10$, $h = 1$ in the symmetry sector $(S^z, \mathcal{F}) = (0, 1)$. Each D_j is randomly chosen from $[-5, 5]$. The density of data points is color coded. The entanglement entropy of each state obeys a volume-law except for $|\bar{B}_{L/2}\rangle$, the symmetric state $|\psi_s\rangle = |+-+ \dots\rangle + |-+-+ \dots\rangle$, and the trivial state $|0\rangle = |00 \dots 0\rangle$. The orange dotted line indicates $S_A = 1.236$, which is obtained from Eq. (3.15) for $L = 10$.

We next examine the time evolution of the half-chain entanglement entropy for several initial states. In the following, we consider the case of even L . The half-chain entanglement entropy of the coherent state $|\beta(t)\rangle$ does not evolve in time. In fact, it is always 0. This can be seen by noting that $|\beta(t)\rangle$ is just a product of two states:

$$|\beta(t)\rangle = e^{-i\mathcal{D}t} e^{-ihS_A^z t} |\beta\rangle_A \otimes e^{-ihS_B^z t} |\beta\rangle_B, \quad (3.22)$$

where $S_{A(B)}^z = \sum_{j \in A(B)} S_j^z$ and

$$|\beta\rangle_{A(B)} := C_{L/2}^{-1} \exp\left(\beta \sum_{j \in A(B)} (S_j^-)^2\right) |\uparrow\rangle_{A(B)} \quad (3.23)$$

with $|\uparrow\rangle_{A(B)} = \otimes_{j \in A(B)} |+\rangle_j$. Let us slightly generalize the initial state by considering a superposition of coherent states with different β , namely, $\sum_{i=1}^n c_i |\beta_i\rangle$. Since $|\beta_i\rangle_L = |\beta_i\rangle_A \otimes |\beta_i\rangle_B$, the entanglement entropy is obtained as [119, 120]

$$S_A = -\frac{\text{Tr}[M^2 \ln M^2]}{\text{Tr}[M^2]} + \ln \text{Tr}[M^2], \quad (3.24)$$

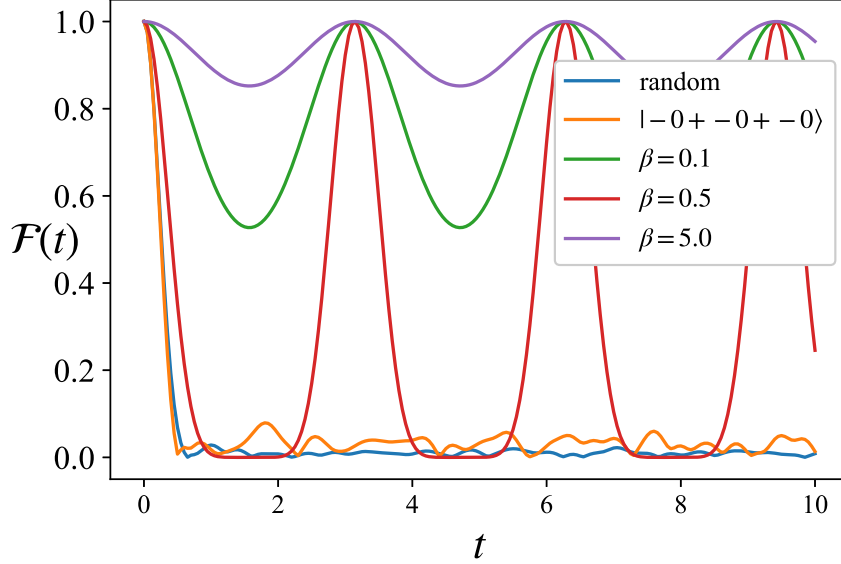


Figure 3.4: The dynamics of the fidelity with $L = 8$, $h = 1$, and D_j ($j = 1, 2, \dots, L$) chosen randomly from $[-1, 1]$. Perfectly periodic revivals can be seen when the initial state is a coherent state, whereas for other generic states the fidelity decays rapidly to zero.

where the matrix elements of M are defined as

$$M_{i,j} = c_i^* c_j \langle \beta_i | \beta_j \rangle_A = \frac{c_i^* c_j (1 + 4\beta_i^* \beta_j)^N}{(1 + 4|\beta_i|^2)^{\frac{N}{2}} (1 + 4|\beta_j|^2)^{\frac{N}{2}}}. \quad (3.25)$$

It is then clear that the entanglement entropy for this class of states is constant in time.

Figure 3.5 shows the time evolution of the half-chain entanglement entropy S_A for several initial states. Clearly, the coherent states and their superposition do not gain entanglement. By contrast, S_A of the product state $|-0+ -0+ -0\rangle$ grows rapidly and saturates near the Page value [58] of a random state

$$S_{\text{Page}} = \frac{L}{2} \ln 3 - \frac{1}{2}. \quad (3.26)$$

3.2.2 Extension for Higher Dimensional Lattices

Here, we consider the generalization of the model H_1 in Eq. (3.11) on a triangular lattice with periodic boundary conditions (Fig. 3.6). Let Λ be the triangular lattice. The Hamiltonian is

$$H_1^{2d}(h, \{D_j\}_j) = C_{\text{SC}}^{2d} + h \sum_{j \in \Lambda} S_j^z + \sum_{j \in \Lambda} D_j (S_j^z)^2, \quad (3.27)$$

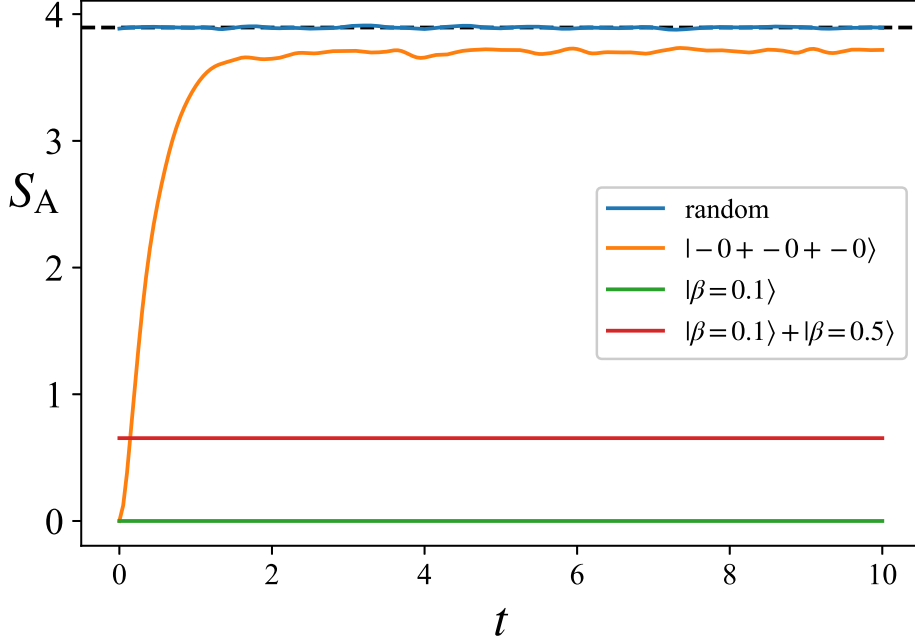


Figure 3.5: Dynamics of the half-chain entanglement entropies with the same setup as Figure 3.4. The dashed line indicates the Page value S_{page} (Eq. (3.26)). Initial coherent states have constant entanglement entropy, but that of $|-0+ -0+ -0\rangle$ rapidly grows and saturates near S_{Page} .

where

$$C_{\text{SC}}^{2\text{d}} = \sum_{\Delta/\nabla} \mathbf{S}_j \cdot (\mathbf{S}_k \times \mathbf{S}_l), \quad (3.28)$$

and the summation is over all triangles. The subscripts j, k , and l are in the clockwise (counterclockwise) order in each upward (downward) triangle.

Analogously to the states $|\bar{B}_n\rangle$ in Eq. (3.13), one can define the following states:

$$|\Psi_n\rangle = (\mathcal{Q}_0^-)^n |\uparrow\uparrow\rangle = \left(\sum_{j \in \Lambda} (S_j^-)^2 \right)^n |\uparrow\uparrow\rangle. \quad (3.29)$$

Since \mathcal{Q}_0^- can be decomposed into $\mathcal{Q}_0^- = Q_X + Q_{\Lambda \setminus X}$ with $Q_X := \sum_{i \in X} (S_i^-)^2$ and $Q_{\Lambda \setminus X} := \mathcal{Q}_0^- - Q_X$ for any $X = \{j, k, l\}$ forming an upward or downward triangle, we obtain

$$|\Psi_n\rangle = \sum_{p=0}^n \binom{n}{p} (Q_X)^p |+++\rangle_X \otimes (Q_{\Lambda \setminus X})^{n-p} |++ \cdots +\rangle_{\Lambda \setminus X}. \quad (3.30)$$

Then, one can show that $\mathbf{S}_j \cdot (\mathbf{S}_k \times \mathbf{S}_l) (Q_X)^p |+++\rangle_X = 0$ for any X and p in the same way as in the one-dimensional case. Therefore, $|\Psi_n\rangle$ is an eigenstate of $C_{\text{SC}}^{2\text{d}}$ with eigenvalue 0. Furthermore, since $D_j(S_j)^2$ acts only on one site, $D_j(S_j)^2 |\Psi_n\rangle = D_j |\Psi_n\rangle$ can be shown

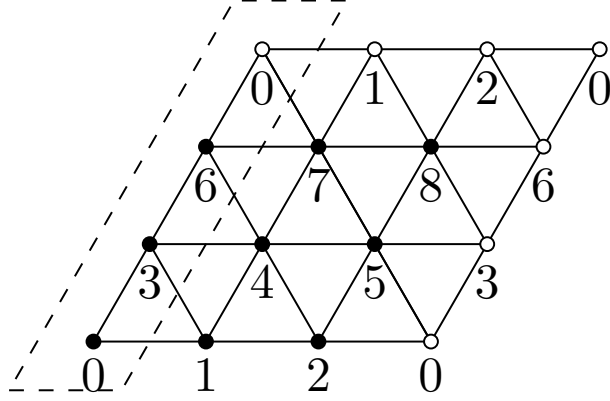


Figure 3.6: An example of the triangular lattice. The integers denote the site indices, and the black and white sites with the same index are identified by the periodic boundary conditions. We take the subsystem A to be the set of sites enclosed by the dashed lines, which is used to calculate the entanglement entropy

in the same way as in the one-dimensional case. Therefore, each $|\Psi_n\rangle$ is an eigenstate of H_1^{2d} in Eq. (3.27) with eigenvalue $h(|\Lambda| - 2n) + \sum_{j=1}^L D_j$, where by $|\Lambda|$ we denote the total number of sites in Λ .

To see whether $|\Psi_n\rangle$ are QMBS, we calculate entanglement entropies in all eigenstates of H_1^{2d} in the symmetry sector with $S^z = 1$. In the calculation, we take the subsystem A to be $\{0, 3, 6\}$ (see Fig. 3.6 for the site labels). As shown in Fig. 3.7, the state $|\Psi_{n=4}\rangle$ has significantly lower entanglement entropy than the other states, indicating that this state is a scar state. We have also checked numerically that the entanglement entropy of $|\Psi_n\rangle$ is extremely low regardless of the choice of the subsystem A .

Note that we can expand it to the model on any graph Λ because the operator \mathcal{Q}_0^- is symmetric under any permutation of sites. Let $\Lambda = (V, E)$ be a graph and we assume the Hamiltonian is

$$H^\Lambda = C_{\text{SC}}^\Lambda + h \sum_{v \in V} S_v^z + \sum_{v \in V} D_v (S_v^z)^2, \quad (3.31)$$

where

$$C_{\text{SC}}^\Lambda = \sum_{\langle ij \rangle, \langle jk \rangle \in E} J_{ijk} \mathbf{S}_i \cdot (\mathbf{S}_j \times \mathbf{S}_k), \quad (3.32)$$

with $J_{ijk} \in \mathbb{R}$ being an arbitrary constant.

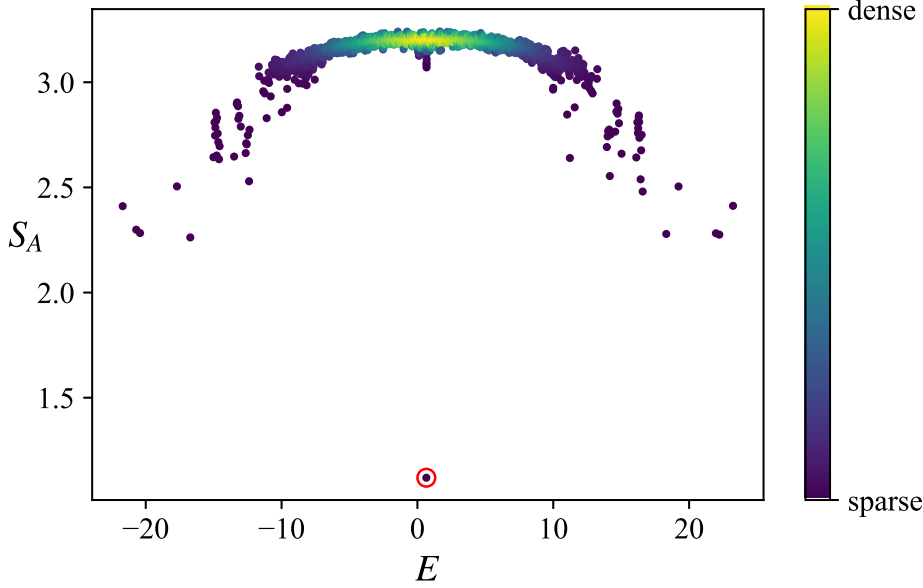


Figure 3.7: Entanglement entropies in all eigenstates of $H_1^{2d}(h, \{D_j\})$ in Eq. (3.27) for $L = 9, h = 1$ in the symmetry sector $S^z = 1$. Each D_j is randomly chosen from $[-1, 1]$. The density of data points is color-coded. The red circle indicate the scar state $|\Psi_{n=4}\rangle$.

3.3 Scarred $|\bar{A}_n\rangle$

3.3.1 Tower of eigenstates

As we have seen in the previous subsection, the key to finding a suitable perturbation is to find an operator that acts on a set of target states as a constant. To find such an operator for $|\bar{A}_n\rangle$, let us take a closer look at these states. The operator \mathcal{O}_π^- that generates $|\bar{A}_n\rangle$ is invariant under translation by two sites. Therefore, considering its action on the two neighboring sites may suggest a suitable operator. The operator \mathcal{O}_π^- acts as $S_j^- - S_{j+1}^-$ at the two neighboring sites $(j, j+1)$, and as a result, we get the states listed in Table 3.1 by repeatedly applying it to the state $|++\rangle_{j,j+1}$.

n	state	$S_j^z + S_{j+1}^z$	$P_{j,j+1}$
0	$ ++\rangle$	2	1
1	$ 0+\rangle - +0\rangle$	1	-1
2	$ -+\rangle - 2 00\rangle + +-\rangle$	0	1
3	$ 0-\rangle - -0\rangle$	-1	-1
4	$ --\rangle$	-2	1

Table 3.1: The explicit form of $(S_j^- - S_{j+1}^-)^n |++\rangle_{j,j+1}$ up to constant factors. The third and fourth columns indicate the eigenvalues of the corresponding operators for each state.

Each state in the table is a simultaneous eigenstate of $S_j^z + S_{j+1}^z$ and $P_{j,j+1}$, the permu-

tation operator between site j and $j+1$. From this result, we see that $(-1)^{S_j^z + S_{j+1}^z} P_{j,j+1} = 1$ holds in the subspace spanned by these states. Therefore, each $|\bar{A}_n\rangle$ is an eigenstate of the following Hamiltonian:

$$H_2(h, \{D_j\}_j) = C_{\text{SC}} + h \sum_{j=1}^L S_j^z + \sum_{j=1}^L D_j (-1)^{S_j^z + S_{j+1}^z} P_{j,j+1}, \quad (3.33)$$

where D_j are any real numbers. One can, in principle, construct a more complicated Hamiltonian involving more than two-spin interactions using the same strategy.

In what follows, we assume that the number of sites L is even and omit the dependence of H_2 on h and D_j unless necessary. Interestingly, the states $|\bar{B}_n\rangle$ are also eigenstates of H_2 since $|\bar{B}_n\rangle$ is totally symmetric, i.e., $P_{i,j} |\bar{B}_n\rangle = |\bar{B}_n\rangle$ for any i, j and $S_j^z + S_{j+1}^z$ is even for any j . We can see from Figure 3.8a that the states $|\bar{A}_n\rangle$ behave as QMBS in this system. On the other hand, the data points for the states $|\bar{B}_n\rangle$ are mostly missing due to the degeneracies.

Since the last term in Eq. (3.33) does not break the $U(1)$ symmetry associated with S^z , we can divide the Hilbert space into subspaces according to the eigenvalues of S^z . The $S^z = 0$ subspace can be further decomposed into two sectors with opposite \mathcal{F} . We have analyzed the level-spacing statistics in the sector $(S^z, \mathcal{F}) = (0, 1)$ and found that the distribution is close to the GUE Wigner-Dyson distribution. We also calculated the r -value and obtained $\langle r \rangle \simeq 0.593$, which is consistent with the GUE.

Figure 3.8b shows the entanglement entropies of eigenstates of H_2 in the sector $S^z = 0$. In the figure, both $|\bar{A}_L\rangle$ and $|\bar{B}_{L/2}\rangle$ can be identified as entanglement outliers, which leads us to the conclusion that $|\bar{B}_n\rangle$ are also QMBS for H_2 . It should be noted that another entanglement outlier, i.e., $|0\rangle = |000\cdots\rangle$ in Figure 3.8b, cannot be thought of as a scar. This is because the projection onto this state, namely $\mathcal{P} = \prod_{j=1}^L (1 - (S_j^z)^2)$, commutes with H_2 , which simply means that this state is uniquely specified by the eigenvalue 1 of \mathcal{P} .

3.3.2 Dynamics

Similarly to the previous section, we introduce a coherent state of \mathcal{O}_π , namely a superposition of $|\bar{A}_n\rangle$ defined by

$$|\alpha\rangle = \tilde{C}_L^{-1} \exp(\alpha \mathcal{O}_\pi^-) |\uparrow\rangle = \tilde{C}_L^{-1} \sum_{n=0}^{2L} \frac{\alpha^n}{n!} |\bar{A}_n\rangle, \quad (3.34)$$

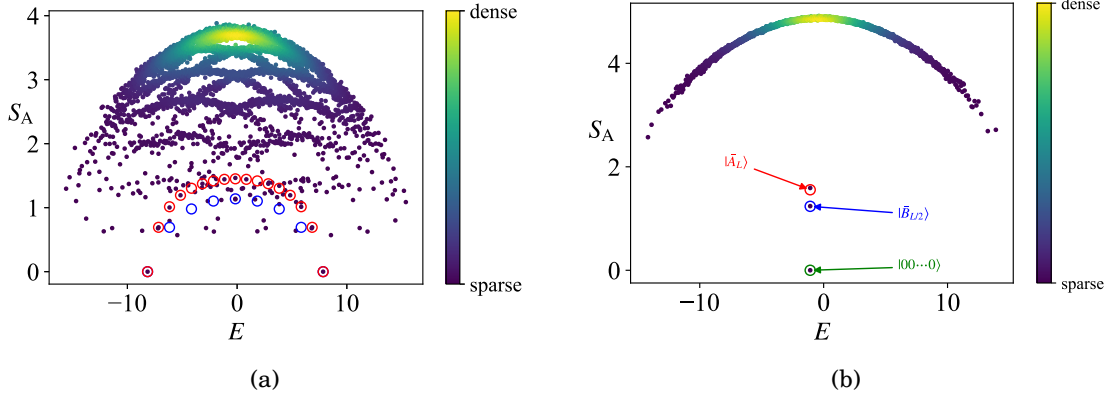


Figure 3.8: (a) Entanglement entropies in all eigenstates in Eq. (3.33) with $L = 10, h = 1$. Each D_j is randomly chosen from $[-1, 1]$. The density of data points is color coded. The states $|\bar{A}_n\rangle$ (red circles) and $|\bar{B}_n\rangle$ (blue circles) have relatively low entanglement entropy. Note that although $|\bar{A}_n\rangle$ and $|\bar{B}_n\rangle$ are eigenstates of $H_2(h, \{D_j\}_j)$, some circles do not overlap with corresponding data points because of degeneracies. (b) Entanglement entropies in all eigenstates of inhomogeneous model Eq. (3.33) for $L = 10, h = 1$ in the symmetry sector $S^z = 0$. Each D_j is randomly chosen from $[-1, 1]$. The density of data points is color coded. The red, blue and green circles indicate $|\bar{A}_L\rangle$, $|\bar{B}_{L/2}\rangle$, and $|0\rangle$, respectively.

where $\tilde{C}_L = (1 + |\alpha|^2)^L$ is the normalization constant. When the initial state is the coherent state $|\alpha\rangle$, the fidelity defined in Eq. (3.20) can be computed as

$$\begin{aligned}
 \mathcal{F}(t) &= \tilde{C}_L^{-2} \left| \sum_{m,n=0}^{2L} \frac{\alpha^{*m} \alpha^n}{m!n!} \langle \bar{A}_m | e^{-iH_2 t} | \bar{A}_n \rangle \right| \\
 &= \tilde{C}_L^{-2} \left| \sum_{n=0}^{2L} \frac{|\alpha|^{2n}}{(n!)^2} e^{iht} \langle \bar{A}_n | \bar{A}_n \rangle \right| \\
 &= \tilde{C}_L^{-2} \left| \sum_{n=0}^{2L} (|\alpha|^2 e^{iht})^n \binom{2L}{n} \right| \\
 &= \left| \frac{1 + |\alpha|^2 e^{iht}}{1 + |\alpha|^2} \right|^{2L}.
 \end{aligned} \tag{3.35}$$

Thus, it attains the maximum fidelity $\mathcal{F}(t) = 1$ periodically with period $T = 2\pi/h$. Figure 3.9 shows the numerical results of the fidelity dynamics with several initial states. Here we set $h = 1$. Clearly, the coherent states attain $\mathcal{F}(t) = 1$ periodically with period 2π , whereas the fidelities of the other states decay rapidly to zero. We also calculated the time evolution of the entanglement entropy for these states and obtained a result similar to that shown in Figure 3.5.

Moreover, since the Hamiltonian (3.33) has two families of QMBS, namely $|\bar{A}_n\rangle$ and $|\bar{B}_n\rangle$, we can consider the dynamics of the superposition of two coherent states. To be

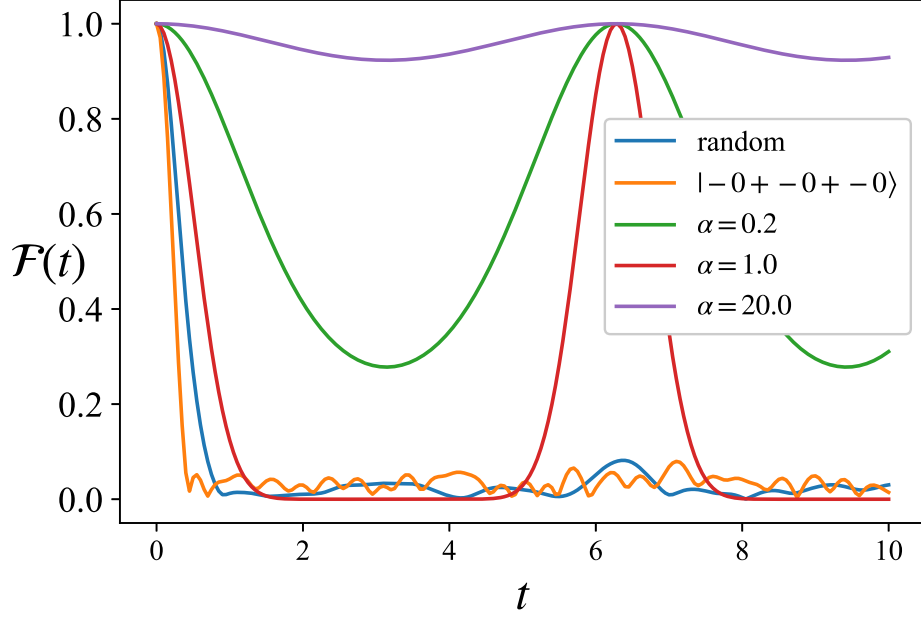


Figure 3.9: The dynamics of the fidelity with $h = 1$, $L = 8$, and D_j ($j = 1, 2, \dots, L$) chosen randomly from $[-1, 1]$. The fidelity shows perfectly periodic revivals when the initial state is a coherent state, whereas it decays rapidly to zero for other generic states.

specific, let us consider the following superposition of $|\alpha\rangle$ and $|\beta\rangle$:

$$|\xi\rangle = \frac{1}{Z}(u|\alpha\rangle + v|\beta\rangle), \quad (3.36)$$

where $u, v \in \mathbb{C}$ are arbitrary constants and Z is the normalization constant. The fidelity between $|\xi\rangle$ and the time evolved state $|\xi(t)\rangle = e^{-iH_2t}|\xi\rangle$ can be expressed as

$$\mathcal{F}(t) = |\langle \xi | \xi(t) \rangle| = \frac{1}{Z^2} \left| |u|^2 \langle \alpha | \alpha(t) \rangle + u^* v \langle \alpha | \beta(t) \rangle + uv^* \langle \beta | \alpha(t) \rangle + |v|^2 \langle \beta | \beta(t) \rangle \right|, \quad (3.37)$$

where $|\alpha(t)\rangle = e^{-iH_2t}|\alpha\rangle$ and $|\beta(t)\rangle = e^{-iH_2t}|\beta\rangle$. To get a more explicit expression for $\mathcal{F}(t)$, let us compute the overlaps. Along the same lines as in Eqs. (3.21, 3.35), one can calculate the first and fourth overlaps in Eq. (3.37) as

$$\langle \alpha | \alpha(t) \rangle = e^{-it(hL+\mathcal{D})} \left(\frac{1 + |\alpha|^2 e^{iht}}{1 + |\alpha|^2} \right)^{2L}, \quad \langle \beta | \beta(t) \rangle = e^{-it(hL+\mathcal{D})} \left(\frac{1 + 4|\beta|^2 e^{2iht}}{1 + 4|\beta|^2} \right)^L, \quad (3.38)$$

where $\mathcal{D} = \sum_{j=1}^L D_j$ and we have used the fact that $|\bar{A}_n\rangle$ and $|\bar{B}_n\rangle$ are eigenstates of H_2 with eigenvalues $h(L-n) + \mathcal{D}$ and $h(L-2n) + \mathcal{D}$, respectively. Next, let us compute the second and third overlaps in Eq. (3.37). To this end, we consider the overlap between $|\bar{A}_m\rangle$ and $|\bar{B}_n\rangle$. Since they are eigenstates of S^z with eigenvalues $L-m$ and $L-2n$, respectively,

it is easy to see that $\langle \bar{A}_m | \bar{B}_n \rangle \propto \delta_{m,2n}$. The overlap for $m = 2n$ is calculated as

$$\begin{aligned} \langle \bar{A}_{2n} | \bar{B}_n \rangle &= \langle \uparrow | (\mathcal{O}_\pi^+)^{2n} (\mathcal{Q}_0^-)^n | \uparrow \rangle \\ &= \frac{(2n)!}{2^n} \langle \uparrow | \left(\sum_{1 \leq j_1 < \dots < j_n \leq L} (S_{j_1}^+)^2 (S_{j_2}^+)^2 \dots (S_{j_n}^+)^2 \right) n! \left(\sum_{1 \leq l_1 < \dots < l_n \leq L} (S_{l_1}^-)^2 (S_{l_2}^-)^2 \dots (S_{l_n}^-)^2 \right) | \uparrow \rangle \\ &= 2^n \cdot (2n)! \cdot n! \cdot \binom{L}{n}, \end{aligned} \quad (3.39)$$

from which we obtain

$$\langle \alpha | \beta(t) \rangle = \frac{e^{-it(hL+\mathcal{D})} (1 + 2(\alpha^*)^2 \beta e^{2iht})^L}{(1 + |\alpha|^2)^L (1 + 4|\beta|^2)^{\frac{L}{2}}}, \quad \langle \beta | \alpha(t) \rangle = \frac{e^{-it(hL+\mathcal{D})} (1 + 2\alpha^2 \beta^* e^{2iht})^L}{(1 + |\alpha|^2)^L (1 + 4|\beta|^2)^{\frac{L}{2}}}. \quad (3.40)$$

Plugging Eqs. (3.38) and (3.40) into Eq. (3.37) yields

$$\begin{aligned} \mathcal{F}(t) &= \frac{1}{Z^2} \left| |u|^2 \left(\frac{1 + |\alpha|^2 e^{iht}}{1 + |\alpha|^2} \right)^{2L} + |v|^2 \left(\frac{1 + 4|\beta|^2 e^{2iht}}{1 + 4|\beta|^2} \right)^L \right. \\ &\quad \left. + u^* v \frac{(1 + 2(\alpha^*)^2 \beta e^{2iht})^L}{(1 + |\alpha|^2)^L (1 + 4|\beta|^2)^{\frac{L}{2}}} + uv^* \frac{(1 + 2\alpha^2 \beta^* e^{2iht})^L}{(1 + |\alpha|^2)^L (1 + 4|\beta|^2)^{\frac{L}{2}}} \right|, \end{aligned} \quad (3.41)$$

with

$$Z^2 = \left| |u|^2 + |v|^2 + \frac{2 \operatorname{Re}\{u^* v (1 + 2(\alpha^*)^2 \beta)\}}{(1 + |\alpha|^2)^L (1 + 4|\beta|^2)^{\frac{L}{2}}} \right|. \quad (3.42)$$

Figure 3.10 shows $\mathcal{F}(t)$ for two different choices of (α, β) . We can see that the fidelity shows revivals with period $2\pi/h$, which is the smallest common period of the two fidelity oscillations shown in Figs. 3.4 and 3.9. Clearly, the trend of the curves is more complicated than the previous ones, with small peaks originating from the interference terms $\langle \alpha | \beta(t) \rangle$ and $\langle \beta | \alpha(t) \rangle$.

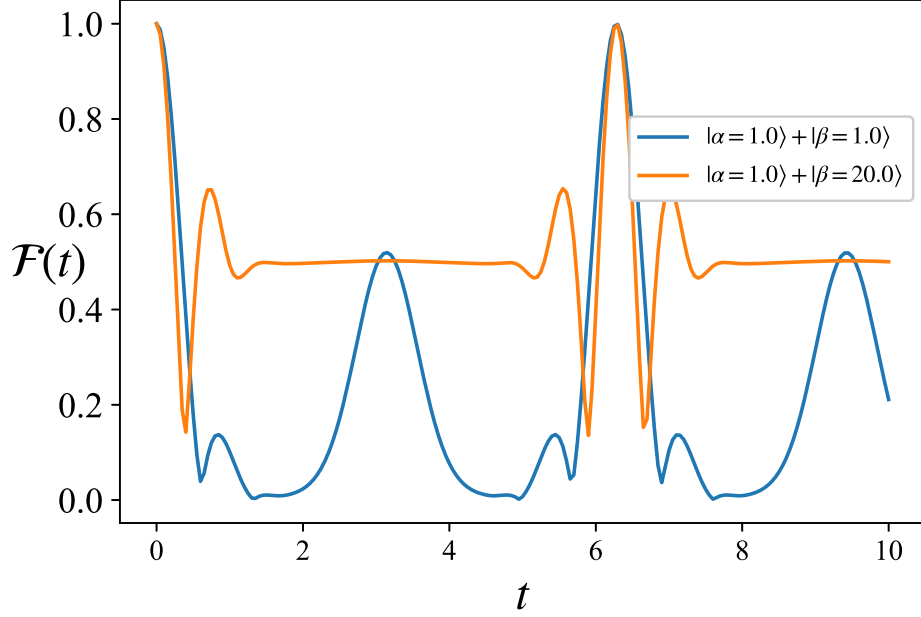


Figure 3.10: The dynamics of the fidelity of the superposition of two coherent states $|\alpha\rangle$ and $|\beta\rangle$ driven by H_2 (Eq. (3.33)) with $h = 1, L = 8$, and $D_j (j = 1, 2, \dots, L)$ chosen randomly from $[-1, 1]$. The period of the revivals is $2\pi/h$.

3.4 Spin-1 AKLT model + scalar spin chirality

3.4.1 Hamiltonian

In this section, we consider another spin-1 model in which the VBS state in Eq. (2.45) is a scar state. The Hamiltonian of the model is given by

$$H(t) = H_{\text{AKLT}} + tC_{\text{SC}}, \quad (3.43)$$

where H_{AKLT} is the AKLT Hamiltonian [107–109]

$$H_{\text{AKLT}} = \sum_{j=1}^L \left[\mathbf{S}_j \cdot \mathbf{S}_{j+1} + \frac{1}{3}(\mathbf{S}_j \cdot \mathbf{S}_{j+1})^2 + \frac{2}{3} \right], \quad (3.44)$$

and C_{SC} is the spin-1 scalar spin chirality (Eq. (3.1)).

The AKLT Hamiltonian H_{AKLT} is invariant under time-reversal Θ , $\text{SU}(2)$ spin rotation, translation \mathcal{T} , bond-centered inversion \mathcal{I}_b , site-centered inversion \mathcal{I}_s , and spin-flip \mathcal{F} . On the other hand, C_{SC} lacks time-reversal and inversion symmetries among them. However, the combined symmetry $\Theta\mathcal{I}_s$ leaves C_{SC} invariant. Therefore, the model $H(t)$ in Eq. (3.43) has $\text{SU}(2)$, translation, spin-flip, and pseudo-time-reversal symmetries. Since the AKLT Hamiltonian is non-integrable, it is quite likely that the model Eq. (3.43) is not integrable either. This is indeed the case as can be seen from Figure 3.11. Clearly, the

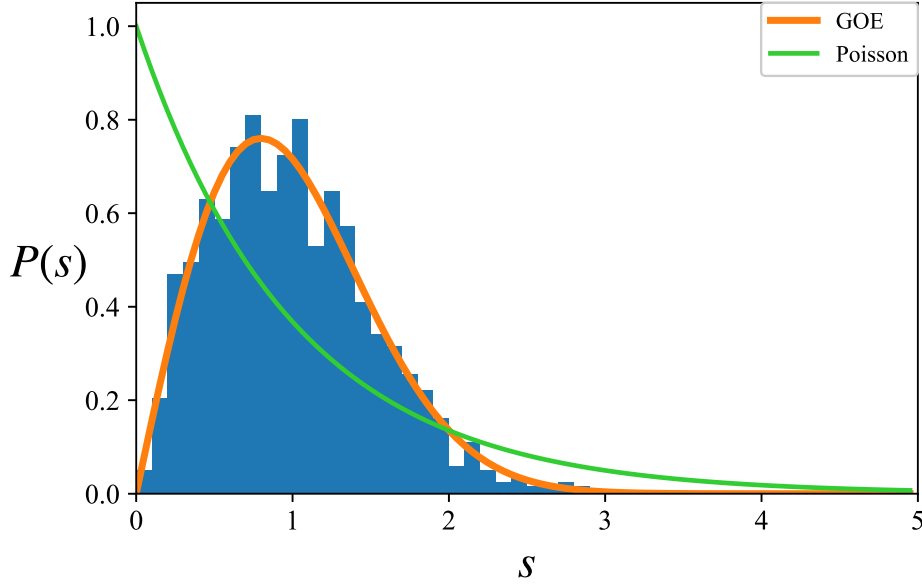


Figure 3.11: Level-spacing statistics in the middle half of the spectrum of the model (3.43) with $t = 3$ and $L = 13$. The data are taken in the symmetry sector where $(S^z, \mathcal{S}, \mathcal{T}, \mathcal{F}) = (0, 0, 1, 1)$. The curves $P(s)_{\text{GOE}}$ (orange) and $P(s)_{\text{Poisson}}$ (green) are shown for comparison. The distribution follows $P(s)_{\text{GOE}}$.

level-spacing distribution is close to the GOE Wigner-Dyson distribution. To provide further evidence for this, we compute the r -value from the histogram and obtain $\langle r \rangle \simeq 0.536$, which agrees with $\langle r_{\text{GOE}} \rangle \simeq 0.536$.

3.4.2 Scar state

The VBS state $|\Psi_{\text{VBS}}\rangle$ in Eq. (2.45) is the zero-energy ground state of H_{AKLT} . Interestingly, one can show that $|\Psi_{\text{VBS}}\rangle$ is an eigenstate of C_{SC} with eigenvalue 0 using its matrix product state representation (see Appendix A.2 for a proof). Thus, $|\Psi_{\text{VBS}}\rangle$ is a simultaneous eigenstate of H_{AKLT} and C_{SC} , and is likely to be a scar state of the system. We checked it by computing half-chain entanglement entropies (Figure 3.12). The obtained results show that the VBS state has a sufficiently low entanglement entropy compared to other states, confirming that it is indeed nonthermal.

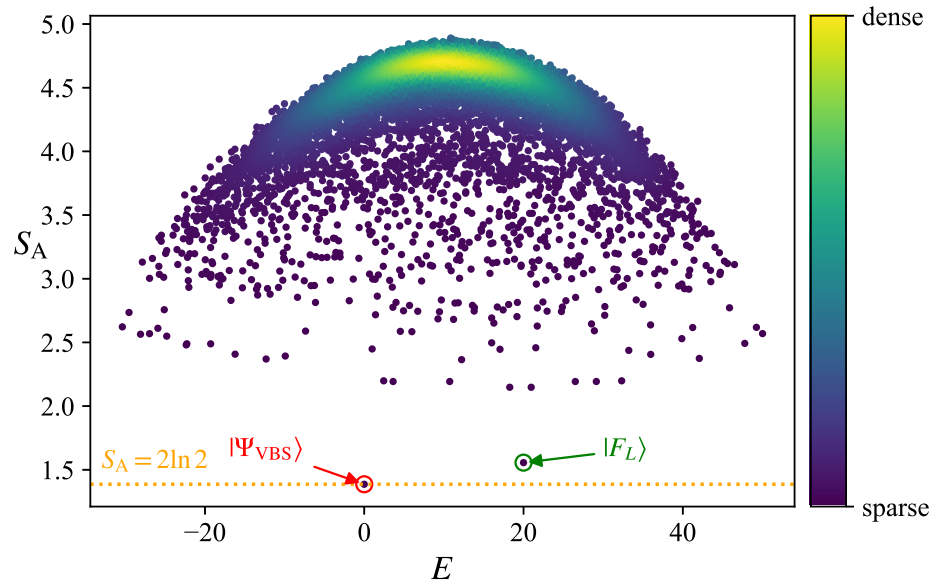


Figure 3.12: Entanglement entropies in all eigenstates of $H(t)$ in Eq. (3.43) with $t = 3$ for $L = 10$ in the $S^z = 0$ sector. The density of data points is color coded. The red and green circles indicate the VBS and ferromagnetic states, respectively. The orange dotted line indicates $S_A = 2 \ln 2 \simeq 1.386$.

CONSTRUCTION OF SCARRED MODELS USING INTEGRABLE BOUNDARY STATES

In this chapter, we introduce another method to construct scarred models. The key to the construction is special states called integrable boundary states [63, 121–124]. They are highly related to conserved quantities of integrable systems. In Section 4.1, we give a review of the integrable boundary states. In Section 4.2, we construct the model with QMBS from the spin-1/2 Majumdar-Ghosh Hamiltonian. Section 4.3 refers to the model with QMBS constructed by the AKLT Hamiltonian and the SU(3) Sutherland model. In Section 4.4, we focused on the spin-1/2 scalar chirality or its deformation, which are the third conserved charges of the XXZ model or the XYZ model, respectively, and we construct models with QMBS. In this chapter, Sections 4.1 - 4.3 are based on Ref. [112], and Section 4.4 is based on preparing paper.

4.1 Integrable Boundary States

4.1.1 Introduction for Integrable Boundary States

Integrable boundary states in lattice models were inspired by those in integrable quantum field theories (QFTs) with boundaries [125] and were formulated by Piroli et al. [123]. Consider a $(1 + 1)$ -dimensional Euclidean field theory with a semi-infinite plane $x \in (-\infty, 0)$ and $y \in (-\infty, \infty)$. Then, the action is given as

$$\mathcal{S}_B = \int_{-\infty}^{\infty} dy \int_{-\infty}^0 dx a(\varphi, \partial_\mu \varphi) + \int_{-\infty}^{\infty} dy b\left(\varphi_B, \frac{d\varphi_B}{dy}\right), \quad (4.1)$$

where $\varphi(x, y)$ is a local bulk field, and $\varphi_B(y) = \varphi(x = 0, y)$ is a boundary field. Similarly, the functionals a and b correspond to the action densities for the bulk and the boundary,

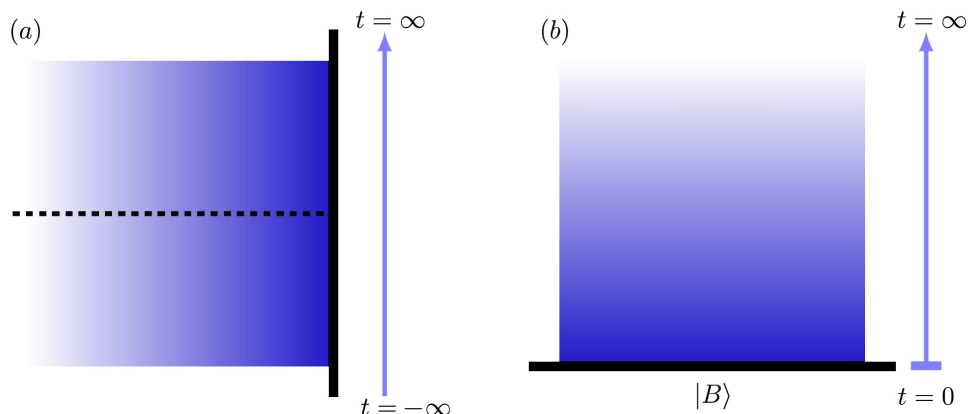


Figure 4.1: Pictorial representation of two-dimensional Euclidean field theory with boundary on $x = 0$. (a) The Euclidean time direction is chosen to be parallel to the boundary (y -direction). The physical Hilbert space is identified as a semi-infinite line at a fixed time $y = y_0$ (dashed line). (b) The Euclidean time direction is chosen to be perpendicular to the boundary (x -direction). The boundary state $|B\rangle$ appears as the initial condition. This figure is reproduced with Creative Commons CC-BY 4.0 license (<https://creativecommons.org/licenses/by/4.0/>) from Ref. [63], ©Elsevier B.V.

respectively. It is related to the Lorentzian field theory through the Wick rotation and that is a normal procedure to apply QFT results for the equilibrium statistical physics¹. Then, there are two ways to obtain the corresponding Hamiltonian. One is to take the Euclidean time axis in the y -direction and identify the coordinate x as the physical Hilbert space. The corresponding Hamiltonian is

$$H_B = \int_{-\infty}^0 dx h(x) + \theta_B, \quad (4.2)$$

where $h(x)$ is the Hamiltonian density in the bulk and θ_B represents a contribution from the boundary. The other approach is to swap the roles of space and time, that is, to take the x -direction as the time axis and the y -direction as corresponding to the space axis. In this situation, the Hamiltonian is written as

$$H = \int_{-\infty}^{\infty} dy h(y). \quad (4.3)$$

Then, the time evolution of the boundary state governed by H_B in Eq. (4.2) [See Figure 4.1 (a)] plays the role of the initial state $|B\rangle$ for H in Eq. (4.3) [See Figure 4.1]. We call it an initial *boundary state*.

Now, consider the bulk action obtained from (4.1) without the boundary, namely,

$$\mathcal{S} = \int_{-\infty}^{\infty} dy \int_{-\infty}^{\infty} dx a(\varphi, \partial_\mu \varphi). \quad (4.4)$$

¹One of the most typical applications of this method is Matsubara Green's function expansion in perturbation theory at finite temperature [126].

If it is integrable, we can find an infinite number of local integrals of motion. These are generated by local fields T_{s+1} and Θ_{s-1} (\bar{T}_{s+1} and $\bar{\Theta}_{s-1}$), which satisfy the continuity equation [127–129]

$$\partial_{\bar{z}} T_{s+1} = \partial_z \Theta_{s-1}, \quad \partial_z \bar{T}_{s+1} = \partial_{\bar{z}} \bar{\Theta}_{s-1}. \quad (4.5)$$

Here, we introduced the complex coordinates $z = x + iy$ and $\bar{z} = x - iy$. The index $s+1 / s-1$ denotes that the positive (negative) spin belongs to the corresponding local field. The spin index s can take values in an infinite set S with positive integers. Then, the integrals of motion can be obtained as

$$P_s = \int_{-\infty}^{\infty} dx (T_{s+1} + \Theta_{s-1}), \quad \bar{P}_s = \int_{-\infty}^{\infty} dx (\bar{T}_{s+1} + \bar{\Theta}_{s-1}). \quad (4.6)$$

The integrable boundary field theory is characterized as infinitely many conservation laws that survive the addition of the boundary term [125]. In this case, the boundary Hamiltonian (4.2) has an infinite number of conserved charges of the form

$$H_B^{(s)} = \int_{-\infty}^0 dx (T_{s+1} + \bar{T}_{s+1} + \Theta_{s-1} + \bar{\Theta}_{s-1}) + \theta_B^{(s)}. \quad (4.7)$$

The index s can be taken in the infinite subset $S_B \subset S$. Since the boundary state $|B\rangle$ reflects the property of the boundary term θ_B in the rotated picture, the following relation holds [125]:

$$(P_s - \bar{P}_s) |B\rangle = 0, \quad s \in S_B. \quad (4.8)$$

Next, when we consider a general integrable one-dimensional lattice system, the space coordinate is discretized by the lattice. To apply the discussion in continuous QFTs to lattice models, the imaginary time and space have to share the same structure, namely, the time should be discretized. In quantum mechanics, the imaginary time w appears in the form of the time evolution operator e^{-wH} . Thus, to discretize the time, we consider the Suzuki-Trotter decomposition [130]

$$e^{-wH} \sim \left(1 - \frac{w}{N} H\right)^N. \quad (4.9)$$

In this picture, we can connect the imaginary time evolution and the transfer matrix [63, 130].

Integrable boundary states in lattice models are inspired by the boundary states in integrable QFTs. Since the boundary state $|B\rangle$ is annihilated by some conserved quantities, it is natural to define their lattice counterparts in such a way that they are annihilated by some combinations of conserved charges in integrable lattice models. Let H be an integrable Hamiltonian, and $Q_n = \sum_{j=1}^L q_{j,n}$ be the n -th conserved quantity of H , where each $q_{j,n}$ is the local operator acting on the n consecutive sites (sites $j, j+1, \dots, j+n-1$).

We can also construct an infinite number of conserved quantities Q_n successively starting from $Q_2 \propto H$ by $Q_{n+1} = [B, Q_n]$, where B is the boost operator² [131–133].

These conserved charges are divided into two groups: parity-even charges Q_{2k} and parity-odd charges Q_{2k+1} . The difference between the groups is the response to the inversion: The parity-even charges have the inversion symmetry $\mathcal{I}Q_{2k}\mathcal{I} = Q_{2k}$. In contrast, the parity-odd charges behave anti-symmetric under the inversion $\mathcal{I}Q_{2k+1}\mathcal{I} = -Q_{2k+1}$ [63], where the inversion operator \mathcal{I} maps the state $|i_1, i_2, \dots, i_L\rangle$ to $|i_L, i_{L-1}, \dots, i_1\rangle$. Finally, by analogy with the fact that $|B\rangle$ vanishes under parity-odd $P_s - \bar{P}_s$, we define integrable boundary state $|\Psi_0\rangle$ as a state that vanishes under any parity-odd charge Q_{2k+1} , namely,

$$Q_{2k+1}|\Psi_0\rangle = 0. \quad (4.10)$$

4.1.2 Method to Construct Models with QMBS from Integrable Boundary States

In the previous subsection, we reviewed the origin of the integrable boundary states. Here, we discuss how to construct models with QMBS using integrable boundary states. Compared to the introduction of integrable boundary states, the construction of models with QMBS using them is extremely simple. Let $|\Psi_0\rangle$ be an integrable boundary state of an integrable system H . Let Q_n ($n = 2, 3, 4, \dots$) be the n -th conserved charge of H . From the definition of the integrable boundary states, $|\Psi_0\rangle$ is annihilated by the odd conserved charge Q_{2k+1} ($k = 1, 2, \dots$) of the integrable Hamiltonian H . In this setup, we prepare a nonintegrable Hamiltonian H_{NI} for which the state $|\Psi_0\rangle$ is an energy eigenstate. Then, $|\Psi_0\rangle$ is clearly an eigenstate of the Hamiltonian

$$H_{\text{scar}}(t_1, t_2, \dots, t_n) = H_{\text{NI}} + \sum_{k=1}^n t_k Q_{2k+1}, \quad (4.11)$$

where $\{t_k\}_{k=1}^n$ are real numbers. If this new Hamiltonian is non-integrable and the energy of $|\Psi_0\rangle$ is in the middle of the spectrum, then $|\Psi_0\rangle$ is likely to be a scar state. Note that this method allows one to construct an enormous number of scarred models by changing parameters $\{t_k\}_{k=1}^n$.

In the above discussion, one may feel that the process to find H_{NI} is quite heuristic. However, since known examples of integrable boundary states are MPS³ [63, 121–124], we can provide some guidance to obtain H_{NI} . It is known that we can construct operators whose unique ground state is a given MPS if the given MPS satisfies a condition called *injectivity* [134]. If an operator \tilde{H} constructed in this way is independent of the conserved charges $\{Q_{2k+1}\}$, we can treat \tilde{H} as the nonintegrable Hamiltonian H_{NI} .

²The boost operator also works for non-difference-form R matrices, see Ref. [131].

³Product states can be regarded as a special case of MPS.

4.2 Spin-1/2 Majumdar-Ghosh Hamiltonian + Scalar Spin Chirality

In this section, we treat the model with the following Hamiltonian with free parameter $t \in \mathbb{R}$:

$$H(t) = H_{\text{MG}} + tC_{\text{SC}}^{1/2}, \quad (4.12)$$

where

$$H_{\text{MG}} = \frac{1}{4} \sum_{j=1}^L [(\sigma_j + \sigma_{j+1} + \sigma_{j+2})^2 - 3], \quad (4.13)$$

is the Majumdar-Ghosh Hamiltonian [82, 83] (see Section 2.3.1) and

$$C_{\text{SC}}^{1/2} = \frac{1}{8} \sum_{j=1}^L \sigma_j \cdot (\sigma_{j+1} \times \sigma_{j+2}), \quad (4.14)$$

is the spin-1/2 scalar spin chirality, which is known as the third conserved charge of the spin-1/2 Heisenberg spin chain [135]. We only consider the case where the model has an even number of sites with periodic boundary conditions. We write $\sigma_j = (\sigma_j^x, \sigma_j^y, \sigma_j^z)$ for the Pauli matrices acting on-site j , namely,

$$\sigma_j^x = \begin{pmatrix} 0 & 1 \\ 1 & 0 \end{pmatrix}_j, \quad \sigma_j^y = \begin{pmatrix} 0 & -i \\ i & 0 \end{pmatrix}_j, \quad \sigma_j^z = \begin{pmatrix} 1 & 0 \\ 0 & -1 \end{pmatrix}_j. \quad (4.15)$$

Before we verify the non-integrability of $H(t)$, we have to enumerate the symmetries of this model. The Majumdar-Ghosh Hamiltonian is invariant under time-reversal Θ : $\sigma_j \mapsto -\sigma_j$, SU(2) spin rotation, translation \mathcal{T} : $\sigma_j \mapsto \sigma_{j+1}$, bond-centered inversion \mathcal{I}_b : $\sigma_j \mapsto \sigma_{L-j+1}$, site-centered inversion \mathcal{I}_s : $\sigma_j \mapsto \sigma_{-j}$, and spin-flip \mathcal{F} : $\sigma_j \mapsto (\sigma_j^x, -\sigma_j^y, -\sigma_j^z)$. Among these symmetries, $C_{\text{SC}}^{1/2}$ does not have time-reversal and bond-centered- and site-centered inversion symmetries. However, it remains invariant under the combination of time reversal and site-centered inversion $\Theta\mathcal{I}_s$. We call it pseudo-time-reversal symmetry; hence, we expect its level-spacing statistics to obey the Wigner-Dyson GOE if it is non-integrable. For convenience, we denote the total spin operator as $S^z = \frac{1}{2} \sum_{j=1}^L \sigma_j^z$ and the SU(2) Casimir operator as $\mathcal{S}^2 = \frac{1}{4} \sum_{j=1}^L \sum_{\alpha=x,y,z} (\sigma_j^\alpha)^2$. For simplicity, we express the eigenvalues of the symmetry operators as the same symbol except for \mathcal{S}^2 , whose eigenvalues are $\mathcal{S}(\mathcal{S} + 1)$.

Figure 4.2 shows the level-spacing statistics in the symmetry sector with $(S^z, \mathcal{S}, \mathcal{T}, \mathcal{F}) = (0, 0, 1, 1)$. It is consistent with the Wigner-Dyson GOE distribution; hence, we conclude that $H_1(t)$ is a non-integrable Hamiltonian. In addition, the r -value of this level spacing is $\langle r \rangle \simeq 0.538$, which is sufficiently close to the r -value of GOE distribution $\langle r_{\text{GOE}} \rangle \simeq 0.536$. Note that when we take large t , the property of the system becomes closer to integrable since $C_{\text{SC}}^{1/2}$ is integrable. Figure 4.3 shows the t dependence of the r -value. It implies that

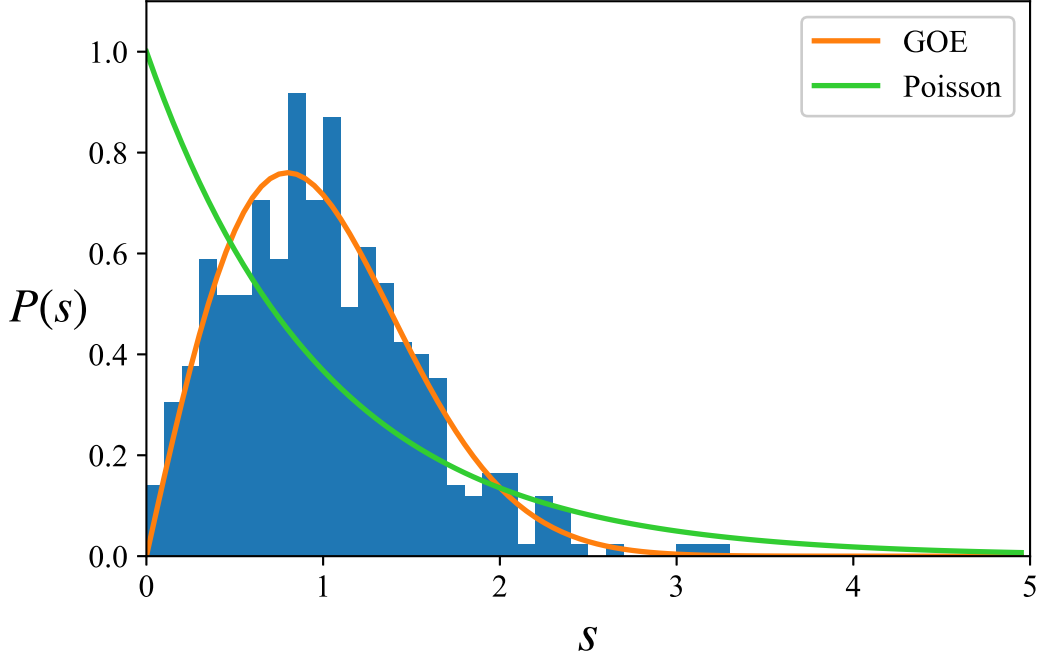


Figure 4.2: Level-spacing statistics in the middle half of the spectrum of $H(t)$ in Eq. (4.12) with $t = 8$ and $L = 20$. The data are taken in the symmetry sector where $(S^z, S, \mathcal{T}, \mathcal{F}) = (0, 0, 1, 1)$. The curves $P(s)_{\text{GOE}}$ (orange) and $P(s)_{\text{Poisson}}$ (green) are shown for comparison. The distribution follows $P(s)_{\text{GOE}}$.

we cannot ignore the effects of integrability when we take $t \sim 10^2$, whereas the models with $t \leq 20$ clearly show non-integrable behavior.

It is shown that the Majumdar-Ghosh Hamiltonian H_{MG} has twofold ground states, which are so-called the dimer states, in some previous research [82, 83, 136], namely,

$$|\Psi_1\rangle = |\text{sing}\rangle_{1,2} \otimes |\text{sing}\rangle_{3,4} \otimes \cdots \otimes |\text{sing}\rangle_{L-1,L}, \quad (4.16)$$

$$|\Psi_2\rangle = |\text{sing}\rangle_{2,3} \otimes |\text{sing}\rangle_{4,5} \otimes \cdots \otimes |\text{sing}\rangle_{L,1}, \quad (4.17)$$

where

$$|\text{sing}\rangle_{i,j} = \frac{1}{\sqrt{2}}(|\uparrow\downarrow\rangle_{i,j} - |\downarrow\uparrow\rangle_{i,j}) \quad (4.18)$$

is the spin singlet-pair state lying on site i and j (See Eqs. (2.19) and (2.20)). These states are related to each other by translation, that is, $|\Psi_2\rangle = \mathcal{T} |\Psi_1\rangle$ and $|\Psi_1\rangle = \mathcal{T} |\Psi_2\rangle$. They are integrable boundary states of the spin-1/2 Heisenberg model [123]. This means that they are annihilated by the odd-order conserved charges of the Heisenberg spin chain. Since C_{SC} is the third-order conserved charge of the Heisenberg model, it annihilates the dimer states $|\Psi_{1,2}\rangle$. Therefore, these states are annihilated by the Hamiltonian $H(t)$ for any t .

We see that these twofold zero-energy states are good candidates for scar states in the model (4.12). To verify these states actually violate the strong ETH, we check the

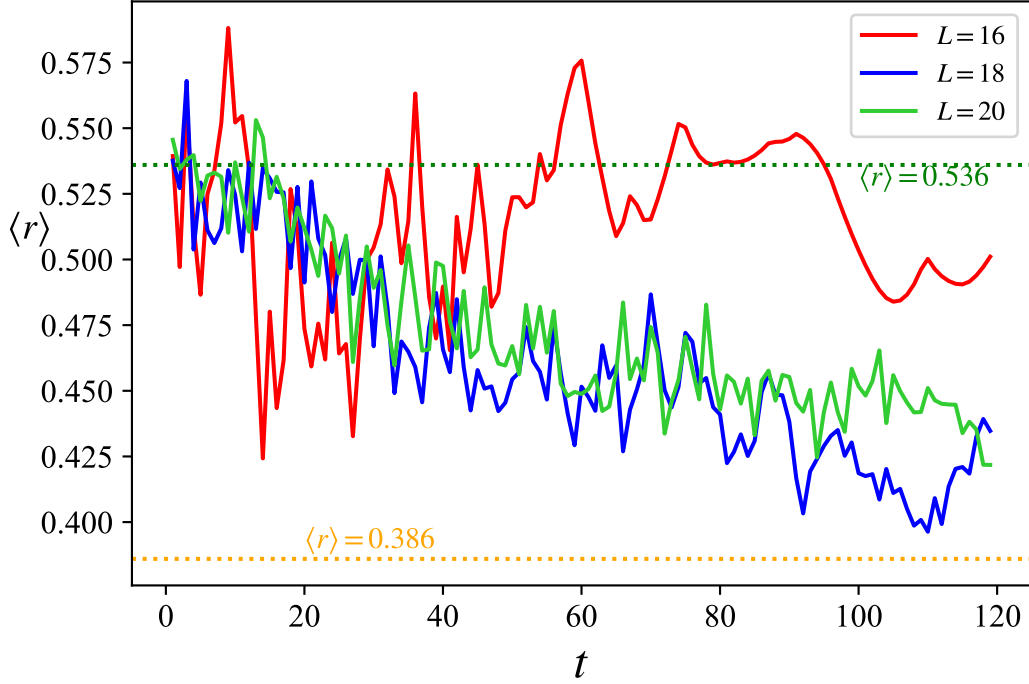


Figure 4.3: The mean level-spacing ratio $\langle r \rangle$ as a function of t for the Hamiltonian (4.12) in the symmetry sector $(S^z, \mathcal{S}, \mathcal{T}, \mathcal{F}) = (0, 0, 1, 1)$ for $L = 16, 18$, and 20 . The green and orange lines indicate $\langle r \rangle = 0.536 \simeq \langle r_{\text{GOE}} \rangle$ and $\langle r \rangle = 0.386 \simeq \langle r_{\text{Poisson}} \rangle$, respectively.

half-chain entanglement entropy for all eigenstates of (4.12). Figure 4.4 shows the entanglement entropies for each eigenstate in the symmetry sector $(S^z, \mathcal{T}) = (0, 1)$ for different lengths L . In this figure, we can see that the symmetrized dimer state $|\text{dimer}\rangle$, which is a superposition of $|\Psi_1\rangle$ and $|\Psi_2\rangle$, that is,

$$|\text{dimer}\rangle = \frac{1}{\sqrt{(2 + (-\frac{1}{2})^{\frac{L}{2}-2})}} (|\Psi_1\rangle + |\Psi_2\rangle), \quad (4.19)$$

shows low entanglement entropy compared to other eigenstates near $E = 0$. Additionally, the entanglement entropy goes up as the system size L does for almost all eigenstates but stays the same for the dimer state ($S_A \simeq 2 \ln 2$). We can obtain a similar result in the sector $(S^z, \mathcal{T}) = (0, -1)$ for the anti-symmetrized dimer state $|\text{dimer}'\rangle \propto |\Psi_1\rangle - |\Psi_2\rangle$. Hence, we can conclude that the states $|\Psi_1\rangle$ and $|\Psi_2\rangle$ are scar states.

Note that we can find another low-entanglement eigenstate in Figure 4.4. We identify that state as the ferromagnetic state $|F_{L/2}\rangle = (\mathcal{S}^-)^{\frac{L}{2}} |\uparrow\uparrow \cdots \uparrow\rangle$, where $\mathcal{S}^- = \mathcal{S}^x - i\mathcal{S}^y$. Its entanglement entropy grows by the sub-volume law, precisely

$$S_A(|F_{L/2}\rangle) \approx \frac{1}{2} \ln L + \frac{1}{2} \ln \frac{e\pi}{8} \quad (L \gg 1). \quad (4.20)$$

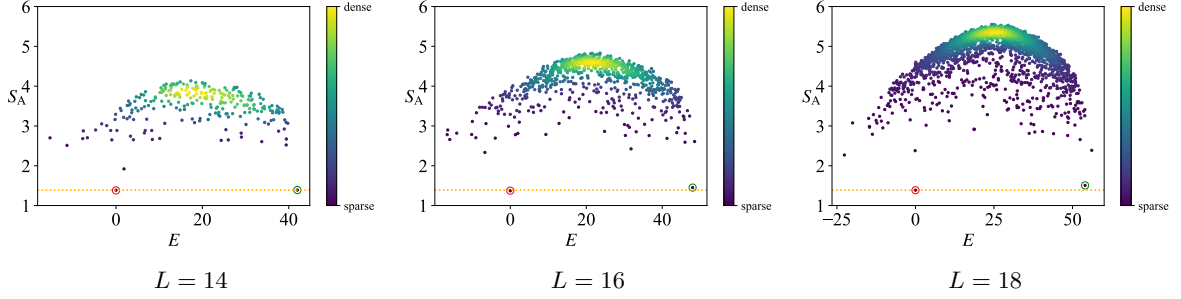


Figure 4.4: Entanglement entropy S_A in all eigenstates of $H(t)$ in Eq. (4.12) with $t = 8$ in the symmetry sector $(S^z, \mathcal{T}) = (0, 1)$ for $L = 14, 16$, and 18 . The density of the data points is color coded. The red and green circles indicate the dimer state $|\text{dimer}\rangle$ and the ferromagnetic state $|F_{L/2}\rangle$, respectively. The orange dotted line indicates $S_A = 2 \ln 2 \simeq 1.386$.

However, it cannot be considered as a QMBS because it belongs to the subspace with the maximum total spin that is isolated by the global $SU(2)$ symmetry, and it appears on the edge of the energy spectrum, which contains only a few states with respect to the dimension of the whole Hilbert space.

As another verification of a violation of ETH, we calculated the expectation value of a macroscopic observable for each eigenstate. We chose the staggered XXX Hamiltonian

$$H_{\text{st}} = \frac{1}{4} \sum_{j=1}^L (1 + (-1)^j \epsilon) \sigma_j \cdot \sigma_{j+1}, \quad (4.21)$$

where ϵ is a small parameter, as an observable. Figure 4.5 shows the numerical calculation of the expectation value of H_{st} for all eigenstates of the Hamiltonian (4.12) in the appropriate symmetric sector. We can see that the expectation value of H_{st} for the dimer state, which is given explicitly

$$\langle \text{dimer} | H_{\text{st}} | \text{dimer} \rangle = - \frac{3L \left[\left(-\frac{1}{2}\right)^{\frac{L}{2}} + \frac{1}{4} \right]}{2 + \left(-\frac{1}{2}\right)^{\frac{L}{2}-2}}, \quad (4.22)$$

is far from other states near $E = 0$. It also implies that $|\Psi_1\rangle$ and $|\Psi_2\rangle$ are the scar states.

Note that our result can be applied to models that contain higher-order conserved charges like Q_5, Q_7, \dots , that is, when we consider the Hamiltonian

$$H(\{t_k\}) = H_{\text{MG}} + \sum_k t_k Q_{2k+1}, \quad (4.23)$$

where t_k is an arbitrary real number, the states $|\Psi_{1,2}\rangle$ are also zero-energy eigenstates of $H(\{t_k\})$. Moreover, we can show that these states are outliers of ETH.

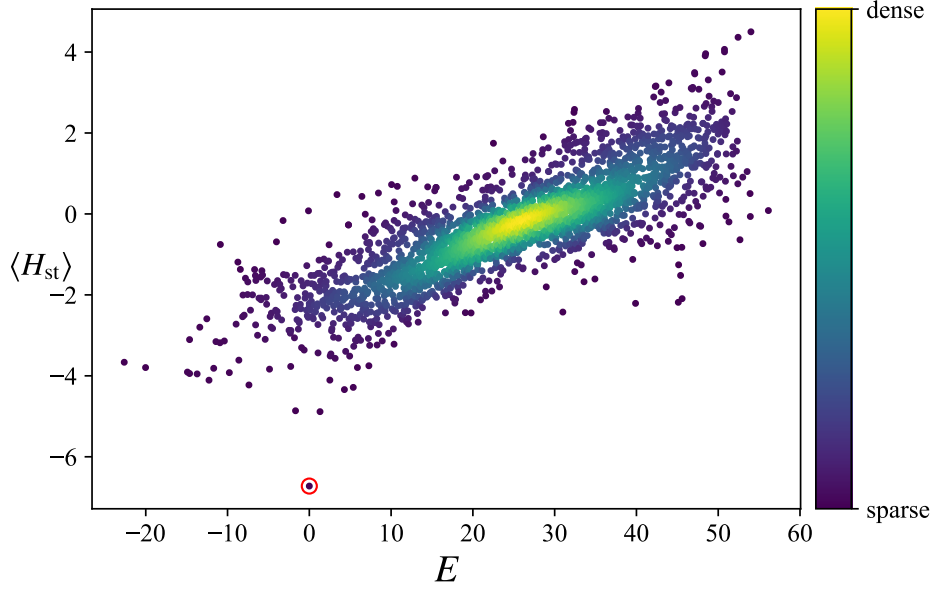


Figure 4.5: The expectation values of H_{st} with $\epsilon = 0.2$ in all eigenstates of $H(t)$ in Eq. (4.12) with $t = 8$, and $L = 18$ in the symmetry sector $(S^z, \mathcal{T}) = (0, 1)$. The density of data points is color coded. The red circle indicates the dimer state $|\text{dimer}\rangle$ with $\langle H_{\text{st}} \rangle \simeq -6.72$, which agrees with the analytical value $\langle H_{\text{st}} \rangle = -1143/170$ obtained from Eq. (4.21).

4.3 AKLT Hamiltonian + Scalar Spin Chirality

4.3.1 AKLT Hamiltonian + SU(3) Scalar Spin Chirality

The other model with QMBS constructed by using integrable boundary states is based on the AKLT model. Consider the Hamiltonian

$$H(t) = H_{\text{AKLT}} + H_3, \quad (4.24)$$

where

$$H_{\text{AKLT}} = \sum_{j=1}^L \left[\mathbf{S}_j \cdot \mathbf{S}_{j+1} + \frac{1}{3} (\mathbf{S}_j \cdot \mathbf{S}_{j+1})^2 + \frac{2}{3} \right] \quad (4.25)$$

is the AKLT Hamiltonian [107–109] and

$$H_3 = \sum_{j=1}^L \sum_{a,b,c=1}^8 f_{abc} \lambda_j^a \lambda_{j+1}^b \lambda_{j+2}^c \quad (4.26)$$

is the third conserved charge of the Sutherland model [137–140]. Here we denote the Gell-Mann matrices acting on site j as λ_j^a ($a = 1, 2, \dots, 8$), in the explicit form

$$\begin{aligned}\lambda^1 &= \begin{pmatrix} 0 & 1 & 0 \\ 1 & 0 & 0 \\ 0 & 0 & 0 \end{pmatrix}, \lambda^2 = \begin{pmatrix} 0 & -i & 0 \\ i & 0 & 0 \\ 0 & 0 & 0 \end{pmatrix}, \lambda^3 = \begin{pmatrix} 1 & 0 & 0 \\ 0 & -1 & 0 \\ 0 & 0 & 0 \end{pmatrix}, \\ \lambda^4 &= \begin{pmatrix} 0 & 0 & 1 \\ 0 & 0 & 0 \\ 1 & 0 & 0 \end{pmatrix}, \lambda^5 = \begin{pmatrix} 0 & 0 & -i \\ 0 & 0 & 0 \\ i & 0 & 0 \end{pmatrix}, \lambda^6 = \begin{pmatrix} 0 & 0 & 0 \\ 0 & 0 & 1 \\ 0 & 1 & 0 \end{pmatrix}, \\ \lambda^7 &= \begin{pmatrix} 0 & 0 & 0 \\ 0 & 0 & -i \\ 0 & i & 0 \end{pmatrix}, \lambda^8 = \frac{1}{\sqrt{3}} \begin{pmatrix} 1 & 0 & 0 \\ 0 & 1 & 0 \\ 0 & 0 & -2 \end{pmatrix},\end{aligned}\tag{4.27}$$

and f_{abc} denotes the structure constants defined by $[\lambda^a, \lambda^b] = 2if_{abc}\lambda^c$. The term H_3 can be regarded as the SU(3) extension of the scalar spin chirality because C_{SC} in Eq. (3.1) can be rewritten as

$$C_{\text{SC}} = \sum_{j=1}^L \sum_{\substack{a,b,c \\ =x,y,z}} \epsilon_{abc} S_j^a S_{j+1}^b S_{j+2}^c,\tag{4.28}$$

where ϵ_{abc} is the Levi-Civita symbol with $\epsilon_{xyz} = 1$, which is known as the structure constant of the SU(2) algebra such that $[S^a, S^b] = 2i\epsilon_{abc}S^c$. Moreover, we can introduce a convenient form of H_3 as follows. Let $P_{i,j}$ be a permutation operator that exchanges states on site i and j such that $P_{i,j} |a\rangle_i \otimes |b\rangle_j = |b\rangle_i \otimes |a\rangle_j$. Then we obtain [141]

$$\sum_{a=1}^8 \lambda_i^a \lambda_j^a = 2P_{i,j} - \frac{1}{3}.\tag{4.29}$$

From this relation and $\sum_c f_{abc}\lambda^c = \frac{1}{2i}[\lambda^a, \lambda^b]$, we obtain another form of (4.26),

$$H_3 = -2i \sum_{j=1}^L (P_{j,j+1,j+2} - P_{j,j+1,j+2}^\dagger),\tag{4.30}$$

where $P_{i,j,k} := P_{j,k}P_{i,j}$ is a three-site ring-exchange operator such that $P_{i,j,k} |a\rangle_i |b\rangle_j |c\rangle_k = |b\rangle_i |c\rangle_j |a\rangle_k$.

This model has the same symmetries as $H(t)$ in Eq. (3.43), i.e., SU(2) spin rotation, translation, spin-flip, and pseudo-time-reversal symmetries. (See Section 3.4 for details).

The AKLT Hamiltonian is invariant under time-reversal Θ , SU(2) spin rotation, translation \mathcal{T} , bond-centered inversion \mathcal{I}_b , site-centered inversion \mathcal{I}_s , and spin-flip \mathcal{F} , whereas H_3 lacks time-reversal and inversion symmetries among them (see Appendix B.2 for a discussion of the SU(2) symmetry of H_3). However, the combined symmetry $\Theta\mathcal{I}_s$ leaves H_3

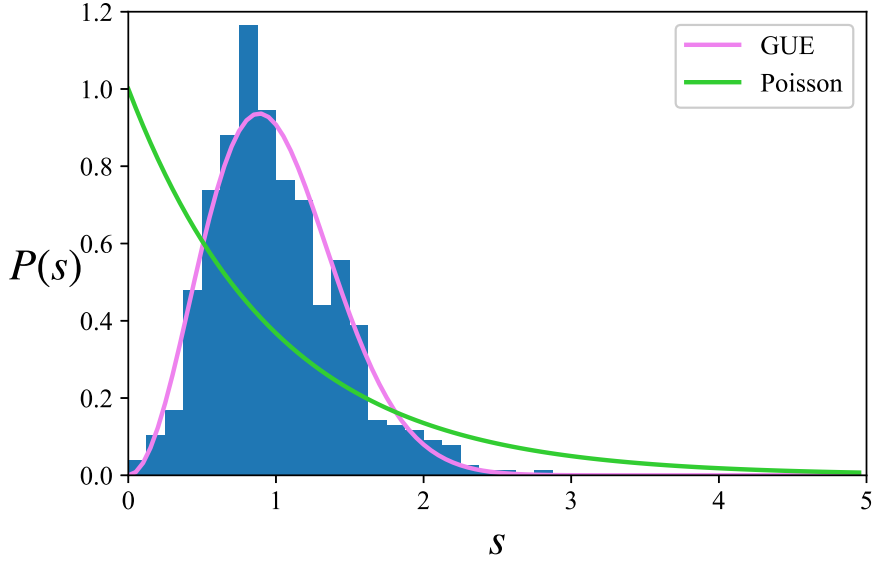


Figure 4.6: Level spacing statistics in the middle half of the spectrum of $H(t)$ in (4.24) with $t = 3$ and $L = 14$. The data are taken in the symmetry sector where $(S^z, S, \mathcal{T}, \mathcal{F}) = (0, 0, 1, 1)$. The curves $P(s)_{\text{GUE}}$ (magenta) and $P(s)_{\text{Poisson}}$ (green) are shown for comparison. The distribution follows $P(s)_{\text{GUE}}$.

invariant. Therefore, the model $H(t)$ in Eq. (4.24) has $\text{SU}(2)$, translation, spin-flip, and pseudo-time-reversal symmetries.

Since the $\text{SU}(3)$ Sutherland model is integrable, the third conserved charge H_3 can be considered as a quantum integrable Hamiltonian as well. On the other hand, the AKLT Hamiltonian is non-integrable. Thus, the model Eq. (4.24), an interpolation between the two, is expected to be non-integrable. To verify this, we compute the level-spacing statistics (Fig. 4.6). The results show that the level-spacing distribution follows the GUE Wigner-Dyson distribution instead of the Poisson distribution, which provides strong evidence that this model is non-integrable. It can also be checked by the r -value $\langle r \rangle \simeq 0.599$, which is close to $\langle r_{\text{GUE}} \rangle \simeq 0.603$. We remark that the model is expected to belong to the GOE class, as it has pseudo-time-reversal symmetry. The observed discrepancy may be due to the crossover between different universality classes [142, 143] or finite-size effects, which are also pronounced in the PXP model [60, 67].

It is widely known that H_{AKLT} has the unique ground state called valence bond solid (VBS) state given as

$$|\Psi_{\text{VBS}}\rangle = \sum_{\{s_j\}} \text{Tr}[A^{s_1} A^{s_2} \cdots A^{s_L}] |s_1, s_2, \dots, s_L\rangle. \quad (4.31)$$

Here, we take the sum over all possible spin configuration $s_j \in \{+, 0, -\}$ and the matrices

A^+ , A^0 and A^- are given by

$$A^+ = \sqrt{\frac{2}{3}}\sigma^+, \quad A^0 = -\sqrt{\frac{1}{3}}\sigma^z, \quad A^- = -\sqrt{\frac{2}{3}}\sigma^-. \quad (4.32)$$

Moreover, the VBS state is an integrable boundary state of the Sutherland model. Therefore, the VBS state is the zero energy state of the Hamiltonian (4.24), and it becomes a good candidate for QMBS in that system. By checking entanglement entropies of the eigenstates of the Hamiltonian (4.24) (Figure 4.7), we conclude that the VBS state $|\Psi_{\text{VBS}}\rangle$ is a QMBS. Moreover, the analytical value of the half-chain entanglement entropy of the VBS state is given as [144, 145]

$$S_A(|\Psi_{\text{VBS}}\rangle) = -3\lambda_A \ln \lambda_A - \lambda_B \ln \lambda_B \quad (4.33)$$

with

$$\lambda_A = \frac{1}{4} \frac{(1 - p^{\lfloor L/2 \rfloor})(1 - p^{\lceil L/2 \rceil})}{1 - p^{L-1}}, \quad (4.34)$$

$$\lambda_B = \frac{1}{4} \frac{(1 + 3p^{\lfloor L/2 \rfloor})(1 + 3p^{\lceil L/2 \rceil})}{1 - p^{L-1}}, \quad (4.35)$$

where $p = -1/3$. $\lfloor x \rfloor$ and $\lceil x \rceil$ denote the floor and ceiling functions, respectively. In the thermodynamic limit, we obtain

$$\lim_{L \rightarrow \infty} S_A(|\Psi_{\text{VBS}}\rangle) = 2 \ln 2. \quad (4.36)$$

It coincides with our numerical calculation shown in Figure 4.7. It shows that $S_A(|\Psi_{\text{VBS}}\rangle)$ obeys a sub-volume law, implying that $|\Psi_{\text{VBS}}\rangle$ is a nonthermal state.

4.3.2 Inhomogeneous generalization

In the previous model, it was necessary to increase t in order to make the energy density of the VBS state (relative to the ground state) finite. However, the problem is that this would increase the effect of H_3 and make the behavior of the system more like that of an integrable system. To avoid such a situation, we consider an inhomogeneous generalization of the AKLT Hamiltonian. In this case, the VBS state is still a zero-energy eigenstate of the inhomogeneous Hamiltonian, yet locating in the middle of the spectrum. The Hamiltonian of the inhomogeneous model is given by

$$\tilde{H}(t) = \tilde{H}_{\text{AKLT}} + tH_3 \quad (4.37)$$

with

$$\tilde{H}_{\text{AKLT}} = \sum_{j=1}^L c_j \left[\mathbf{S}_j \cdot \mathbf{S}_{j+1} + \frac{1}{3}(\mathbf{S}_j \cdot \mathbf{S}_{j+1})^2 + \frac{2}{3} \right]. \quad (4.38)$$

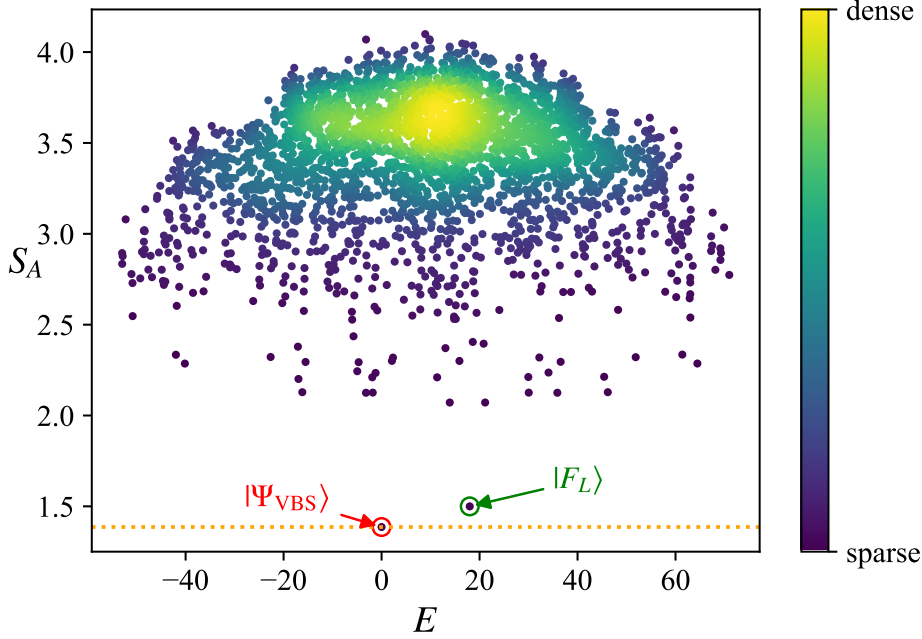


Figure 4.7: Entanglement entropies in all eigenstates of $H(t)$ in Eq. (4.24) for $L = 9$, $t = 3$ in the $S^z = 0$ sector. The density of data points is color coded. The points enclosed by the red and green circles indicate the VBS state $|\Psi_{\text{VBS}}\rangle$ and ferromagnetic state $|F_L\rangle$, respectively. The orange dotted line indicates $S_A = 2 \ln 2 \simeq 1.386$.

In principle, each coefficient c_j can be any real number. However, for our purpose, we choose $|c_j| \lesssim t$ in order to keep the magnitudes of the two terms (\tilde{H}_{AKLT} and H_3) comparable. In the following, we set $t \simeq 1$ and draw c_j uniformly from the interval $[-1, 1]$, in which case the model is no longer invariant under the combination of Θ and \mathcal{I}_s .

Like $H(t)$ in Eq. (4.24), $\tilde{H}(t)$ in Eq. (4.37) is also non-integrable. As Figure 4.8 shows, the level-spacing statistics of the model behave as that of the GUE. Also, the calculated r -value $r \simeq 0.598$ is compatible with the r -value of the GUE $\langle r_{\text{GUE}} \rangle \simeq 0.603$.

In order to check whether the VBS state is a scar state, we compute entanglement entropies. The results are shown in Figure 4.9. Clearly, there are two entanglement outliers. The one at $E = 0$ is the VBS state. The other one that is also far from other ordinary states is the ferromagnetic state. Its energy is $2 \sum c_j$ (see Appendix B.3), and it is a trivial state rather than a scar because of the $\text{SU}(2)$ symmetry of the model (4.37).

We provide further evidence that the VBS state is a scar state in this model. To this end, we study the expectation values of some physical observable in all energy eigenstates. The physical quantity we consider here is the AKLT Hamiltonian (4.25) whose expectation value in a normalized state $|\psi\rangle$ is denoted as $\langle H_{\text{AKLT}} \rangle := \langle \psi | H_{\text{AKLT}} | \psi \rangle$. Figure 4.10 shows the numerical result for the distribution of $\langle H_{\text{AKLT}} \rangle$. Clearly, the VBS

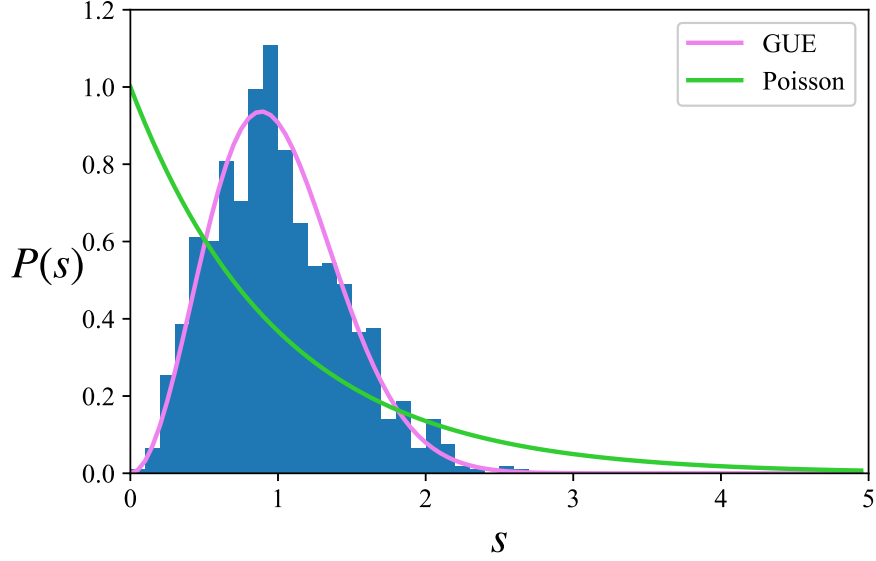


Figure 4.8: Level-spacing statistics in the middle half of the spectrum of the inhomogeneous model $\tilde{H}(t)$ in Eq. (4.37) with $t = 1$ and $L = 11$. Each c_j is randomly chosen from $[-1, 1]$. The data are taken in the symmetry sector where $(S^z, \mathcal{S}, \mathcal{F}) = (0, 0, 1)$. The curves $P_{\text{GUE}}(s)$ (magenta) and $P_{\text{Poisson}}(s)$ (green) are shown for comparison. The distribution follows $P_{\text{GUE}}(s)$.

state at $(0, 0)$ can be distinguished from other eigenstates.

4.3.3 Further Generalizations

Now we generalize the model in the previous subsection in two ways. First, we consider a generalization of the spin-1 AKLT model to include next-nearest-neighbor interactions. Based on the results obtained in [146, 147], we find that the VBS state in Eq. (2.45) is annihilated by

$$\tilde{H}'_{\text{AKLT}} = \sum_{j=1}^L d_j \left[\mathbf{S}_j \cdot \mathbf{S}_{j+1} + \mathbf{S}_{j+1} \cdot \mathbf{S}_{j+2} + \frac{1}{2} \mathbf{S}_j \cdot \mathbf{S}_{j+2} - \frac{1}{2} (\mathbf{S}_j \cdot \mathbf{S}_{j+2})^2 + 3 \right], \quad (4.39)$$

where each coefficient d_j can be any real number. This means that adding this term to the Hamiltonian $\tilde{H}(t)$ in Eq. (4.37) leaves the scar state unaffected. Second, we consider higher-order conserved charges Q_{2k+1} ($k > 1$) of the SU(3) Sutherland model, whose explicit expressions can be found in Ref. [133]. Since the VBS state is an integrable boundary state, it is annihilated by all Q_{2k+1} (see Appendix B.1). Thus, adding these terms with arbitrary coefficients does not affect the scar state. Combining these two generalizations

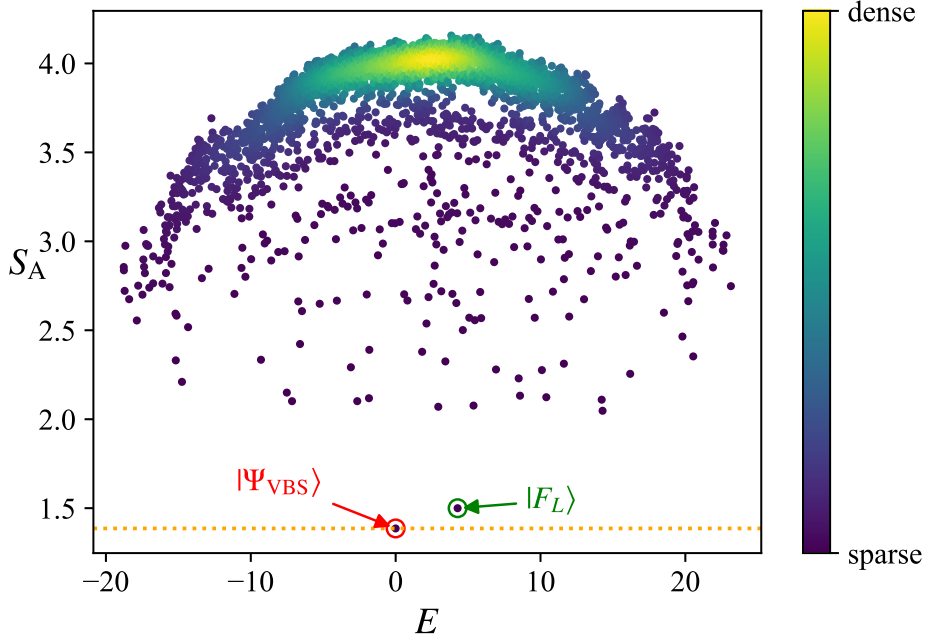


Figure 4.9: Entanglement entropies in all eigenstates of the inhomogeneous model $\tilde{H}(t)$ in Eq. (4.37) for $L = 9, t = 1$ in the $S^z = 0$ sector. The density of data points is color coded. Each c_j is randomly chosen from $[-1, 1]$. The red and green circles indicate the VBS and the ferromagnetic states, respectively. The orange dotted line indicates $S_A = 2 \ln 2$.

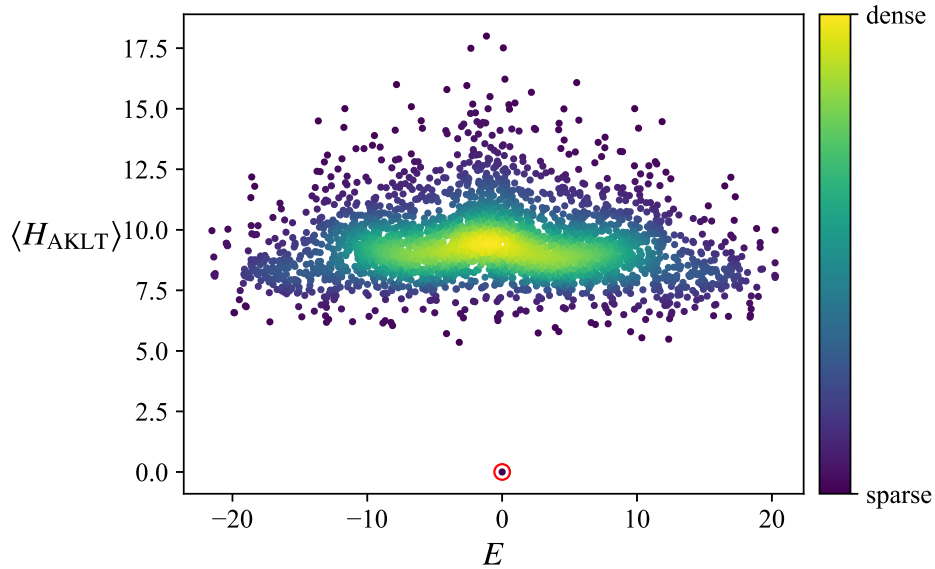


Figure 4.10: The expectation values of H_{AKLT} in all eigenstates of (4.37) with $t = 1, L = 9$ in the symmetry sector where $S^z = 0$. The density of data points is color coded. The red circle indicates the VBS state.

leads to the following Hamiltonian

$$\tilde{H}(t_1, t_2, \dots, t_n) = \tilde{H}(t_1) + \tilde{H}'_{\text{AKLT}} + \sum_{k=2}^n t_k Q_{2k+1}, \quad (4.40)$$

in which the VBS state survives as a scar state.

Let us finally discuss higher-spin generalizations. The spin-1 AKLT model can be generalized to models with $\text{SO}(5)$ and more generally $\text{SO}(2l+1)$ symmetry [148–150]. The exact ground states of these models, which we dub $\text{SO}(2l+1)$ VBS states, take the form of a matrix product state built from $2l+1$ gamma matrices. According to the general theory of integrable boundary states [122], the $\text{SO}(2l+1)$ VBS state is an integrable boundary state of the $\text{SU}(2l+1)$ Heisenberg model, meaning that the state is annihilated by all parity-odd conserved charges of the model. Thus, the construction of deformed models proceeds in much the same way as in the $\text{SU}(2)$ case. We also note that the parent Hamiltonian of the $\text{SO}(2l+1)$ VBS state can be inhomogeneous, like the one in Eq. (4.38). We thus expect that the models constructed in this way are non-integrable for general l and can be thought of as scarred models.

4.4 Scarred Models Related to XXZ Model and XYZ model

In the previous sections, models that we constructed have only one QMBS. It is inconvenient to consider the dynamics of QMBS in such models since the dynamics of an eigenstate is trivial. In this section, we introduce examples of models with multiple QMBS.

It is known that the XXZ Hamiltonian

$$H_{\text{XXZ}} = \sum_{j=1}^L (\sigma_j^x \sigma_{j+1}^x + \sigma_j^y \sigma_{j+1}^y + \Delta \sigma_j^z \sigma_{j+1}^z), \quad (4.41)$$

and the XYZ Hamiltonian

$$H_{\text{XYZ}} = \sum_{j=1}^L (J_x \sigma_j^x \sigma_{j+1}^x + J_y \sigma_j^y \sigma_{j+1}^y + J_z \sigma_j^z \sigma_{j+1}^z), \quad (4.42)$$

are integrable under appropriate boundary conditions [151, 152].

4.4.1 XXZ model

We consider the following Hamiltonian

$$H_1(s, h_y) = C_{\text{SC}} + s H_{\text{pert}} + h_y S^y, \quad (4.43)$$

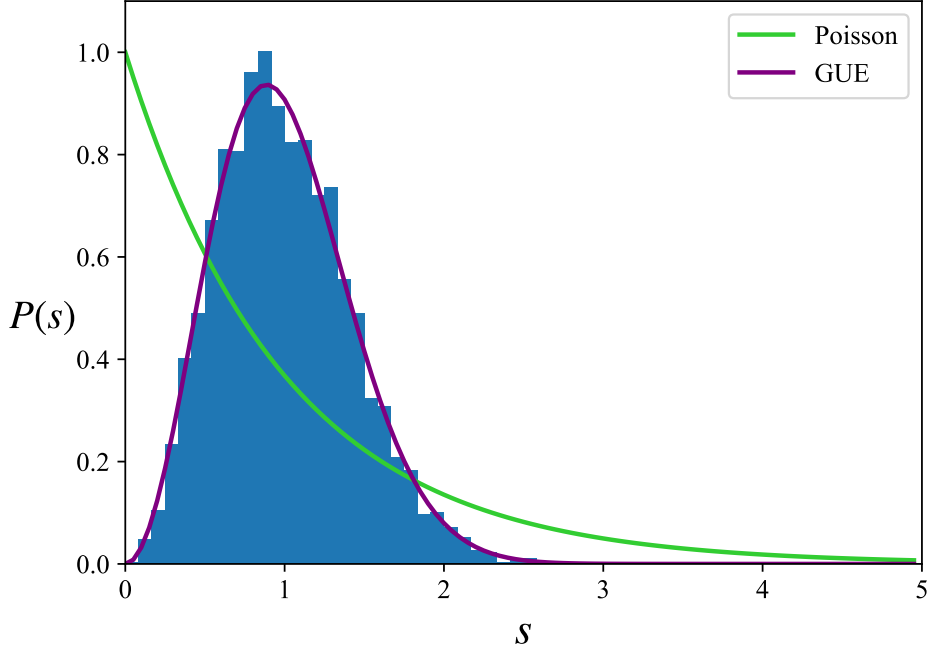


Figure 4.11: Level-spacing statistics in the middle half of the spectrum of $H_1(s, h_y)$ (Eq. (4.43)) with $s = 1$, $h_y = 1$ and $L = 16$. The arbitrary constants c_j are randomly chosen from $[-1, 1]$. The data are taken in the symmetry sector with $S^y = 0$.

with

$$C_{\text{SC}} = \sum_{j=1}^L \sigma_j \cdot (\sigma_{j+1} \times \sigma_{j+2}), \quad (4.44)$$

$$H_{\text{pert}} = \sum_{j=1}^L c_j (\sigma_j^x \sigma_{j+1}^x - \sigma_j^y \sigma_{j+1}^y + \sigma_j^z \sigma_{j+1}^z + 1), \quad (4.45)$$

$$S^y = \sum_{j=1}^L \sigma_j^y, \quad (4.46)$$

where each $c_j \in \mathbb{R}$ is a random constant. We note that C_{SC} is not only the third conserved charge of the Heisenberg model, but also of the XXZ model. We can see that the perturbation term H_{pert} makes the whole Hamiltonian nonintegrable. The level spacing statistics of the Hamiltonian (Figure 4.11) show that its level-spacing statistics coincide with the GUE Wigner-Dyson distribution. In addition, its r -value $\langle r \rangle \simeq 0.596$ agrees with one of the GUE distribution $\langle r_{\text{GUE}} \rangle \simeq 0.603$.

As mentioned in Ref. [63], two-site product states are integrable boundary states of the XXZ model. Thus, we focus on two-site product eigenstates of H_{pert} . We focus on the

tilted Néel (q -Néel) states

$$|\psi_1(\alpha)\rangle = \frac{1}{\sqrt{\mathcal{N}}} [(-\alpha |\uparrow\rangle + |\downarrow\rangle) \otimes (|\uparrow\rangle + \alpha |\downarrow\rangle)]^{\otimes \frac{L}{2}}, \quad (4.47)$$

$$|\psi_2(\alpha)\rangle = \frac{1}{\sqrt{\mathcal{N}}} [(|\uparrow\rangle + \alpha |\downarrow\rangle) \otimes (-\alpha |\uparrow\rangle + |\downarrow\rangle)]^{\otimes \frac{L}{2}}, \quad (4.48)$$

with the normalized constant $\mathcal{N} = (|\alpha|^2 + 1)^L$ and an arbitrary constant $\alpha \in \mathbb{C}$. These states are related to each other by the one-site translation \mathcal{T} .

The tilted Néel states are zero-energy eigenstates of C_{SC} because they are integrable boundary states of the XXZ model [63]. In addition, since H_{pert} is a sum of the projection operators on $\frac{1}{\sqrt{2}}(|\uparrow\uparrow\rangle_{j,j+1} + |\downarrow\downarrow\rangle_{j,j+1})$, $|\psi_{1,2}(\alpha)\rangle$ are zero-energy eigenstates of H_{pert} . On the other hand, they are not eigenstates of \mathcal{S}^y . However, thanks to the arbitrariness of the parameter $\alpha \in \mathbb{C}$, $|\psi_{1,2}(\alpha)\rangle$ can be written as a linear combination of eigenstates of \mathcal{S}^y . To make the following discussion easier, we use the basis in which σ_j^y is diagonal, namely,

$$|+\rangle = \frac{1}{\sqrt{2}}(|\uparrow\rangle + i|\downarrow\rangle), \quad |-\rangle = \frac{1}{\sqrt{2}}(|\uparrow\rangle - i|\downarrow\rangle), \quad (4.49)$$

which satisfy $\sigma^y |\pm\rangle = \pm |\pm\rangle$. With respect to this basis, we can rewrite $|\psi_1(\alpha)\rangle$ as

$$\begin{aligned} |\psi_1(\alpha)\rangle &\propto \left[-\frac{1}{\sqrt{2}}\{(\alpha + i)|+\rangle + (\alpha - i)|-\rangle\} \right] \otimes \left[\frac{1}{\sqrt{2}}\{(1 - i\alpha)|+\rangle + (1 + i\alpha)|-\rangle\} \right] \otimes \cdots \\ &\propto ((\alpha + i)|+\rangle + (\alpha - i)|-\rangle) \otimes (-i(\alpha + i)|+\rangle + i(\alpha - i)|-\rangle) \otimes \cdots \\ &\propto (z|+\rangle + |-\rangle) \otimes (z|+\rangle - |-\rangle) \otimes \cdots, \end{aligned} \quad (4.50)$$

where $z = \frac{\alpha+i}{\alpha-i}$. Finally, we obtain

$$|\psi_1(\alpha)\rangle \propto \sum_{n=0}^L z^{L-n} |\Psi_n\rangle, \quad (4.51)$$

where $|\Psi_0\rangle := |++++\cdots\rangle$ and $|\Psi_n\rangle = (\tilde{O}_\pi^-)^n |\Psi_0\rangle$ with

$$\tilde{O}_\pi^- = \sum_{j=1}^L (-1)^j \tilde{\sigma}_j^-, \quad (4.52)$$

where $\tilde{\sigma}_j^- = (\sigma_j^z - i\sigma_j^x)/2$. Since $z \in \mathbb{C} \setminus \{1\}$ can be taken arbitrary, we conclude that each $|\Psi_n\rangle$ is an eigenstate of the Hamiltonian (4.43) with eigenvalue $(\frac{L}{2} - n)h_y$. Their half-chain entanglement entropies (Figure 4.12) are extremely lower than those of other eigenstates. It suggests that the states $|\tilde{\Psi}_n\rangle$ are the exact QMBS of the Hamiltonian in Eq. (4.43).

4.4.2 XYZ model

It is known that the tilted Néel states are integrable boundary states of the XYZ model as well (See Appendix B.4):

$$H_{\text{XYZ}} = \sum_{j=1}^L h_{j,j+1}^{\text{XYZ}} = \sum_{j=1}^L (J_x \sigma_j^x \sigma_{j+1}^x + J_y \sigma_j^y \sigma_{j+1}^y + J_z \sigma_j^z \sigma_{j+1}^z). \quad (4.53)$$

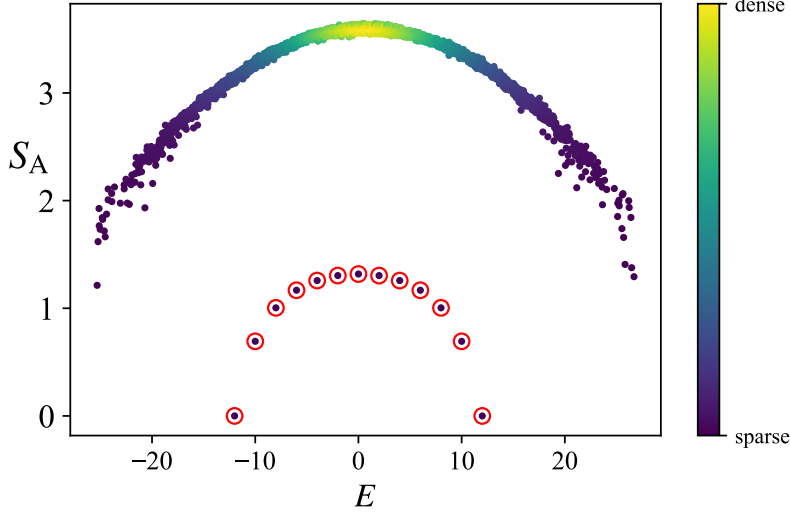


Figure 4.12: The half-chain entanglement entropy and eigenenergy for all eigenstates of $H_1(t=1, h_y=1)$ in Eq. (4.43) with $L=12$. The arbitrary constants c_j are randomly chosen from $[-1, 1]$. The red circle indicates the half-chain entanglement entropy and energy of $|\tilde{\Psi}_n\rangle$.

Therefore, its third conserved quantity, Q_3 , annihilates these states. This means that $|\tilde{\Psi}_n\rangle$ are eigenstates of the following Hamiltonian:

$$H_2(s, h_y) = Q_3 + sH_{\text{pert}} + h_y S^y. \quad (4.54)$$

We can calculate Q_3 using the Boost operator $B = \sum_j j h_{j,j+1}^{\text{XYZ}}$:

$$Q_3 \propto i \sum_{j=1}^L [h_{j,j+1}^{\text{XYZ}}, h_{j+1,j+2}^{\text{XYZ}}] \quad (4.55)$$

$$\propto i \sum_{j=1}^L \left[x \tilde{h}_{j,j+1}^{\text{XXZ}} + y E_j, x \tilde{h}_{j+1,j+2}^{\text{XXZ}} + y E_{j+1} \right], \quad (4.56)$$

where

$$x = \frac{J_x + J_y}{2}, \quad y = \frac{J_x - J_y}{2}, \quad (4.57)$$

$$\tilde{h}_{j,j+1}^{\text{XXZ}} = \sigma_j^x \sigma_{j+1}^x + \sigma_j^y \sigma_{j+1}^y + \Delta \sigma_j^z \sigma_{j+1}^z, \quad \left(\Delta = \frac{2J_z - J_x + J_y}{J_x + J_y} \right), \quad (4.58)$$

$$E_j = \sigma_j^x \sigma_{j+1}^x - \sigma_j^y \sigma_{j+1}^y + \sigma_j^z \sigma_{j+1}^z + 1. \quad (4.59)$$

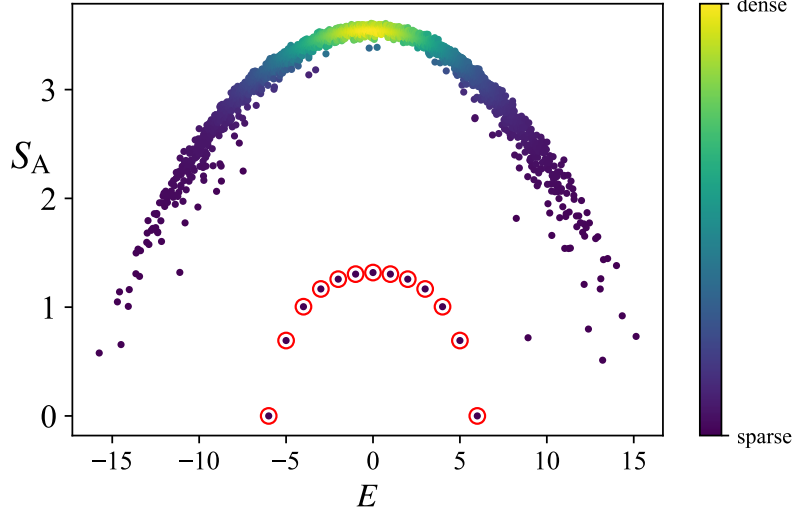


Figure 4.13: The half-chain entanglement entropy and eigenenergy of the all eigenstates of $H_2(t = 1.0, h_y = 0.5)$ in Eq. (4.54) with $L = 12$. The arbitrary constants c_j are randomly chosen from $[-1, 1]$. The density of data points is color coded. The red circles indicate the scar states $|\tilde{\Psi}_n\rangle$.

After a lengthy calculation, we obtain [153]

$$Q_3 = \sum_{j=1}^L \hat{\sigma}_j \cdot (\bar{\sigma}_{j+1} \times \hat{\sigma}_{j+2}) \quad (4.60)$$

$$= \sum_{j=1}^L \sum_{\lambda, \mu, \nu} \epsilon_{\lambda\mu\nu} \frac{J_x J_y J_z}{J_\mu} \sigma_j^\lambda \sigma_{j+1}^\mu \sigma_{j+2}^\nu, \quad (4.61)$$

where $\sum_{\lambda, \mu, \nu}$ is shorthand for $\sum_{\lambda \in \{x, y, z\}} \sum_{\mu \in \{x, y, z\}} \sum_{\nu \in \{x, y, z\}}$ and

$$\hat{\sigma}_j^\mu = \sqrt{J_\mu} \sigma_j^\mu, \quad (4.62)$$

$$\bar{\sigma}_j^\mu = \sqrt{\frac{J_x J_y J_z}{J_\mu}} \sigma_j^\mu, \quad (4.63)$$

and $\epsilon_{\lambda\mu\nu}$ is the Levi-Civita symbol with $\epsilon_{xyz} = 1$. Figure 4.13 shows the numerical calculation of entanglement entropies for all energy eigenstates of the Hamiltonian (4.54). It suggests that the states $|\tilde{\Psi}_n\rangle$ show low entanglement entropy in comparison to other eigenstates in the middle of the spectrum. Thus, we can conclude the states $|\tilde{\Psi}_n\rangle$ are exact scar states of the Hamiltonian (4.54).

4.4.2.1 Dynamics

To reveal the non-thermal features of the scar states, we observe their dynamical behavior. We consider the one-dimensional model H_2 in Eq. (4.54). We prepare the Néel state $|\mathbb{Z}_2\rangle = |\uparrow\downarrow\uparrow\downarrow\cdots\rangle = |\psi_1(z \rightarrow 1)\rangle$ as a superposition of the scar states and $|\mathbb{Z}_3\rangle = |\uparrow\uparrow\downarrow\cdots\rangle$ as an initial thermal state.

First, we calculate the time evolution of the fidelity: $\mathcal{F}(t) := |\langle\phi(t=0)|\phi(t)\rangle| = |\langle\phi|e^{-iH_2t}|\phi\rangle|$. Figure 4.14 shows the numerical result of the fidelity of $|\mathbb{Z}_2\rangle$ and $|\mathbb{Z}_3\rangle$. It shows that the Néel state shows perfect periodic revival, which implies it never reaches thermalization, while the fidelity of $|\mathbb{Z}_3\rangle$ decays rapidly to zero.

Since $|\mathbb{Z}_2\rangle = |\psi_1(z \rightarrow 1)\rangle$ is a zeroenergy eigenstate of $H(s, h_y = 0)$, we obtain the explicit form of the fidelity:

$$\begin{aligned} & \left| \langle \mathbb{Z}_2 | e^{-itH_2(s, h_y)} | \mathbb{Z}_2 \rangle \right| \\ &= \left| \langle \mathbb{Z}_2 | e^{-ith_y S^y} | \mathbb{Z}_2 \rangle \right| \\ &= \left| \left(\langle \uparrow | e^{-ith_y \sigma^y} | \uparrow \rangle \times \langle \downarrow | e^{-ith_y \sigma^y} | \downarrow \rangle \right)^{\frac{L}{2}} \right| \\ &= \cos^L(h_y t). \end{aligned} \quad (4.64)$$

Therefore, we conclude that the fidelity of $|\mathbb{Z}_2\rangle$ shows perfectly periodic behavior with period $T = \frac{\pi}{h_y}$. In general, it implies the existence of QMBS [118].

We have also checked the time evolution of a correlation function with an appropriate initial state $|\phi\rangle$:

$$C_r^x(t) = \frac{1}{L} \sum_{j=1}^L \langle \phi(t) | \sigma_j^x \sigma_{j+r}^x | \phi(t) \rangle. \quad (4.65)$$

Figure 4.15 shows the numerical result for the time evolution of $C_r^x(t)$ for $|\mathbb{Z}_2\rangle$ and $|\mathbb{Z}_3\rangle$. We can also see that $|\mathbb{Z}_2\rangle$ shows periodic behavior whereas the correlation function of $|\mathbb{Z}_3\rangle$ rapidly decreases. We can calculate the correlation function in $|\mathbb{Z}_2(t)\rangle$ as

$$\begin{aligned} C_r^x(t) &= \frac{1}{L} \sum_{j=1}^L \langle \mathbb{Z}_2 | e^{itH_2(s, h_y)} \sigma_j^x \sigma_{j+r}^x e^{-itH_2(s, h_y)} | \mathbb{Z}_2 \rangle \\ &= \frac{1}{2} \left(\langle \mathbb{Z}_2 | e^{ith_y S^y} \sigma_1^x \sigma_{1+r}^x e^{-ith_y S^y} | \mathbb{Z}_2 \rangle + \langle \mathbb{Z}_2 | e^{ith_y S^y} \sigma_2^x \sigma_{2+r}^x e^{-ith_y S^y} | \mathbb{Z}_2 \rangle \right) \\ &= \frac{1}{2} \left(\langle \uparrow | e^{ith_y \sigma^y} \sigma^x e^{-ith_y \sigma^y} | \uparrow \rangle \cdot \langle v_r | e^{ith_y \sigma^y} \sigma^x e^{-ith_y \sigma^y} | v_r \rangle \right. \\ &\quad \left. + \langle \downarrow | e^{ith_y \sigma^y} \sigma^x e^{-ith_y \sigma^y} | \downarrow \rangle \cdot \langle v_{r+1} | e^{ith_y \sigma^y} \sigma^x e^{-ith_y \sigma^y} | v_{r+1} \rangle \right) \\ &= \frac{1}{2} \left(\sin(2h_y t) \times (-1)^r \sin(2h_y t) + [-\sin(2h_y t)] \times (-1)^{r+1} \sin(2h_y t) \right) \\ &= (-1)^r \sin^2(2h_y t), \end{aligned} \quad (4.66)$$

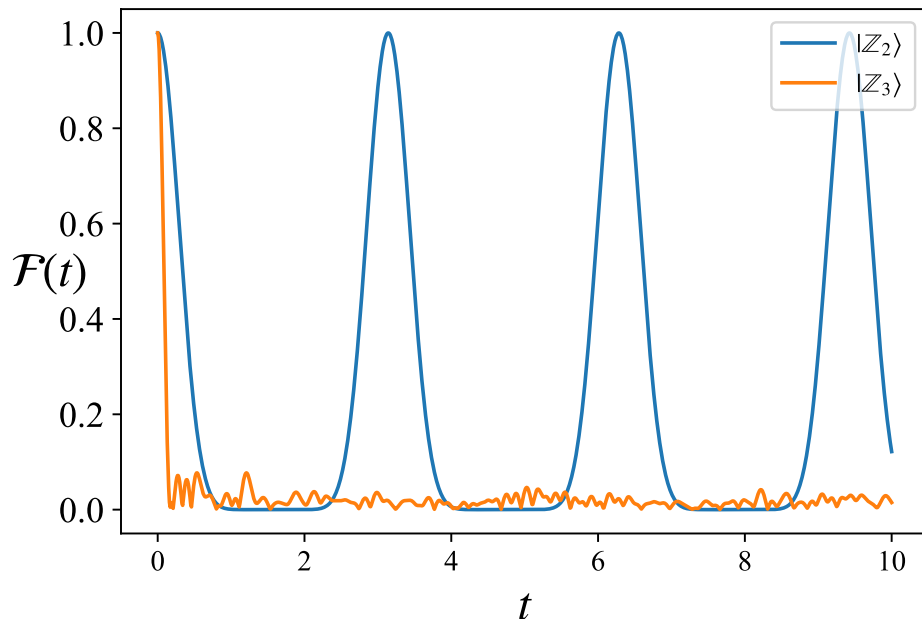


Figure 4.14: The time dependence of the fidelity of $|\mathbb{Z}_2\rangle$ and $|\mathbb{Z}_3\rangle$ driven by $H_2(s = 1, h_y = 1)$ in Eq. (4.54) with $J_x, J_y, J_z \in [-1, 1]$ and $L = 12$.

where $|v_r\rangle = |\uparrow\rangle$ when r is even and $|v_r\rangle = |\downarrow\rangle$ when r is odd, respectively. Therefore, the correlation function of $|\mathbb{Z}_2\rangle$ is a periodic function with the period $T = \frac{\pi}{2h_y}$. The analytical calculation agrees with the numerical calculation (see Figure 4.15).

4.4.3 Extension for Higher Dimensional Lattices

We can find scar states in higher-dimensional models in the same way as in one-dimensional models. Let us consider the following two-dimensional Hamiltonian on the square lattice Λ (Figure 4.16):

$$H^{2d}(s) = C_{\text{SC}}^{2d} + sH_{\text{pert}}^{2d}, \quad (4.67)$$

where

$$C_{\text{SC}}^{2d} = \sum_{j \in \Lambda} \sum_{a=1}^3 \sum_{b=a+1}^4 \sigma_{j+e_a} \cdot (\sigma_j \times \sigma_{j+e_b}), \quad (4.68)$$

$$H_{\text{pert}}^{2d} = \sum_{\langle i,j \rangle} c_{i,j} (\sigma_i^x \sigma_j^x - \sigma_i^y \sigma_j^y + \sigma_i^z \sigma_j^z + 1), \quad (4.69)$$

and $(e_1, e_2, e_3, e_4) = (-e_x, -e_y, e_y, e_x)$, where e_x and e_y denote the unit vector along x -direction and y -direction, respectively (see Figure 4.16). We can choose constants $c_{i,j} \in \mathbb{R}$ arbitrarily. The operator Q_3^{2d} is expressed graphically as

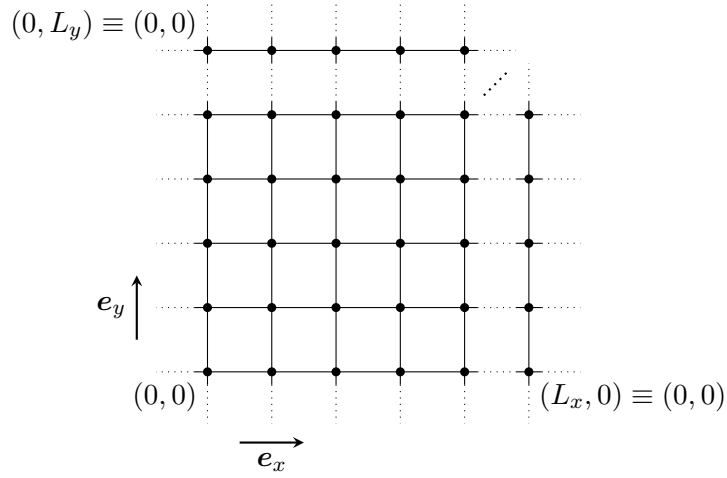


Figure 4.16: An example of the $L_x \times L_y$ square lattice. Due to the periodic boundary conditions, $(mL_x + x, nL_y + y) \equiv (x, y)$ with any $m, n \in \mathbb{Z}$.

eigenstates of the Hamiltonian (4.67). The two-dimensional tilted Néel states are given as

$$|\psi_1^{2d}(\alpha)\rangle = \bigotimes_{j \in \Lambda} |\chi_j\rangle, \quad (4.73)$$

where

$$|\chi_j\rangle = \begin{cases} -\alpha |\uparrow\rangle + |\downarrow\rangle & j_x + j_y \equiv 0 \pmod{2} \\ |\uparrow\rangle + \alpha |\downarrow\rangle & j_x + j_y \equiv 1 \pmod{2} \end{cases}, \quad (4.74)$$

and

$$|\psi_2^{2d}(\alpha)\rangle = \mathcal{T}_x |\psi_1^{2d}(\alpha)\rangle = \mathcal{T}_y |\psi_1^{2d}(\alpha)\rangle, \quad (4.75)$$

where \mathcal{T}_x and \mathcal{T}_y are the translation operators along the x -axis and y -axis, respectively. These states can be decomposed into the eigenstates of $\mathcal{S}^y = \sum_{j \in \Lambda} \sigma_j^y$, denoting $|\tilde{\Psi}_n^{2d}\rangle$, as in the case of the one-dimensional lattice. The states $|\tilde{\Psi}_n^{2d}\rangle$ are given as

$$|\tilde{\Psi}_n^{2d}\rangle = \mathcal{O}_{2d}^- |++ \cdots +\rangle, \quad (4.76)$$

with

$$\mathcal{O}_{2d}^- = \sum_{j \in \Lambda} (-1)^{(j_x + j_y)} \tilde{\sigma}_j^-. \quad (4.77)$$

To calculate the entanglement entropy of these states, we divide the lattice Λ to $\Lambda = \Lambda_A \sqcup \bar{\Lambda}_A$, where $\Lambda_A = \{j \in \Lambda | j_y < L_y/2\}$, and calculate an entanglement entropy S_A of the sublattice Λ_A for each eigenstate in the $\mathcal{S}^y = 0$ sector. Figure 4.17 shows that $|\tilde{\Psi}_{n=L/2}^{2d}\rangle$ has extremely low entanglement.

Finally, we remark that our result can be extended to XYZ-based models and models on any bipartite graph. Here, a graph $\Lambda = (V, E)$ is bipartite if there exists a direct sum

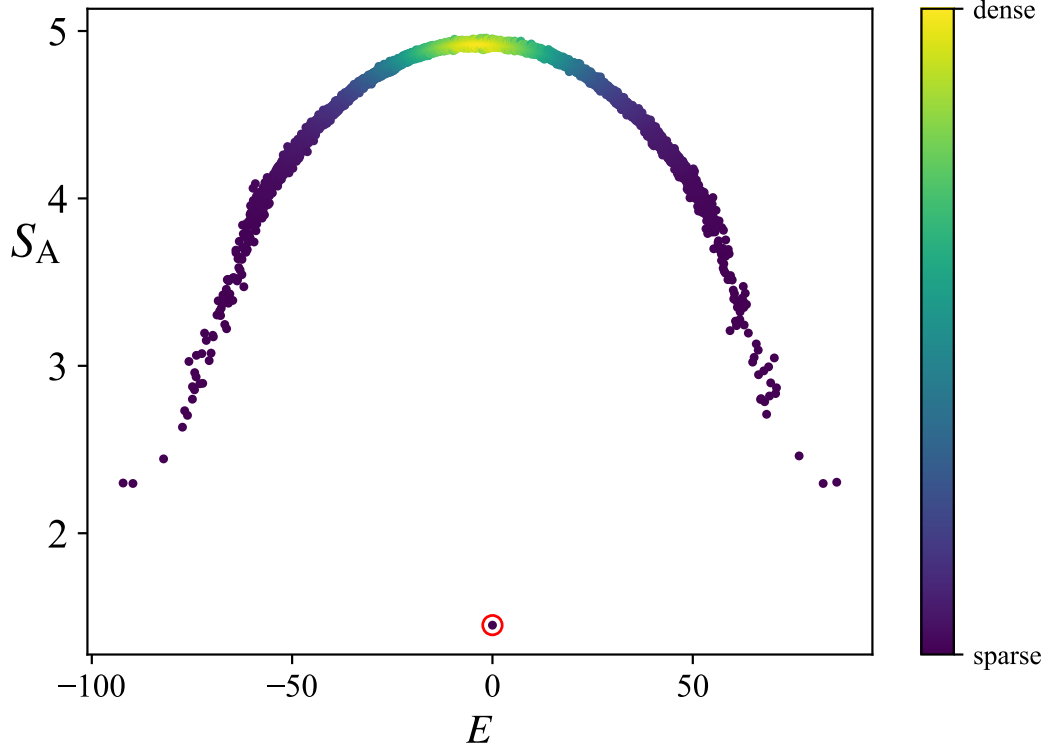


Figure 4.17: The entanglement entropies and energies for all eigenstates of the Hamiltonian (4.67) with $(L_x, L_y) = (4, 4)$ in the sector $\mathcal{S}^y = 0$. The red circle indicates $|\Psi_{n=L/2}^{2d}\rangle$.

decomposition of the set of vertices $V = V_A \sqcup V_B$ such that any edge $e \in E$ connects a vertex in V_A and one in V_B . For a bipartite graph $\Lambda = (V, E)$, we introduce the following Hamiltonian

$$H^\Lambda(t, h_y) = Q^\Lambda + tH_{\text{pert}}^\Lambda + h_y \mathcal{S}^{y, \Lambda}, \quad (4.78)$$

with

$$Q^\Lambda = \sum_{\langle ij \rangle, \langle jk \rangle \in E} \hat{\sigma}_i \cdot (\bar{\sigma}_j \times \hat{\sigma}_k), \quad (4.79)$$

$$H_{\text{pert}}^\Lambda = \sum_{\langle ij \rangle \in E} c_{\langle ij \rangle} (\sigma_i^x \sigma_j^x - \sigma_i^y \sigma_j^y + \sigma_i^z \sigma_j^z + 1), \quad (4.80)$$

$$\mathcal{S}^{y, \Lambda} = \sum_{v \in V} \sigma_v^y, \quad (4.81)$$

where $c_{\langle ij \rangle} \in \mathbb{R}$ are arbitrary constants. Then, we can show that the states

$$|\Psi_n^\Lambda\rangle = (\mathcal{O}_\Lambda^-)^n \bigotimes_{v \in V} |+\rangle_v, \quad (4.82)$$

with

$$\mathcal{O}_{\Lambda}^{-} = \sum_{v_a \in V_A} \tilde{\sigma}_{v_a}^{-} - \sum_{v_b \in V_B} \tilde{\sigma}_{v_b}^{-}, \quad (4.83)$$

are eigenstates of $H^{\Lambda}(t, h_y)$. We can verify that these states do not satisfy the strong ETH through the same discussion as in the one- or two-dimensional cases.

SUMMARY AND DISCUSSIONS

In this chapter, we summarize our results in this thesis and provide an outlook. We have constructed new classes of quantum spin models with multibody interactions that exhibit QMBS using two different methods: The first method focuses on the spin-1 scalar spin chirality C_{SC} and uses RSGA method. The second method uses integrable boundary states. We demonstrated that the QMBS in the models behave differently from thermal states by comparing their spectral, dynamical, and entanglement properties with those of other typical states.

In Chapter 3, we introduced three classes of models with QMBS constructed by RSGA. The first and second models are focused on a tower of the eigenstates in the scalar spin chirality. We constructed these models by adding perturbations to preserve the RSGA structure. This method is a standard method to construct models with QMBS, and several previous studies have used it to construct models with QMBS [59, 93, 154]. In particular, the models we constructed in Chapter 3 are similar to those suggested by Tang et al. [155], where the authors constructed models with towers of scar states generated by irreducible tensor operators. However, their main focus is on spin-1/2 systems, whereas our work is primarily concerned with spin-1 systems. In addition, we demonstrated that our method allows for the construction of two-dimensional models with QMBS.

In Chapter 4, we use integrable boundary states to construct models with QMBS. This procedure is quite different from those proposed in previous studies, and this method can provide a class of models with as many QMBS as these. For example, using another combination of conserved charges $\{Q_{2k+1}\}_{k=1,2,\dots}$, one can construct a family of new models in which an integrable boundary state is an exact zero-energy state. We also provide higher-dimensional extension of some of the models constructed by using integrable boundary

states.

We believe that these results can serve as a solid basis for understanding QMBS and nonthermal behavior in quantum many-body systems. Since research on QMBS is comparatively new, attempts to understand QMBS in a unified manner have only recently begun [156]. Therefore, it is important to propose new classes of models with QMBS for revealing the hidden properties of QMBS.

In future research, it would be interesting to construct non-integrable quantum field theories with QMBS by extending our method since the idea of integrable boundary states can be traced back to those of integrable quantum field theories [125]. In this regard, we note that QMBS in continuous models have also been discussed in previous studies [157–160]. As another extension of our research, it would be interesting to find the correspondence between integrable lattice systems and models with QMBS that originate from integrable boundary states. For example, there exist some previous studies that found explicit forms of conserved charges in integrable lattice systems [161, 162]. We can start from these conserved charges and construct integrable boundary states and models with QMBS. In addition, Eck and Fendley found invertible maps between integrable models that share the same algebra [163]. It would be interesting to construct another class of models with QMBS by using these maps on models that we constructed by using integrable boundary states.

Another direction worth investigating is to apply our methods to open quantum and periodically driven systems. Previous studies have shown that there are some open or driven systems that fail to thermalize at late times [164–168], where algebraic approaches were also widely used. Finally, it would also be interesting to extend the notion of integrable boundary states to such systems and construct models that exhibit non-thermalizing dynamics. In this respect, dissipative systems described by integrable Lindblad superoperators [169–173] and integrable Floquet systems [174–177] may serve as a good starting point for constructing concrete examples.



SUPPLEMENTAL MATERIALS FOR CHAPTER 3

A.1 Zero energy states of C_{SC}

In this section, we prove that $|\bar{A}_n\rangle$, $|\bar{B}_n\rangle$, and $|K_{0,p}\rangle$ are annihilated by C_{SC} . We also derive a lower bound on the number of zero-energy states of C_{SC} .

A.1.1 $C_{\text{SC}}|\bar{A}_n\rangle = 0$

To prove $C_{\text{SC}}|\bar{A}_n\rangle = 0$, we first prove the following:

Theorem A.1. *Consider C_{SC} with an even number of sites L . Then the following relations hold:*

$$C_{\text{SC}}\mathcal{O}_{\pi}^{-}|\uparrow\rangle = 0, \quad (\text{A.1})$$

$$C_{\text{SC}}(\mathcal{O}_{\pi}^{-})^2|\uparrow\rangle = 0, \quad (\text{A.2})$$

$$[\mathcal{O}_{\pi}^{-}, [\mathcal{O}_{\pi}^{-}, [\mathcal{O}_{\pi}^{-}, C_{\text{SC}}]]] = 0. \quad (\text{A.3})$$

Proof. We first prove Eq. (A.1). We can write $\mathcal{O}_{\pi}^{-}|\uparrow\rangle$ in the S^z basis as

$$\mathcal{O}_{\pi}^{-}|\uparrow\rangle = \sqrt{2} \sum_{j=1}^L (-1)^j |j\rangle, \quad (\text{A.4})$$

where we have used the short-hand notation $|j\rangle := |+\cdots+0_j+\cdots+\rangle$. Then we find $C_{\text{SC}}|j\rangle = i(|j-2\rangle - |j+2\rangle)$, which yields

$$C_{\text{SC}}\mathcal{O}_{\pi}^{-}|\uparrow\rangle = \sqrt{2}i \sum_{j=1}^L (-1)^j (|j-2\rangle - |j+2\rangle) = 0. \quad (\text{A.5})$$

We can also see this as follows. First note that $C_{\text{SC}}\mathcal{O}_{\pi}^{-}|\uparrow\rangle$ is odd under the site-centered inversion \mathcal{I}_s . We then note that it is invariant under translation by two sites \mathcal{T}^2 . However, there is no single-magnon state (a linear combination of $|j\rangle$) that is compatible with these constraints. Thus, $C_{\text{SC}}\mathcal{O}_{\pi}^{-}|\uparrow\rangle$ must vanish identically.

Next, we consider Eq. (A.2). By acting on $|\uparrow\rangle$ with \mathcal{O}_{π}^{-} twice, we get

$$(\mathcal{O}_{\pi}^{-})^2|\uparrow\rangle = 2 \left(2 \sum_{1 \leq j < k \leq L} (-1)^{j+k} |j, k\rangle + \sum_{j=1}^L |\bar{j}\rangle \right), \quad (\text{A.6})$$

where $|j, k\rangle := |+\cdots+0_j+\cdots+0_k+\cdots+\rangle$ and $|\bar{j}\rangle := |+\cdots+-_j+\cdots+\rangle$. We can rewrite the first term as

$$\sum_{j < k} (-1)^{j+k} |j, k\rangle = \sum_{j=1}^L \left(\sum_{r=1}^{L/2-1} (-1)^r |j, j+r\rangle + (-1)^{\frac{L}{2}} \left| j, j + \frac{L}{2} \right\rangle \right). \quad (\text{A.7})$$

We now examine the action of C_{SC} on $|j, j+r\rangle$. For $r \geq 3$, we get

$$C_{\text{SC}}|j, j+r\rangle = i(|j-2, j+r\rangle - |j+2, j+r\rangle + |j, j+r-2\rangle - |j, j+r+2\rangle) \quad (r \geq 3). \quad (\text{A.8})$$

Therefore, we obtain

$$C_{\text{SC}} \sum_{j=1}^L |j, j+r\rangle = 0 \quad (r \geq 3). \quad (\text{A.9})$$

Next, we consider the case with $r = 2$. In this case, the action of C_{SC} is

$$\begin{aligned} C_{\text{SC}}|j, j+2\rangle = & i(|j-2, j+2\rangle - 2|j-1, j+2\rangle + |j+1, j+2\rangle + |\bar{j}\rangle \\ & - |\overline{j+2}\rangle + 2|j, j+3\rangle - |j, j+1\rangle - |j, j+4\rangle), \end{aligned} \quad (\text{A.10})$$

which yields

$$C_{\text{SC}} \sum_{j=1}^L |j, j+2\rangle = 0. \quad (\text{A.11})$$

Similarly, for $|j, j+1\rangle$, we obtain

$$C_{\text{SC}}|j, j+1\rangle = i(|j-2, j+1\rangle - |j-1, j+1\rangle + 2|\overline{j+1}\rangle - 2|\bar{j}\rangle + |j, j+2\rangle - |j, j+3\rangle). \quad (\text{A.12})$$

Thus, we have

$$\sum_{j=1}^L C_{\text{SC}}|j, j+1\rangle = 0. \quad (\text{A.13})$$

We next examine $|\bar{j}\rangle$. Acting with C_{SC} on $|\bar{j}\rangle$, we obtain

$$C_{\text{SC}}|\bar{j}\rangle = i(|j-2, j\rangle - 2|j-1, j\rangle + 2|j, j+1\rangle + |j, j+2\rangle). \quad (\text{A.14})$$

Thus, we have

$$\sum_{j=1}^L C_{\text{SC}} |\bar{j}\rangle = 0. \quad (\text{A.15})$$

Putting this all together, we get

$$C_{\text{SC}}(\mathcal{O}_\pi^-)^2 |\uparrow\rangle = 0. \quad (\text{A.16})$$

Finally, we consider Eq. (A.3). Since C_{SC} is a sum of terms of the form $S_j^\alpha S_{j+1}^\beta S_{j+2}^\gamma$ ($\{\alpha, \beta, \gamma\} = \{+, -, z\}$) and \mathcal{O}_π^- is a linear combination of S_k^- , the nested commutator $[\mathcal{O}_\pi^-, [\mathcal{O}_\pi^-, [\mathcal{O}_\pi^-, C_{\text{SC}}]]]$ is a sum of $S_j^- S_{j+1}^- S_{j+2}^-$. Let $O_j^{\alpha\beta\gamma} := [\mathcal{O}_\pi^-, [\mathcal{O}_\pi^-, [\mathcal{O}_\pi^-, S_j^\alpha S_{j+1}^\beta S_{j+2}^\gamma]]]$ for $\{\alpha, \beta, \gamma\} = \{+, -, z\}$, we obtain

$$\begin{aligned} O_j^{+-z} &= 3[\mathcal{O}_\pi^-, [\mathcal{O}_\pi^-, S_j^+]] S_{j+1}^- [\mathcal{O}_\pi^-, S_{j+2}^z] \\ &= 3 \cdot (-2) \cdot (-1)^{2j} S_j^- \cdot S_{j+1}^- \cdot (-1)^{j+2} S_{j+2}^- \end{aligned} \quad (\text{A.17})$$

$$= -6(-1)^{j+2} S_j^- S_{j+1}^- S_{j+2}^-, \quad (\text{A.18})$$

$$\begin{aligned} O_j^{-+z} &= 3S_j^- [\mathcal{O}_\pi^-, [\mathcal{O}_\pi^-, S_{j+1}^+]] [\mathcal{O}_\pi^-, S_{j+2}^z] \\ &= 3 \cdot S_j^- \cdot (-2) \cdot (-1)^{2(j+1)} S_{j+1}^- \cdot (-1)^{j+2} S_{j+2}^- \end{aligned} \quad (\text{A.19})$$

$$= -6(-1)^{j+2} S_j^- S_{j+1}^- S_{j+2}^-. \quad (\text{A.20})$$

Hence, $O_j^{+-z} = O_j^{-+z}$. Similarly, one can show that $O_j^{-z+} = O_j^{+z-}$ and $O_j^{z+-} = O_j^{z-+}$. Therefore, we have

$$[\mathcal{O}_\pi^-, [\mathcal{O}_\pi^-, [\mathcal{O}_\pi^-, C_{\text{SC}}]]] = \frac{i}{2} \sum_{j=1}^L \sum_{\alpha, \beta, \gamma} \tau_{\alpha\beta\gamma} O_j^{\alpha\beta\gamma} = 0. \quad (\text{A.21})$$

□

From Theorem A.1, $C_{\text{SC}} |\bar{A}_n\rangle = 0$ follows immediately.

A.1.2 $C_{\text{SC}} |\bar{B}_n\rangle = 0$

Next we prove that $C_{\text{SC}} |\bar{B}_n\rangle = 0$. To this end, we first prove the following:

Theorem A.2. *The following relations are true.*

$$[\mathcal{Q}_0^-, C_{\text{SC}}] |\uparrow\rangle = 0, \quad (\text{A.22})$$

$$[\mathcal{Q}_0^-, [\mathcal{Q}_0^-, C_{\text{SC}}]] |\uparrow\rangle = 0, \quad (\text{A.23})$$

$$[\mathcal{Q}_0^-, [\mathcal{Q}_0^-, [\mathcal{Q}_0^-, C_{\text{SC}}]]] = 0. \quad (\text{A.24})$$

Proof. We consider the coherent state $|\beta\rangle$, which can be written as

$$|\beta\rangle \propto e^{\beta \mathcal{Q}_0^-} |\uparrow\rangle = \prod_{j=1}^L (1 + \beta (S_j^-)^2) |\uparrow\rangle = \bigotimes_{j=1}^L |\psi_\beta\rangle_j, \quad (\text{A.25})$$

where $|\psi_\beta\rangle_j = |+\rangle_j + 2\beta|-\rangle_j$. One can prove that $|\beta\rangle$ is annihilated by C_{SC} . This can be seen as follows. First note that $S_j^+ |\psi_\beta\rangle_j = 2\sqrt{2}\beta|0\rangle_j$ and $S_j^- |\psi_\beta\rangle_j = \sqrt{2}|0\rangle_j$, and hence $(S_j^+ S_k^- - S_j^- S_k^+) |\psi_\beta\rangle_j \otimes |\psi_\beta\rangle_k = 0$. Next, we note that each summand of C_{SC} can be cast in the form:

$$\begin{aligned} & \mathbf{S}_j \cdot (\mathbf{S}_{j+1} \times \mathbf{S}_{j+2}) \\ &= \frac{i}{2} \left\{ (S_j^+ S_{j+1}^- - S_j^- S_{j+1}^+) S_{j+2}^z + (S_{j+1}^+ S_{j+2}^- - S_{j+1}^- S_{j+2}^+) S_j^z + (S_{j+2}^+ S_j^- - S_{j+2}^- S_j^+) S_{j+1}^z \right\}. \end{aligned} \quad (\text{A.26})$$

From this, it is clear that each summand annihilates $|\beta\rangle$, and hence $C_{\text{SC}} e^{\beta Q_0^-} |\uparrow\rangle = 0$. Acting with $e^{-\beta Q_0^-}$ from the left on both sides of this equation and expanding it by the Baker-Campbell-Hausdorff formula, we have

$$\left(C_{\text{SC}} - \beta [Q_0^-, C_{\text{SC}}] + \frac{\beta^2}{2} [Q_0^-, [Q_0^-, C_{\text{SC}}]] + \dots \right) |\uparrow\rangle = 0, \quad (\text{A.27})$$

which proves Eqs. (A.22) and (A.23) since $\beta \in \mathbb{C}$ can be taken arbitrarily.

Finally, we show Eq. (A.24). Let $Q_j^{\alpha\beta\gamma} = [Q_0^-, [Q_0^-, [Q_0^-, S_j^\alpha S_{j+1}^\beta S_{j+2}^\gamma]]]$ ($\alpha, \beta, \gamma = +, -, \text{ or } z$). Then, we obtain

$$\begin{aligned} Q_j^{+-z} &= 3[Q_0^-, [Q_0^-, S_j^+]] S_{j+1}^- [Q_0^-, S_{j+2}^z] \\ &= 3 \cdot (-8(S_j^-)^3) \cdot S_{j+1}^- \cdot 2(S_{j+2}^-)^2 = 0. \end{aligned} \quad (\text{A.28})$$

In the same way, one can show $Q_j^{-+z} = Q_j^{-z+} = Q_j^{+z-} = Q_j^{z+-} = Q_j^{z-+} = 0$. Therefore,

$$[Q_0^-, [Q_0^-, [Q_0^-, C_{\text{SC}}]]] = \frac{i}{2} \sum_{j=1}^L \sum_{\alpha, \beta, \gamma} \tau_{\alpha\beta\gamma} Q_j^{\alpha\beta\gamma} = 0. \quad (\text{A.29})$$

□

From Theorem A.2, $C_{\text{SC}} |\bar{B}_n\rangle = 0$ follows immediately.

A.1.3 $C_{\text{SC}} |K_{0,p}\rangle = 0$

Here we prove that $C_{\text{SC}} |K_{0,p}\rangle = 0$. From Eq. (3.10), each $|K_{0,p}\rangle$ can be expressed as a linear combination of $|\Phi_n\rangle = \sum_{j=1}^L |j, j+n\rangle$, where $n = 0, 1, \dots, \lfloor L/2 \rfloor$ and $|j, j\rangle = |\bar{j}\rangle$. However, it has already been shown by Eqs. (A.9), (A.11), (A.13), and (A.15) that these states are annihilated by C_{SC} . Therefore, $|K_{0,p}\rangle$ are zero-energy states of C_{SC} .

A.1.4 Lower bound on the number of zero-energy states

In this subsection, we derive a lower bound on the number of zero-energy states of C_{SC} . We follow the argument in Ref. [60], where the authors obtained a lower bound on the

number of zero-energy states of the PXP model. The key point is that the site-centered inversion \mathcal{I}_s anticommutes with the Hamiltonian C_{SC} in Eq. (3.1), i.e., $\mathcal{I}_s C_{\text{SC}} = -C_{\text{SC}} \mathcal{I}_s$.

Let \mathcal{H} be the Hilbert space of a spin-1 chain of length L . This Hilbert space can be decomposed as $\mathcal{H} = \mathcal{K}_e \oplus \mathcal{K}_o$, where $\mathcal{K}_e = \{|\psi\rangle \in \mathcal{H} \mid \mathcal{I}_s |\psi\rangle = |\psi\rangle\}$ and $\mathcal{K}_o = \{|\psi\rangle \in \mathcal{H} \mid \mathcal{I}_s |\psi\rangle = -|\psi\rangle\}$. It follows from $\{\mathcal{I}_s, C_{\text{SC}}\} = 0$ that if $|\psi\rangle \in \mathcal{K}_{e/o}$ then $C_{\text{SC}} |\psi\rangle \in \mathcal{K}_{o/e}$. Therefore, C_{SC} can be written in block-matrix form as

$$C_{\text{SC}} = \begin{pmatrix} O & D_{\text{SC}}^\dagger \\ D_{\text{SC}} & O \end{pmatrix}. \quad (\text{A.30})$$

Here the operator D_{SC} can be regarded as a linear map from \mathcal{K}_e to \mathcal{K}_o . Let $\text{Im } D_{\text{SC}}$ and $\text{Ker } D_{\text{SC}}$ be the image and kernel of D_{SC} , respectively. It is clear that if $|\psi\rangle \in \text{Ker } D_{\text{SC}}$, then $|\psi\rangle$ is annihilated by C_{SC} . Thus, the dimension of $\text{Ker } D_{\text{SC}}$ gives a lower bound on the number of zero-energy states. We now apply the rank-nullity theorem to estimate $\dim \text{Ker } D_{\text{SC}}$. The theorem implies that

$$\dim \text{Im } D_{\text{SC}} + \dim \text{Ker } D_{\text{SC}} = \dim \mathcal{K}_e, \quad (\text{A.31})$$

Since $\dim \text{Im } D_{\text{SC}} \leq \dim \mathcal{K}_o$, we have

$$\dim \text{Ker } D_{\text{SC}} \geq \dim \mathcal{K}_e - \dim \mathcal{K}_o, \quad (\text{A.32})$$

which gives a lower bound on the number of zero-energy states.

Before deriving a general expression for the RHS of Eq. (A.32), let us consider a simple example that illustrates the strategy. For $L = 3$, the Hilbert space \mathcal{H} is spanned by 27 states. Consider the inversion about site 2. Then \mathcal{K}_e is spanned by the states of the forms $|s_1, s_2, s_1\rangle$ and $|s_1, s_2, s_3\rangle + |s_3, s_2, s_1\rangle$ ($s_1 < s_3$). The number of these states amounts to $9 + 9 = 18$. On the other hand, \mathcal{K}_o is spanned by the states of the form $|s_1, s_2, s_3\rangle - |s_3, s_2, s_1\rangle$ ($s_1 < s_3$), the number of which amounts to 9. Thus, $\dim \mathcal{K}_e - \dim \mathcal{K}_o = 9$.

The above example clearly illustrates that the difference between the dimensions of even and odd subspaces counts the number of product states invariant under \mathcal{I}_s . Let \mathcal{N}_L be the number of such states for the L -site system. Let \mathcal{Z}_L be the exact number of zero-energy states of C_{SC} . It is easy to see that $\mathcal{N}_L = 3^{\frac{L+1}{2}}$ for L odd and $\mathcal{N}_L = 3^{\frac{L+2}{2}}$ for L even. These results can be summarized as $\mathcal{Z}_L \geq \mathcal{N}_L = 3^{\lfloor \frac{L}{2} \rfloor + 1}$, which proves that \mathcal{Z}_L grows exponentially with the system size. Table A.1 shows the comparison between \mathcal{Z}_L obtained by exact diagonalization and the bound \mathcal{N}_L . Clearly, \mathcal{Z}_L grows more rapidly than \mathcal{N}_L . We expect that a better lower bound can be obtained by considering other symmetries of the Hamiltonian, but leave this possibility for future work. We note in passing that a lower bound on \mathcal{Z}_L for general spin quantum number σ can also be derived in a similar manner; the result is $\mathcal{Z}_L \geq (2\sigma + 1)^{\lfloor \frac{L}{2} \rfloor + 1}$.

L	3	4	5	6	7	8	9	10	11
\mathcal{Z}_L	11	35	45	127	141	435	473	1451	1553
\mathcal{N}_L	9	27	27	81	81	243	243	729	729

 Table A.1: The number of zero-energy states (\mathcal{Z}_L) and the bound (\mathcal{N}_L) up to $L = 11$ sites.

A.2 Proof of $C_{\text{SC}} |\Psi_{\text{VBS}}\rangle = 0$

In this section, we show

$$C_{\text{SC}} |\Psi_{\text{VBS}}\rangle = 0. \quad (\text{A.33})$$

First, we rewrite $|\Psi_{\text{VBS}}\rangle$ as

$$|\Psi_{\text{VBS}}\rangle = 3^{-L/2} \text{Tr}[A_1 A_2 \cdots A_L], \quad A_j = \begin{pmatrix} |0\rangle_j & -\sqrt{2}|+\rangle_j \\ \sqrt{2}|-\rangle_j & -|0\rangle_j \end{pmatrix}. \quad (\text{A.34})$$

Next, we introduce a convenient representation of C_{SC} :

$$\mathbf{S}_j \cdot (\mathbf{S}_{j+1} \times \mathbf{S}_{j+2}) = \frac{i}{2} \tau_{\alpha\beta\gamma} S_j^\alpha S_{j+1}^\beta S_{j+2}^\gamma, \quad (\text{A.35})$$

where $\alpha, \beta, \gamma \in \{+, -, z\}$ and τ is the totally anti-symmetric tensor with $\tau_{+-z} = 1$. Then, by acting on $|\Psi_{\text{VBS}}\rangle$ with each term, we obtain

$$\tau_{\alpha\beta\gamma} S_j^\alpha S_{j+1}^\beta S_{j+2}^\gamma |\Psi_{\text{VBS}}\rangle = 3^{-L/2} \text{Tr}[A_1 \cdots A_{j-1} B_{j,j+1,j+2}^{\alpha\beta\gamma} A_{j+3} \cdots], \quad (\text{A.36})$$

where

$$B_{j,j+1,j+2}^{+-z} = \sqrt{2} \begin{pmatrix} |+-\rangle & -|-+-\rangle \\ 2|00-\rangle - |+-\rangle & -\sqrt{2}|0-\rangle \end{pmatrix}, \quad (\text{A.37})$$

$$B_{j,j+1,j+2}^{+z-} = \sqrt{2} \begin{pmatrix} 0 & -|++-\rangle \\ -|+-\rangle & \sqrt{2}(|+-\rangle - |0+-\rangle) \end{pmatrix}, \quad (\text{A.38})$$

$$B_{j,j+1,j+2}^{-z+} = \sqrt{2} \begin{pmatrix} \sqrt{2}(|0-\rangle - |-+0\rangle) & |-++\rangle \\ |--\rangle & 0 \end{pmatrix}, \quad (\text{A.39})$$

$$B_{j,j+1,j+2}^{-+z} = \sqrt{2} \begin{pmatrix} \sqrt{2}|0+-\rangle & |-++\rangle - 2|00+\rangle \\ |+-\rangle & -\sqrt{2}|-0+\rangle \end{pmatrix}, \quad (\text{A.40})$$

$$B_{j,j+1,j+2}^{z+-} = \sqrt{2} \begin{pmatrix} -\sqrt{2}|+0-\rangle & 2|+00\rangle - |++-\rangle \\ -|-+-\rangle & \sqrt{2}|-+0\rangle \end{pmatrix}, \quad (\text{A.41})$$

$$B_{j,j+1,j+2}^{z-+} = \sqrt{2} \begin{pmatrix} -\sqrt{2}|+-0\rangle & |+-+\rangle \\ |--\rangle - 2|-00\rangle & \sqrt{2}|-0+\rangle \end{pmatrix}, \quad (\text{A.42})$$

and $B_{j,j+1,j+2}^{\alpha\beta\gamma} = 0$ for any other choice of (α, β, γ) . Therefore, we obtain

$$\mathbf{S}_j \cdot (\mathbf{S}_{j+1} \times \mathbf{S}_{j+2}) |\Psi_{\text{VBS}}\rangle = 3^{-L/2} \text{Tr}[A_1 \cdots A_{j-1} B_{j,j+1,j+2} A_{j+3} \cdots], \quad (\text{A.43})$$

where

$$\begin{aligned}
 B_{j,j+1,j+2} &= \frac{i}{2} \sum_{\alpha,\beta,\gamma \in \{+,-,z\}} B_{j,j+1,j+2}^{\alpha\beta\gamma} \\
 &= i \begin{pmatrix} |0 - +\rangle - |- + 0\rangle + |0 + -\rangle - |+ - 0\rangle & \sqrt{2}(|+00\rangle - |00+\rangle + |- + +\rangle - |+ + -\rangle) \\ \sqrt{2}(|00-\rangle - |-00\rangle + |- - +\rangle - |+ - -\rangle) & |+ - 0\rangle + |- + 0\rangle - |0 - +\rangle - |0 + -\rangle \end{pmatrix}.
 \end{aligned} \tag{A.44}$$

Then, we can decompose $B_{j,j+1,j+2}$ into

$$B_{j,j+1,j+2} = A_j C_{j+1,j+2} - C_{j,j+1} A_{j+2}, \tag{A.45}$$

where

$$C_{j,j+1} = i \begin{pmatrix} |+ -\rangle + |- +\rangle - |00\rangle & 0 \\ 0 & |+ -\rangle + |- +\rangle - |00\rangle \end{pmatrix} \tag{A.46}$$

Therefore, we have

$$\begin{aligned}
 C_{\text{SC}} |\Psi_{\text{VBS}}\rangle &= 3^{-L/2} \sum_{j=1}^L \{ \text{Tr}[A_1 \cdots A_{j-1} A_j C_{j+1,j+2} A_{j+3} \cdots A_L] \\
 &\quad - \text{Tr}[A_1 \cdots A_{j-1} C_{j,j+1} A_{j+2} A_{j+3} \cdots A_L] \} \\
 &= 0.
 \end{aligned} \tag{A.47}$$

SUPPLEMENTAL MATERIALS FOR CHAPTER 4

B.1 Proof that $|\Psi_{\text{VBS}}\rangle$ is an integrable boundary state

In this section, we prove that the VBS state $|\Psi_{\text{VBS}}\rangle$ in Eq. (2.45) is an integrable boundary state of the Sutherland model [137]. The Hamiltonian of the model is defined as

$$H_S = - \sum_{i=1}^L (P_{i,i+1} - 1), \quad (\text{B.1})$$

commuting with H_3 in Sec. 4.3. The quantum integrability of the model can be summarized by the transfer matrix $T(\lambda)$,

$$T(\lambda) = \text{Tr}_a \left(\prod_{j=1}^L R_{a,j}(\lambda) \right), \quad (\text{B.2})$$

with the R matrix

$$R_{a,j}(\lambda) = \frac{1}{\lambda + i} (\lambda + iP_{a,j}) \quad (\text{B.3})$$

satisfying the celebrated Yang–Baxter equation. The sub-index a stands for the 3-dimensional auxiliary space, which is traced over in Eq. (B.2), resulting in an operator acting only on the physical Hilbert space. From the Yang–Baxter equation, it is easy to deduce that $T(\lambda)$ is in involution,

$$[T(\lambda), T(\mu)] = 0, \quad \forall \lambda, \mu \in \mathbb{C}. \quad (\text{B.4})$$

Moreover, we have

$$H_S = -i \frac{\partial}{\partial \lambda} \log T(\lambda) \Big|_{\lambda=0}, \quad H_3 = -2i \frac{\partial^2}{\partial \lambda^2} \log T(\lambda) \Big|_{\lambda=0}. \quad (\text{B.5})$$

As shown in [63], for an integrable boundary state $|\Psi_0\rangle$ with even system size L ,

$$Q_{2k+1}|\Psi_0\rangle = 0 \quad (k = 1, 2, \dots) \quad \Leftrightarrow \quad T(\lambda)|\Psi_0\rangle = \mathcal{I}_b T(\lambda) \mathcal{I}_b |\Psi_0\rangle, \quad (\text{B.6})$$

where \mathcal{I}_b is the spatial inversion operator such that

$$\mathcal{I}_b = \prod_{j=1}^{L/2} P_{j,L-j+1}. \quad (\text{B.7})$$

Our aim is to show that the VBS state $|\Psi_{\text{VBS}}\rangle$ satisfies the condition (B.6) with the Sutherland model transfer matrix. To begin with, for any similarity transformation with local density,

$$U = \prod_{j=1}^L u_j, \quad (\text{B.8})$$

the transfer matrix $T(\lambda)$ commutes with it, i.e.,

$$UT(\lambda)U^{-1} = \text{Tr}_a \left(\prod_{j=1}^L u_j R_{a,j}(\lambda) u_j^{-1} \right) = \text{Tr}_a \left(\prod_{j=1}^L u_a^{-1} R_{a,j}(\lambda) u_a \right) = T(\lambda), \quad (\text{B.9})$$

using (B.3). We choose the similarity transformation to be

$$u_j = \frac{1}{\sqrt{2}} \begin{pmatrix} 1 & i & 0 \\ 0 & 0 & -\sqrt{2} \\ -1 & i & 0 \end{pmatrix}_j, \quad (\text{B.10})$$

such that after acting with U^{-1} on $|\Psi_{\text{VBS}}\rangle$, we get [63]

$$U^{-1} |\Psi_{\text{VBS}}\rangle = 3^{-L/2} |\Psi_0\rangle, \quad |\Psi_0\rangle = \sum_{\{s\}} \text{Tr} [B_{s_1} B_{s_2} \cdots B_{s_L}] |s_1, s_2, \cdots s_L\rangle, \quad (\text{B.11})$$

where

$$B_+ = \sigma^x, \quad B_0 = \sigma^y, \quad B_- = \sigma^z. \quad (\text{B.12})$$

Acting on $|\Psi_0\rangle$ with the parity operator, we have

$$\mathcal{I}_b |\Psi_0\rangle = \sum_{\{s\}} \text{Tr} [B_{s_1}^T B_{s_2}^T \cdots B_{s_L}^T] |s_1, s_2, \cdots s_L\rangle = \sum_{\{s\}} (-1)^{n_0} \text{Tr} [B_{s_1} B_{s_2} \cdots B_{s_L}] |s_1, s_2, \cdots s_L\rangle, \quad (\text{B.13})$$

where the superscript T denotes transpose and n_0 counts the number of spin 0 in state $|s_1, s_2, \cdots s_L\rangle$. Since the transfer matrix $T(\lambda)$ is a matrix product operator, we can express the state

$$T(\lambda) \text{Tr} [B_{s_1} B_{s_2} \cdots B_{s_L}] |s_1, s_2, \cdots s_L\rangle = \text{Tr} [C_{s_1} C_{s_2} \cdots C_{s_L}] |s_1, s_2, \cdots s_L\rangle, \quad (\text{B.14})$$

where the matrices C_s ($s = +, 0, -$) are 6-dimensional. In addition, one can show that there exists a similarity transformation V such that

$$C_{\pm}^T = VC_{\pm}V^{-1}, \quad C_0^T = -VC_0V^{-1}, \quad (\text{B.15})$$

i.e.

$$\begin{aligned} \mathcal{I}_b \text{Tr}[C_{s_1}C_{s_2}\cdots C_{s_L}]|s_1, s_2, \cdots s_L\rangle &= \text{Tr}[C_{s_1}^T C_{s_2}^T \cdots C_{s_L}^T]|s_1, s_2, \cdots s_L\rangle \\ &= (-1)^{n_0} \text{Tr}[C_{s_1}C_{s_2}\cdots C_{s_L}]|s_1, s_2, \cdots s_L\rangle. \end{aligned} \quad (\text{B.16})$$

We are now ready to show that $|\Psi_0\rangle$ is an integrable boundary state. Using Eqs. (B.13), (B.14), and (B.16), we have

$$\begin{aligned} \mathcal{I}_b T(\lambda) \mathcal{I}_b |\Psi_0\rangle &= \mathcal{I}_b \sum_{\{s\}} (-1)^{n_0} \text{Tr}[C_{s_1}C_{s_2}\cdots C_{s_L}]|s_1, s_2, \cdots s_L\rangle \\ &= \sum_{\{s\}} (-1)^{2n_0} \text{Tr}[C_{s_1}C_{s_2}\cdots C_{s_L}]|s_1, s_2, \cdots s_L\rangle \\ &= T(\lambda)|\Psi_0\rangle. \end{aligned} \quad (\text{B.17})$$

From this, we find

$$\mathcal{I} T(\lambda) \mathcal{I} |\Psi_{\text{VBS}}\rangle = 3^{-L/2} U \mathcal{I} T(\lambda) \mathcal{I} |\Psi_0\rangle = 3^{-L/2} U T(\lambda) |\Psi_0\rangle = T(\lambda) |\Psi_{\text{VBS}}\rangle, \quad (\text{B.18})$$

which shows that the VBS state is an integrable boundary state of the Sutherland model.

B.2 SU(2) symmetry of H_3

In this section, we provide a proof that H_3 in (4.26) has global SU(2) symmetry. As in the main text, we define the total spin operators by $\mathcal{S}^\alpha = \sum_{j=1}^L S_j^\alpha$ ($\alpha = x, y, z$), where S_j^α is the spin-1 operator at site j in Eq. (3.2). They are the generators of the global SU(2), i.e., for any $U \in \text{SU}(2)$ there exists $\{\theta_\alpha\}$ such that $U = \exp\left(i \sum_{\alpha \in \{x, y, z\}} \theta_\alpha \mathcal{S}^\alpha\right)$. Any U can be decomposed into $U = 1 + X$, where X is a polynomial in $\{\mathcal{S}^x, \mathcal{S}^y, \mathcal{S}^z\}$. Thus, to prove that $[H_3, U] = 0$ for all $U \in \text{SU}(2)$, it suffices to show $[H_3, \mathcal{S}^\alpha] = 0$ for all $\alpha \in \{x, y, z\}$.

For simplicity, we introduce the SU(3) generators $T^a := \lambda^a/2$ satisfying $[T^a, T^b] = i f_{abc} T^c$, in terms of which $H_3/8$ is written as

$$\frac{1}{8} H_3 = \sum_{j=1}^L f_{abc} T_j^a T_{j+1}^b T_{j+2}^c, \quad (\text{B.19})$$

where the summation over repeated indices a, b , and c is implied. Due to the tracelessness of the SU(2) generators, S_j^x, S_j^y , and S_j^z can be written as linear combinations of the SU(3)

generators. By $\text{Tr}[T^a T^b] = \frac{1}{2} \delta_{ab}$ [178], we have $S_j^\alpha = 2 \text{Tr}_j[S_j^\alpha T_j^u] T_j^u$. Now we calculate the commutator

$$\frac{1}{8} \left[H_3, \sum_{k=1}^L T_k^u \right] = \left[\sum_{j=1}^L f_{abc} T_j^a T_{j+1}^b T_{j+2}^c, \sum_{k=1}^L T_k^u \right] \quad (\text{B.20})$$

$$= \sum_{j=1}^L f_{abc} \left([T_j^a, T_j^u] T_{j+1}^b T_{j+2}^c + T_j^a [T_{j+1}^b, T_{j+1}^u] T_{j+2}^c + T_j^a T_{j+1}^b [T_{j+2}^c, T_{j+2}^u] \right) \quad (\text{B.21})$$

$$= i \sum_{j=1}^L f_{abc} \left(f_{auv} T_j^v T_{j+1}^b T_{j+2}^c + f_{buv} T_j^a T_{j+1}^v T_{j+2}^c + f_{cuv} T_j^a T_{j+1}^b T_{j+2}^v \right) \quad (\text{B.22})$$

$$= i \sum_{j=1}^L \underbrace{(f_{vbc} f_{vua} + f_{avc} f_{vub} + f_{abv} f_{vuc})}_{(*)} T_j^a T_{j+1}^b T_{j+2}^c. \quad (\text{B.23})$$

Then it follows from the Jacobi identity that $(*) = 0$, which yields the desired result $[H_3, S^\alpha] = 0$ ($\alpha = x, y, z$), i.e., the global $\text{SU}(2)$ symmetry of H_3 .

B.3 Eigenenergy of ferromagnetic states

In this section, we compute the energy of the ferromagnetic states, which are eigenstates of the Hamiltonian $H(t)$ in Eq. (4.24). The ferromagnetic states are defined as $|F_n\rangle = (\mathcal{S}^-)^n |F_0\rangle$, where $|F_0\rangle = |++\cdots+\rangle$ and $0 \leq n \leq 2L$. Because H_{AKLT} and H_3 commute with \mathcal{S}^- (see Appendix B.2), all ferromagnetic states $|F_n\rangle$ have the same energy. Thus it suffices to consider the energy of $|F_0\rangle$.

Since $|F_0\rangle$ is invariant under any permutation, we have $P_{j,j+1,j+2} |F_0\rangle = P_{j,j+1,j+2}^\dagger |F_0\rangle = |F_0\rangle$. Thus we obtain

$$H_3 |F_0\rangle = \sum_{j=1}^L (P_{j,j+1,j+2} - P_{j,j+1,j+2}^\dagger) |F_0\rangle = 0, \quad (\text{B.24})$$

and hence $H_3 |F_n\rangle = H_3 |F_0\rangle = 0$ for all n . Moreover, since $(\mathbf{S}_j \cdot \mathbf{S}_{j+1}) |F_0\rangle = |F_0\rangle$ for all j , we obtain

$$H_{\text{AKLT}} |F_0\rangle = \sum_{j=1}^L \left[1 + \frac{1}{3} + \frac{2}{3} \right] |F_0\rangle = 2L |F_0\rangle. \quad (\text{B.25})$$

Therefore, the ferromagnetic states are eigenstates of $H(t)$ with eigenvalue $2L$. A similar calculation shows that the eigenenergy of the ferromagnetic states in the inhomogeneous model (4.37) is $2 \sum_j c_j$.

B.4 Proof that tilted-Néel states are integrable boundary states

In this section, we prove that the tilted-Néel states are integrable boundary states. Let us fix $\eta, \tau \in \mathbb{C}$ with $\text{Im}\{\tau\} > 0$ ¹, the R -matrix of XYZ model is given as [179, 180]

$$R(u) = \begin{pmatrix} a(u) & & & d(u) \\ & b(u) & c(u) & \\ & c(u) & b(u) & \\ d(u) & & & a(u) \end{pmatrix}, \quad (\text{B.26})$$

with

$$a(u) = \frac{\theta_4(\eta|2\tau)\theta_1(u + \eta|2\tau)}{\theta_1(\eta|2\tau)\theta_4(u + \eta|2\tau)}, \quad (\text{B.27})$$

$$b(u) = \frac{\theta_4(\eta|2\tau)\theta_1(u|2\tau)}{\theta_1(\eta|2\tau)\theta_4(u|2\tau)}, \quad (\text{B.28})$$

$$c(u) = 1, \quad (\text{B.29})$$

$$d(u) = \frac{\theta_1(u + \eta|2\tau)\theta_1(\eta|2\tau)}{\theta_4(u + \eta|2\tau)\theta_4(\eta|2\tau)}, \quad (\text{B.30})$$

where $\theta_{1,4}$ are the Jacobi theta functions [181]. This R -matrix satisfies the regularization condition $R_{i,j}(u = 0) = P_{i,j}$, where $R_{i,j}$ is the R -matrix acting on $\mathcal{H}_i \otimes \mathcal{H}_j$ and $P_{i,j}$ is a permutation operator such that $P_{i,j}(|x\rangle_i \otimes |y\rangle_j) = |y\rangle_i \otimes |x\rangle_j$.

This R -matrix satisfies the following Yang-Baxter equation (Figure B.1):

$$R_{1,2}(u - v)R_{1,3}(u)R_{2,3}(v) = R_{2,3}(v)R_{1,3}(u)R_{1,2}(u - v). \quad (\text{B.31})$$

From this R -matrix, we can define the transfer matrix T :

$$T(u) = \text{Tr}_a \left[\prod_{j=1}^{\overleftarrow{L}} R_{a,j} \left(u - \frac{\eta}{2} \right) \right], \quad (\text{B.32})$$

where the product is defined as $\overleftarrow{\prod}_{j=1}^L A_j := A_L A_{L-1} \cdots A_1$. Taking the derivative of the logarithm of this transfer matrix yields the Hamiltonian and higher-order conserved charges:

$$Q_n = \partial_u^{(n-1)} \log T(u)|_{u=\frac{\eta}{2}}, \quad (\text{B.33})$$

$$H \propto \partial_u \log T(u)|_{u=\frac{\eta}{2}} \propto Q_2. \quad (\text{B.34})$$

Then we can translate the statement we want to prove in the language of the transfer matrix:

¹ η and τ are defined from the ratio of the model parameters J_x, J_y and J_z .

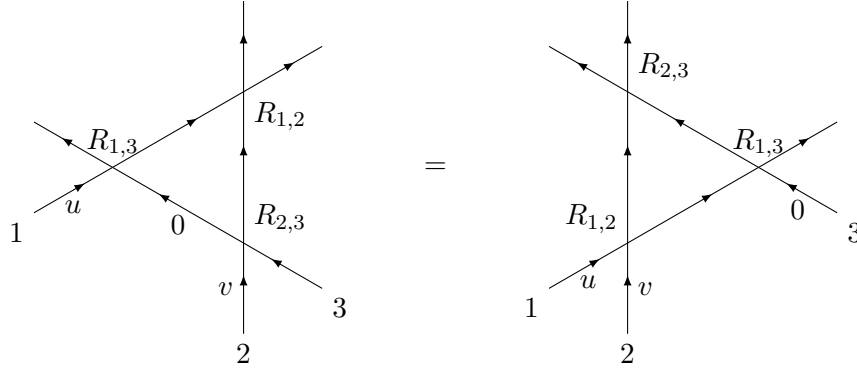


Figure B.1: Graphical representation of the Yang-Baxter equation (Eq. (B.31)). We denote $R_{a,b}(u-v) = a \begin{array}{c} \xrightarrow{u} \\ \uparrow v \\ \downarrow b \end{array}$. The diagram is meant to be read from down to up, corresponding to reading (B.31) from right to left.

Theorem B.1. For $j = 1, 2$ and any $q \in \mathbb{C}$, the following relation holds.

$$T(u) |\psi_j(q)\rangle = \mathcal{I}_b T(u) \mathcal{I}_b |\psi_j(q)\rangle, \quad (\text{B.35})$$

where $|\psi_j(q)\rangle$ is given in Eqs. (4.47) and (4.48), and \mathcal{I}_b is the bond-center-inversion operator defined as

$$\mathcal{I}_b = \prod_{j=1}^{L/2} P_{j,L-j+1}. \quad (\text{B.36})$$

Since we aim to obtain integrable boundary states, we have to consider boundary conditions other than the periodic boundary condition. To describe a situation on the boundary, we introduce the boundary Yang-Baxter equation [34, 63, 182]:

$$R_{1,2}(u-v) K_{R,1}(u) R_{2,1}(u+v) K_{R,2}(v) = K_{R,2}(v) R_{2,1}(u+v) K_{R,1}(u) R_{1,2}(u-v), \quad (\text{B.37})$$

$$R_{1,2}(-u+v) K_{L,1}^t(u) R_{2,1}^t(-u-v-2\eta) K_{L,2}^t(v) = K_{L,2}^t(v) R_{2,1}(-u-v-2\eta) K_{L,1}^t(u) R_{1,2}^t(-u+v), \quad (\text{B.38})$$

where the superscript t denotes the transposition. The matrix $K_{R(L)}$ corresponds to the right (left) boundary condition [63]. Introducing an ansatz that K_{\pm} is diagonal yields its solution

$$K_{R,\cdot}(u) = \begin{pmatrix} \frac{\theta_1(\xi+u|2\tau)}{\theta_4(\xi+u|2\tau)} & 0 \\ 0 & \frac{\theta_1(\xi-u|2\tau)}{\theta_4(\xi-u|2\tau)} \end{pmatrix}, \quad (\text{B.39})$$

$$K_{L,\cdot}(u) = \begin{pmatrix} \frac{\theta_1(\xi-u-\eta|2\tau)}{\theta_4(\xi-u-\eta|2\tau)} & 0 \\ 0 & \frac{\theta_1(\xi+u+\eta|2\tau)}{\theta_4(\xi+u+\eta|2\tau)} \end{pmatrix}, \quad (\text{B.40})$$

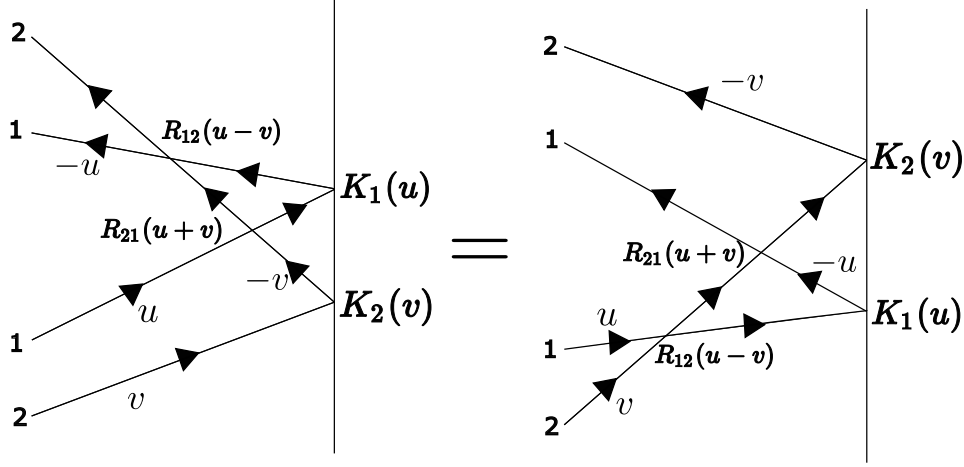


Figure B.2: Graphical representation of the boundary Yang-Baxter equation (Eq. (B.37)). The diagram is meant to be read from down to up, corresponding reading (B.37) from right to left. Note that the signs of the rapidities u and v change on the boundary because of the reflection.

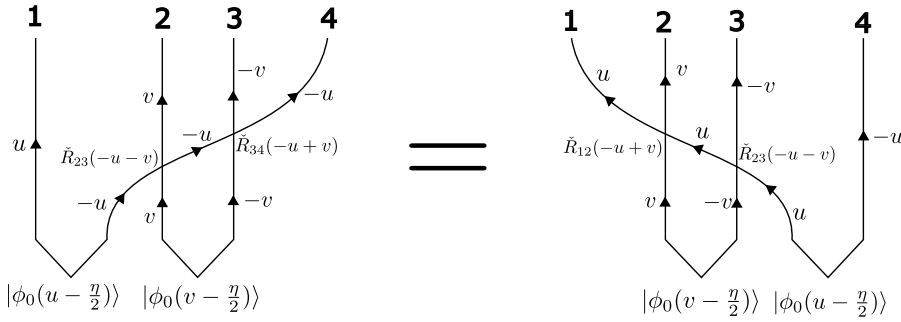


Figure B.3: Graphical representation of the reflection equation (Eq. (B.41)). The diagram is meant to be read from down to up, corresponding reading (B.41) from right to left.

where $\xi \in \mathbb{C}$ is a free parameter. By considering the $\pi/2$ rotation on the Euclidean space-time, we naturally obtain the reflection equation (Figure B.3):

$$\begin{aligned} & \check{R}_{3,4}(-u+v) \check{R}_{2,3}(-u-v) \left| \phi_0(u - \frac{\eta}{2}) \right\rangle_{1,2} \left| \phi_0(v - \frac{\eta}{2}) \right\rangle_{3,4} \\ &= \check{R}_{1,2}(-u+v) \check{R}_{2,3}(-u-v) \left| \phi_0(v - \frac{\eta}{2}) \right\rangle_{1,2} \left| \phi_0(u - \frac{\eta}{2}) \right\rangle_{3,4}, \end{aligned} \quad (\text{B.41})$$

where $\check{R}_{a,b} = R_{a,b} P_{a,b}$ and $|\phi_0(u)\rangle = -K_{12}(u) |\uparrow\uparrow\rangle + K_{11}(u) |\uparrow\downarrow\rangle - K_{22}(u) |\downarrow\uparrow\rangle + K_{21}(u) |\downarrow\downarrow\rangle$. Since we assume K -matrix is diagonal, $|\phi_0\rangle$ becomes a q -dimer state, namely,

$$|\phi_0(u)\rangle = K_{11}(u) |\uparrow\downarrow\rangle - K_{22}(u) |\downarrow\uparrow\rangle. \quad (\text{B.42})$$

Therefore, by applying Eq. (B.41) repeatedly and taking a limit $v \rightarrow 0$, we obtain

$$\prod_{j=1}^{\overleftarrow{L}} R_{L+1,j}(-u) \left(|W\rangle_{0,L+1} \otimes |\phi_0\rangle^{\otimes \frac{L}{2}} \right) = \prod_{j=1}^{\overleftarrow{L}} R_{0,L+1-j}(-u) \left(|\phi_0\rangle^{\otimes \frac{L}{2}} \otimes |W\rangle_{0,L+1} \right), \quad (\text{B.43})$$

where $|\phi_0\rangle = |\phi_0(-\frac{\eta}{2})\rangle = K_{11}(-\frac{\eta}{2})|\uparrow\downarrow\rangle - K_{22}(-\frac{\eta}{2})|\downarrow\uparrow\rangle$ and $|W\rangle_{0,L+1} = K_{11}(u - \frac{\eta}{2})|\uparrow\downarrow\rangle - K_{22}(u - \frac{\eta}{2})|\downarrow\uparrow\rangle$. The sites 0 and $L+1$ are auxiliary sites corresponding to the left and right boundaries, respectively.

Finally, by tracing out the auxiliary space (sites 0 and $L+1$), we get

$$\text{Tr}_{L+1} \left[\prod_{j=1}^{\overleftarrow{L}} R_{L+1,j}(-u) \right] |\phi_0\rangle^{\otimes \frac{L}{2}} = \text{Tr}_0 \left[\prod_{j=1}^{\overleftarrow{L}} R_{0,L+1-j}(-u) \right] |\phi_0\rangle^{\otimes \frac{L}{2}}. \quad (\text{B.44})$$

It implies

$$T(u) |\phi_0\rangle^{\otimes \frac{L}{2}} = \mathcal{IT}(u) \mathcal{I} |\phi_0\rangle^{\otimes \frac{L}{2}}. \quad (\text{B.45})$$

Since $|\phi_0\rangle^{\otimes \frac{L}{2}}$ can be written as a linear combination of the tilted Néel states, namely,

$$\begin{aligned} |\phi_0(\xi)\rangle^{\otimes \frac{L}{2}} &= \left[\frac{\theta_1(\xi - \frac{\eta}{2} | 2\tau)}{\theta_4(\xi - \frac{\eta}{2} | 2\tau)} |\uparrow\downarrow\rangle - \frac{\theta_1(\xi + \frac{\eta}{2} | 2\tau)}{\theta_4(\xi + \frac{\eta}{2} | 2\tau)} |\downarrow\uparrow\rangle \right]^{\otimes \frac{L}{2}} \\ &\propto |\psi_1(\alpha)\rangle - |\psi_2(\beta)\rangle \\ &= (-\alpha^{-1} + \beta) |\uparrow\downarrow\rangle + (\alpha + \beta^{-1}) |\downarrow\uparrow\rangle, \end{aligned} \quad (\text{B.46})$$

where

$$\begin{aligned} \alpha &= \pm \frac{\sqrt{b}\sqrt{ab-4}}{2\sqrt{a}} - \frac{b}{2}, \\ \beta &= \pm \frac{\sqrt{a}\sqrt{ab-4}}{2\sqrt{b}} - \frac{a}{2}, \end{aligned} \quad (\text{B.47})$$

with

$$a = \frac{\theta_1(\xi - \frac{\eta}{2} | 2\tau)}{\theta_4(\xi - \frac{\eta}{2} | 2\tau)}, \quad b = \frac{\theta_1(\xi + \frac{\eta}{2} | 2\tau)}{\theta_4(\xi + \frac{\eta}{2} | 2\tau)}. \quad (\text{B.48})$$

BIBLIOGRAPHY

- [1] L. Boltzmann, Weitere studien über das wärmegleichgewicht unter gasmolekülen, Wien. Ber. **66**, 275 (1872).
- [2] L. Boltzmann, Bemerkungen über einige Probleme der mechanischen Wärmetheorie, Wien. Ber. **75**, 62 (1877).
- [3] L. Boltzmann, Über die Eigenschaften monocyclischer und anderer damit verwandter Systeme., Wien. Ber. **92**, 853 (1885).
- [4] J. von Neumann, Beweis des Ergodensatzes und des H-Theorems in der neuen Mechanik, *Z. Phys.* **57**, 30 (1929).
- [5] L. Boltzmann, Einige allgemeine sätze über Wärmegleichgewicht, Wien. Ber. **63**, 670 (1871).
- [6] J. von Plato, Boltzmann’s ergodic hypothesis, *Arch. Hist. Exact Sci.* **42**, 71 (1991).
- [7] T. Mori, T. N. Ikeda, E. Kaminishi, and M. Ueda, Thermalization and prethermalization in isolated quantum systems: a theoretical overview, *J. Phys. B: At. Mol. Opt. Phys.* **51**, 112001 (2018).
- [8] H. Tasaki, Typicality of thermal equilibrium and thermalization in isolated macroscopic quantum systems, *J. Stat. Phys.* **163**, 937 (2016).
- [9] J. L. Lebowitz, From time-symmetric microscopic dynamics to time-asymmetric macroscopic behavior: an overview, in *Boltzmann’s legacy*, ESI Lectures in Mathematics and Physics, edited by G. Gallavotti, W. Reiter, and J. Yngvason (2008) pp. 63–88, international Symposium on Boltzmann, Erwin Schrodinger Int Inst Math Phys, Vienna, AUSTRIA, JUN 07-09, 2006.
- [10] S. Sugiura, Typicality and Ergodicity, in *Formulation of Statistical Mechanics Based on Thermal Pure Quantum States* (Springer Singapore, Singapore, 2017) pp. 5–14.

- [11] S. Goldstein, J. L. Lebowitz, R. Tumulka, and N. Zanghi, Long-time behavior of macroscopic quantum systems: Commentary accompanying the English translation of John von Neumann's 1929 article on the quantum ergodic theorem, [Eur. Phys. J. H **35**, 173 \(2010\)](#).
- [12] L. D'Alessio, Y. Kafri, A. Polkovnikov, and M. Rigol, From quantum chaos and eigenstate thermalization to statistical mechanics and thermodynamics, [Adv. Phys. **65**, 239 \(2016\)](#).
- [13] S. Goldstein, J. L. Lebowitz, C. Mastrodonato, R. Tumulka, and N. Zanghi, Normal typicality and von Neumann's quantum ergodic theorem, [Proc. R. Soc. A **466**, 3203 \(2010\)](#).
- [14] P. Reimann, Foundation of statistical mechanics under experimentally realistic conditions, [Phys. Rev. Lett. **101**, 190403 \(2008\)](#).
- [15] C. Gogolin and J. Eisert, Equilibration, thermalisation, and the emergence of statistical mechanics in closed quantum systems, [Rep. Prog. Phys. **79**, 056001 \(2016\)](#).
- [16] M. D. Choi, Almost commuting matrices need not be nearly commuting, [Proc. Amer. Math. Soc. **102**, 529 \(1988\)](#).
- [17] W. De Roeck, C. Maes, and K. Netočný, Quantum macrostates, equivalence of ensembles, and an H-theorem, [J. Math. Phys. **47**, 073303 \(2006\)](#).
- [18] S. Goldstein, D. A. Huse, J. L. Lebowitz, and R. Tumulka, Thermal Equilibrium of a Macroscopic Quantum System in a Pure State, [Phys. Rev. Lett. **115**, 100402 \(2015\)](#).
- [19] S. Goldstein, D. A. Huse, J. L. Lebowitz, and R. Tumulka, Macroscopic and microscopic thermal equilibrium, [Ann. Phys. \(Berlin\) **529**, 1600301 \(2017\)](#).
- [20] S. Popescu, A. J. Short, and A. Winter, Entanglement and the foundations of statistical mechanics, [Nat. Phys. **2**, 754 \(2006\)](#).
- [21] S. Goldstein, J. L. Lebowitz, R. Tumulka, and N. Zanghi, Canonical typicality, [Phys. Rev. Lett. **96**, 050403 \(2006\)](#).
- [22] M. P. Müller, E. Adlam, L. Masanes, and N. Wiebe, Thermalization and Canonical Typicality in Translation-Invariant Quantum Lattice Systems, [Commun. Math. Phys. **340**, 499 \(2015\)](#).
- [23] J. M. Deutsch, Quantum statistical mechanics in a closed system, [Phys. Rev. A **43**, 2046 \(1991\)](#).

- [24] M. Srednicki, Chaos and quantum thermalization, [Phys. Rev. E **50**, 888 \(1994\)](#).
- [25] M. Ueda, Quantum equilibration, thermalization and prethermalization in ultra-cold atoms, [Nat. Rev. Phys. **2**, 669 \(2020\)](#).
- [26] M. Srednicki, The approach to thermal equilibrium in quantized chaotic systems, [J. Phys. A: Math. Gen. **32**, 1163 \(1999\)](#).
- [27] J. M. Deutsch, Eigenstate thermalization hypothesis, [Rep. Prog. Phys. **81**, 082001 \(2018\)](#).
- [28] S. Moudgalya, B. A. Bernevig, and N. Regnault, Quantum many-body scars and Hilbert space fragmentation: a review of exact results, [Rep. Prog. Phys. **85**, 086501 \(2022\)](#).
- [29] J.-S. Caux and J. Mossel, Remarks on the notion of quantum integrability, [J. Stat. Mech.: Theory Exp. **2011** \(02\), P02023](#).
- [30] W. Miller, S. Post, and P. Winternitz, Classical and quantum superintegrability with applications, [J. Phys. A: Math. Theor. **46**, 423001 \(2013\)](#).
- [31] M. Brenes, T. LeBlond, J. Goold, and M. Rigol, Eigenstate Thermalization in a Locally Perturbed Integrable System, [Phys. Rev. Lett. **125**, 070605 \(2020\)](#).
- [32] B. Bertini, F. Heidrich-Meisner, C. Karrasch, T. Prosen, R. Steinigeweg, and M. Žnidarič, Finite-temperature transport in one-dimensional quantum lattice models, [Rev. Mod. Phys. **93**, 025003 \(2021\)](#).
- [33] M. Gaudin, Boundary Energy of a Bose Gas in One Dimension, [Phys. Rev. A **4**, 386 \(1971\)](#).
- [34] E. K. Sklyanin, Boundary conditions for integrable quantum systems, [J. Phys. A: Math. Gen. **21**, 2375 \(1988\)](#).
- [35] P. W. Anderson, Absence of Diffusion in Certain Random Lattices, [Phys. Rev. **109**, 1492 \(1958\)](#).
- [36] A. Pal and D. A. Huse, Many-body localization phase transition, [Phys. Rev. B **82**, 174411 \(2010\)](#).
- [37] R. Nandkishore and D. A. Huse, Many-Body Localization and Thermalization in Quantum Statistical Mechanics, [Annu. Rev. Condens. Matter Phys. **6**, 15 \(2015\)](#).
- [38] D. A. Abanin and Z. Papić, Recent progress in many-body localization, [Ann. Phys. \(Berlin\) **529**, 1700169 \(2017\)](#).

- [39] F. Alet and N. Laflorencie, Many-body localization: An introduction and selected topics, [C. R. Phys.](#) **19**, 498 (2018).
- [40] D. A. Abanin, E. Altman, I. Bloch, and M. Serbyn, Colloquium: Many-body localization, thermalization, and entanglement, [Rev. Mod. Phys.](#) **91**, 021001 (2019).
- [41] D. J. Luitz, N. Laflorencie, and F. Alet, Many-body localization edge in the random-field Heisenberg chain, [Phys. Rev. B](#) **91**, 081103 (2015).
- [42] M. Žnidarič, T. Prosen, and P. Prelovšek, Many-body localization in the Heisenberg XXZ magnet in a random field, [Phys. Rev. B](#) **77**, 064426 (2008).
- [43] S. Moudgalya and O. I. Motrunich, Hilbert Space Fragmentation and Commutant Algebras, [Phys. Rev. X](#) **12**, 011050 (2022).
- [44] P. Sala, T. Rakovszky, R. Verresen, M. Knap, and F. Pollmann, Ergodicity Breaking Arising from Hilbert Space Fragmentation in Dipole-Conserving Hamiltonians, [Phys. Rev. X](#) **10**, 011047 (2020).
- [45] S. Zhang, M. Karbach, G. Müller, and J. Stolze, Charge and spin dynamics in the one-dimensional $t - J_z$ and $t - J$ models, [Phys. Rev. B](#) **55**, 6491 (1997).
- [46] C. D. Batista and G. Ortiz, Quantum Phase Diagram of the $t - J_z$ Chain Model, [Phys. Rev. Lett.](#) **85**, 4755 (2000).
- [47] T. Rakovszky, P. Sala, R. Verresen, M. Knap, and F. Pollmann, Statistical localization: From strong fragmentation to strong edge modes, [Phys. Rev. B](#) **101**, 125126 (2020).
- [48] C. D. Batista and G. Ortiz, Generalized Jordan-Wigner Transformations, [Phys. Rev. Lett.](#) **86**, 1082 (2001).
- [49] O. Bohigas, M. J. Giannoni, and C. Schmit, Characterization of Chaotic Quantum Spectra and Universality of Level Fluctuation Laws, [Phys. Rev. Lett.](#) **52**, 1 (1984).
- [50] M. V. Berry, Quantizing a classically ergodic system: Sinai's billiard and the KKR method, [Ann. Phys. \(N. Y.\)](#) **131**, 163 (1981).
- [51] T. Prosen and M. Robnik, Energy level statistics in the transition region between integrability and chaos, [J. Phys. A: Math. Gen.](#) **26**, 2371 (1993).
- [52] D. Szász-Schagrin, B. Pozsgay, and G. Takács, Weak integrability breaking and level spacing distribution, [SciPost Phys.](#) **11**, 37 (2021).

-
- [53] Y. Y. Atas, E. Bogomolny, O. Giraud, and G. Roux, Distribution of the Ratio of Consecutive Level Spacings in Random Matrix Ensembles, [Phys. Rev. Lett. **110**, 084101 \(2013\)](#).
- [54] R. Islam, R. Ma, P. M. Preiss, M. Eric Tai, A. Lukin, M. Rispoli, and M. Greiner, Measuring entanglement entropy in a quantum many-body system, [Nature \(London\) **528**, 77 \(2015\)](#).
- [55] D. S. Bhakuni and A. Sharma, Entanglement and thermodynamic entropy in a clean many-body-localized system, [J. Phys.: Condens. Matter **32**, 255603 \(2020\)](#).
- [56] J. M. Deutsch, H. Li, and A. Sharma, Microscopic origin of thermodynamic entropy in isolated systems, [Phys. Rev. E **87**, 042135 \(2013\)](#).
- [57] J. M. Deutsch, Thermodynamic entropy of a many-body energy eigenstate, [New J. Phys. **12**, 075021 \(2010\)](#).
- [58] D. N. Page, Average entropy of a subsystem, [Phys. Rev. Lett. **71**, 1291 \(1993\)](#).
- [59] O. Vafek, N. Regnault, and B. A. Bernevig, Entanglement of exact excited eigenstates of the Hubbard model in arbitrary dimension, [SciPost Phys. **3**, 043 \(2017\)](#).
- [60] C. J. Turner, A. A. Michailidis, D. A. Abanin, M. Serbyn, and Z. Papić, Quantum scarred eigenstates in a Rydberg atom chain: Entanglement, breakdown of thermalization, and stability to perturbations, [Phys. Rev. B **98**, 155134 \(2018\)](#).
- [61] N. Shiraishi and T. Mori, Systematic Construction of Counterexamples to the Eigenstate Thermalization Hypothesis, [Phys. Rev. Lett. **119**, 030601 \(2017\)](#).
- [62] N. Shibata, N. Yoshioka, and H. Katsura, Onsager's Scars in Disordered Spin Chains, [Phys. Rev. Lett. **124**, 180604 \(2020\)](#).
- [63] L. Piroli, B. Pozsgay, and E. Vernier, What is an integrable quench?, [Nucl. Phys. **925**, 362 \(2017\)](#).
- [64] H. Bernien, S. Schwartz, A. Keesling, H. Levine, A. Omran, H. Pichler, S. Choi, A. S. Zibrov, M. Endres, M. Greiner, V. Vuletić, and M. D. Lukin, Probing many-body dynamics on a 51-atom quantum simulator, [Nature \(London\) **551**, 579 \(2017\)](#).
- [65] E. J. Heller, Bound-State Eigenfunctions of Classically Chaotic Hamiltonian Systems: Scars of Periodic Orbits, [Phys. Rev. Lett. **53**, 1515 \(1984\)](#).
- [66] L. A. Bunimovich, On the ergodic properties of nowhere dispersing billiards, [Comm. Math. Phys. **65**, 295 \(1979\)](#).

- [67] C. J. Turner, A. A. Michailidis, D. A. Abanin, M. Serbyn, and Z. Papić, Weak ergodicity breaking from quantum many-body scars, [Nat. Phys. **14**, 745 \(2018\)](#).
- [68] M. Serbyn, D. A. Abanin, and Z. Papić, Quantum many-body scars and weak breaking of ergodicity, [Nat. Phys. **17**, 675 \(2021\)](#).
- [69] D. Bluvstein, H. Levine, G. Semeghini, T. T. Wang, S. Ebadi, M. Kalinowski, A. Keesling, N. Maskara, H. Pichler, M. Greiner, V. Vuletić, and M. D. Lukin, A quantum processor based on coherent transport of entangled atom arrays, [Nature \(London\) **604**, 451 \(2022\)](#).
- [70] P. Zhang, H. Dong, Y. Gao, L. Zhao, J. Hao, J.-Y. Desaulles, Q. Guo, J. Chen, J. Deng, B. Liu, W. Ren, Y. Yao, X. Zhang, S. Xu, K. Wang, F. Jin, X. Zhu, B. Zhang, H. Li, C. Song, Z. Wang, F. Liu, Z. Papić, L. Ying, H. Wang, and Y.-C. Lai, Many-body Hilbert space scarring on a superconducting processor, [Nat. Phys. **19**, 120 \(2023\)](#).
- [71] E. J. Gustafson, A. C. Y. Li, A. Khan, J. Kim, D. M. Kurkcuoglu, M. S. Alam, P. P. Orth, A. Rahmani, and T. Iadecola, Preparing quantum many-body scar states on quantum computers, [Quantum **7**, 1171 \(2023\)](#).
- [72] P. Schauß, M. Cheneau, M. Endres, T. Fukuhara, S. Hild, A. Omran, T. Pohl, C. Gross, S. Kuhr, and I. Bloch, Observation of spatially ordered structures in a two-dimensional Rydberg gas, [Nature \(London\) **491**, 87 \(2012\)](#).
- [73] P. Schauß, J. Zeiher, T. Fukuhara, S. Hild, M. Cheneau, T. Macrì, T. Pohl, I. Bloch, and C. Groß, Crystallization in Ising quantum magnets, [Science **347**, 1455 \(2015\)](#).
- [74] J. Zeiher, J.-y. Choi, A. Rubio-Abadal, T. Pohl, R. Van Bijnen, I. Bloch, and C. Gross, Coherent many-body spin dynamics in a long-range interacting Ising chain, [Phys. Rev. X **7**, 041063 \(2017\)](#).
- [75] H. Labuhn, D. Barredo, S. Ravets, S. De Léséleuc, T. Macrì, T. Lahaye, and A. Browaeys, Tunable two-dimensional arrays of single Rydberg atoms for realizing quantum Ising models, [Nature \(London\) **534**, 667 \(2016\)](#).
- [76] P. Weinberg and M. Bukov, QuSpin: a Python package for dynamics and exact diagonalisation of quantum many body systems part I: spin chains, [SciPost Phys. **2**, 003 \(2017\)](#).
- [77] P. Weinberg and M. Bukov, QuSpin: a Python package for dynamics and exact diagonalisation of quantum many body systems. Part II: bosons, fermions and higher spins, [SciPost Phys. **7**, 020 \(2019\)](#).

-
- [78] S. Choi, C. J. Turner, H. Pichler, W. W. Ho, A. A. Michailidis, Z. Papić, M. Serbyn, M. D. Lukin, and D. A. Abanin, Emergent SU(2) Dynamics and Perfect Quantum Many-Body Scars, [Phys. Rev. Lett. **122**, 220603 \(2019\)](#).
- [79] C.-J. Lin and O. I. Motrunich, Exact Quantum Many-Body Scar States in the Rydberg-Blockaded Atom Chain, [Phys. Rev. Lett. **122**, 173401 \(2019\)](#).
- [80] W. W. Ho, S. Choi, H. Pichler, and M. D. Lukin, Periodic Orbits, Entanglement, and Quantum Many-Body Scars in Constrained Models: Matrix Product State Approach, [Phys. Rev. Lett. **122**, 040603 \(2019\)](#).
- [81] K. Omiya and M. Müller, Quantum many-body scars in bipartite Rydberg arrays originating from hidden projector embedding, [Phys. Rev. A **107**, 023318 \(2023\)](#).
- [82] C. K. Majumdar and D. K. Ghosh, On Next-Nearest-Neighbor Interaction in Linear Chain. I, [J. Math. Phys. **10**, 1388 \(1969\)](#).
- [83] C. K. Majumdar and D. K. Ghosh, On Next-Nearest-Neighbor Interaction in Linear Chain. II, [J. Math. Phys. **10**, 1399 \(1969\)](#).
- [84] L. Onsager, Crystal Statistics. I. A Two-Dimensional Model with an Order-Disorder Transition, [Phys. Rev. **65**, 117 \(1944\)](#).
- [85] L. Dolan and M. Grady, Conserved charges from self-duality, [Phys. Rev. D **25**, 1587 \(1982\)](#).
- [86] B. Davies, Onsager's algebra and superintegrability, [J. Phys. A: Math. Gen. **23**, 2245 \(1990\)](#).
- [87] B. Davies, Onsager's algebra and the Dolan–Grady condition in the nonselfdual case, [J. Math. Phys. **32**, 2945 \(1991\)](#).
- [88] A. B. Zamolodchikov and V. A. Fateev, Model Factorized S-Matrix and an Integrable Spin-1 Heisenberg Chain, *Sov. J. Nucl. Phys.* **32**, 298 (1980).
- [89] A. G. Bytsko, On integrable Hamiltonians for higher spin XXZ chain, [J. Math. Phys. **44**, 3698 \(2003\)](#).
- [90] P. P. Kulish, N. Y. Reshetikhin, and E. K. Sklyanin, Yang-Baxter equation and representation theory: I, [Lett. Math. Phys. **5**, 393 \(1981\)](#).
- [91] K. Sogo, Ground state and low-lying excitations in the Heisenberg XXZ chain of arbitrary spin S , [Phys. Lett. A **104**, 51 \(1984\)](#).

- [92] D. K. Mark, C.-J. Lin, and O. I. Motrunich, Unified structure for exact towers of scar states in the Affleck-Kennedy-Lieb-Tasaki and other models, [Phys. Rev. B **101**, 195131 \(2020\)](#).
- [93] S. Moudgalya, N. Regnault, and B. A. Bernevig, η -pairing in Hubbard models: From spectrum generating algebras to quantum many-body scars, [Phys. Rev. B **102**, 085140 \(2020\)](#).
- [94] C. D. Batista, Canted spiral: An exact ground state of XXZ zigzag spin ladders, [Phys. Rev. B **80**, 180406 \(2009\)](#).
- [95] J. Wouters, H. Katsura, and D. Schuricht, Exact ground states for interacting Kitaev chains, [Phys. Rev. B **98**, 155119 \(2018\)](#).
- [96] M. Schechter and T. Iadecola, Weak Ergodicity Breaking and Quantum Many-Body Scars in Spin-1 XY Magnets, [Phys. Rev. Lett. **123**, 147201 \(2019\)](#).
- [97] S. Chattopadhyay, H. Pichler, M. D. Lukin, and W. W. Ho, Quantum many-body scars from virtual entangled pairs, [Phys. Rev. B **101**, 174308 \(2020\)](#).
- [98] T. Iadecola and M. Schechter, Quantum many-body scar states with emergent kinetic constraints and finite-entanglement revivals, [Phys. Rev. B **101**, 024306 \(2020\)](#).
- [99] D. K. Mark and O. I. Motrunich, η -pairing states as true scars in an extended Hubbard model, [Phys. Rev. B **102**, 075132 \(2020\)](#).
- [100] K. Pakrouski, P. N. Pallegar, F. K. Popov, and I. R. Klebanov, Many-Body Scars as a Group Invariant Sector of Hilbert Space, [Phys. Rev. Lett. **125**, 230602 \(2020\)](#).
- [101] S. Moudgalya, N. Regnault, and B. A. Bernevig, Entanglement of exact excited states of Affleck-Kennedy-Lieb-Tasaki models: Exact results, many-body scars, and violation of the strong eigenstate thermalization hypothesis, [Phys. Rev. B **98**, 235156 \(2018\)](#).
- [102] A. Hallam, J.-Y. Desaulles, and Z. Papić, Embedding Semiclassical Periodic Orbits into Chaotic Many-Body Hamiltonians, [Phys. Rev. Lett. **131**, 110401 \(2023\)](#).
- [103] A. O. Barut and A. Böhm, Dynamical groups and mass formula, [Phys. Rev. **139**, B1107 \(1965\)](#).
- [104] Y. Dothan, M. Gell-Mann, and Y. Ne'eman, Series of hadron energy levels as representations of non-compact groups, [Phys. Lett. **17**, 148 \(1965\)](#).
- [105] B. Buča, J. Tindall, and D. Jaksch, Non-stationary coherent quantum many-body dynamics through dissipation, [Nat. Commun. **10**, 1730 \(2019\)](#).

-
- [106] M. Medenjak, B. Buča, and D. Jaksch, Isolated Heisenberg magnet as a quantum time crystal, [Phys. Rev. B **102**, 041117 \(2020\)](#).
- [107] I. Affleck, T. Kennedy, E. H. Lieb, and H. Tasaki, Rigorous results on valence-bond ground states in antiferromagnets, [Phys. Rev. Lett. **59**, 799 \(1987\)](#).
- [108] I. Affleck, T. Kennedy, E. H. Lieb, and H. Tasaki, Valence bond ground states in isotropic quantum antiferromagnets, [Commun. Math. Phys. **115**, 477 \(1988\)](#).
- [109] H. Tasaki, *Physics and Mathematics of Quantum Many-Body Systems* (Springer, New York, 2020).
- [110] A. Klumper, A. Schadschneider, and J. Zittartz, Equivalence and solution of anisotropic spin-1 models and generalized t-J fermion models in one dimension, [J. Phys. A: Math. Gen. **24**, L955 \(1991\)](#).
- [111] S. Moudgalya, S. Rachel, B. A. Bernevig, and N. Regnault, Exact excited states of nonintegrable models, [Phys. Rev. B **98**, 235155 \(2018\)](#).
- [112] K. Sanada, Y. Miao, and H. Katsura, Quantum many-body scars in spin models with multibody interactions, [Phys. Rev. B **108**, 155102 \(2023\)](#).
- [113] K. Fujiwara, Y. Kato, T. Seki, K. Nomura, K. Takanashi, Y. Motome, and A. Tsukazaki, Tuning scalar spin chirality in ultrathin films of the kagome-lattice ferromagnet Fe₃Sn, [Commun. Mater. **2**, 113 \(2021\)](#).
- [114] Y. Taguchi, Y. Oohara, H. Yoshizawa, N. Nagaosa, and Y. Tokura, Spin Chirality, Berry Phase, and Anomalous Hall Effect in a Frustrated Ferromagnet, [Science **291**, 2573 \(2001\)](#).
- [115] X. G. Wen, F. Wilczek, and A. Zee, Chiral spin states and superconductivity, [Phys. Rev. B **39**, 11413 \(1989\)](#).
- [116] K. Lee, R. Melendrez, A. Pal, and H. J. Changlani, Exact three-colored quantum scars from geometric frustration, [Phys. Rev. B **101**, 241111\(R\) \(2020\)](#).
- [117] K. Lee, A. Pal, and H. J. Changlani, Frustration-induced emergent hilbert space fragmentation, [Phys. Rev. B **103**, 235133 \(2021\)](#).
- [118] A. M. Alhambra, A. Anshu, and H. Wilming, Revivals imply quantum many-body scars, [Phys. Rev. B **101**, 205107 \(2020\)](#).
- [119] Y.-Y. Shi, L.-M. Duan, and G. Vidal, Classical simulation of quantum many-body systems with a tree tensor network, [Phys. Rev. A **74**, 022320 \(2006\)](#).

- [120] H. Katsura, N. Kawashima, A. N. Kirillov, V. E. Korepin, and S. Tanaka, Entanglement in valence-bond-solid states on symmetric graphs, [J. Phys. A: Math. Theor.](#) **43**, 255303 (2010).
- [121] M. De Leeuw, C. Kristjansen, and G. Linardopoulos, Scalar one-point functions and matrix product states of AdS/dCFT, [Phys. Lett. B](#) **781**, 238 (2018).
- [122] B. Pozsgay, L. Piroli, and E. Vernier, Integrable matrix product states from boundary integrability, [SciPost Phys.](#) **6**, 062 (2019).
- [123] L. Piroli, E. Vernier, P. Calabrese, and B. Pozsgay, Integrable quenches in nested spin chains I: the exact steady states, [J. Stat. Mech.: Theory Exp.](#) **2019**, 063103.
- [124] B. Pozsgay, Overlaps with arbitrary two-site states in the XXZ spin chain, [J. Stat. Mech.: Theory Exp.](#) **2018**, 053103.
- [125] S. Ghoshal and A. Zamolodchikov, Boundary S-Matrix and Boundary State in Two-Dimensional Integrable Quantum Field Theory, [Int. J. Mod. Phys. A](#) **09**, 3841 (1994).
- [126] T. Matsubara, A New Approach to Quantum-Statistical Mechanics, [Prog. Theor. Phys.](#) **14**, 351 (1955).
- [127] A. B. Zamolodchikov, Integrable field theory from conformal field theory, in *Integrable systems in quantum field theory and statistical mechanics*, Adv. Stud. Pure Math., Vol. 19 (Academic Press, Boston, MA, 1989) pp. 641–674.
- [128] A. B. Zamolodchikov, Integrals of Motion and S-Matrix of the (Scaled) $T = T_c$ Ising Model With Magnetic Field, [Int. J. Mod. Phys. A](#) **04**, 4235 (1989).
- [129] F. Smirnov and A. Zamolodchikov, On space of integrable quantum field theories, [Nucl. Phys. B](#) **915**, 363 (2017).
- [130] L. Piroli, B. Pozsgay, and E. Vernier, From the quantum transfer matrix to the quench action: the Loschmidt echo in XXZ Heisenberg spin chains, [J. Stat. Mech.: Theory Exp.](#) **2017** (2), 023106.
- [131] M. De Leeuw, A. Pribytok, and P. Ryan, Classifying integrable spin-1/2 chains with nearest neighbour interactions, [J. Phys. A: Math. Theor.](#) **52**, 505201 (2019).
- [132] E. K. Sklyanin, Quantum Inverse Scattering Method. Selected Topics (1992), [arXiv:hep-th/9211111 \[hep-th\]](#).

-
- [133] M. Grabowski and P. Mathieu, Structure of the Conservation Laws in Quantum Integrable Spin Chains with Short Range Interactions, *Ann. Phys. (N. Y.)* **243**, 299 (1995).
- [134] D. Perez-Garcia, F. Verstraete, M. Wolf, and J. Cirac, Matrix product state representations, *Quantum Inf. Comput.* **7**, 401 (2007), (*Preprint* [arXiv:quant-ph/0608197](https://arxiv.org/abs/quant-ph/0608197) [[quant-ph](#)]).
- [135] H. Frahm and C. Rödenbeck, Properties of the chiral spin liquid state in generalized spin ladders, *J. Phys. A: Math. Gen.* **30**, 4467 (1997).
- [136] W. J. Caspers, K. M. Emmett, and W. Magnus, The Majumdar-Ghosh chain. Twofold ground state and elementary excitations, *J. Phys. A: Math. Gen.* **17**, 2687 (1984).
- [137] B. Sutherland, Model for a multicomponent quantum system, *Phys. Rev. B* **12**, 3795 (1975).
- [138] C. K. Lai, Lattice gas with nearest-neighbor interaction in one dimension with arbitrary statistics, *J. Math. Phys.* **15**, 1675 (1974).
- [139] G. V. Uimin, One-dimensional problem for $S = 1$ with modified antiferromagnetic Hamiltonian, *Zh. Eksp. Teor. Fiz. Pis. Red.* **12**, 332 (1970), [*JETP Lett.* **12**, 225 (1970)].
- [140] M. P. Grabowski and P. Mathieu, Integrability test for spin chains, *J. Phys. A: Math. Gen.* **28**, 4777 (1995).
- [141] J.-Y. Chen, S. Capponi, A. Wietek, M. Mambrini, N. Schuch, and D. Poilblanc, $SU(3)_1$ Chiral Spin Liquid on the Square Lattice: A View from Symmetric Projected Entangled Pair States, *Phys. Rev. Lett.* **125**, 017201 (2020).
- [142] S. Schierenberg, F. Bruckmann, and T. Wettig, Wigner surmise for mixed symmetry classes in random matrix theory, *Phys. Rev. E* **85**, 061130 (2012).
- [143] D. Kundu, S. Kumar, and S. Sen Gupta, Signatures of spectral crossovers in the short-and long-range spectral correlations of a disordered spin-chain with Kramers degeneracy, *Phys. Rev. B* **107**, 094205 (2023).
- [144] T. Hirano and Y. Hatsugai, Entanglement entropy of one-dimensional gapped spin chains, *J. Phys. Soc. Jpn.* **76**, 074603 (2007).
- [145] H. Katsura, T. Hirano, and Y. Hatsugai, Exact analysis of entanglement in gapped quantum spin chains, *Phys. Rev. B* **76**, 012401 (2007).

- [146] C. Lange, A. Klümper, and J. Zittartz, Exact groundstates for antiferromagnetic spin-one chains with nearest and next-nearest neighbour interactions, *Z. Phys. B* **96**, 267 (1994).
- [147] H. Nakano and M. Takahashi, Long-ranged interacting $S=1$ spin chain with the exact valence-bond-solid state, *Phys. Rev. B* **54**, 9000 (1996).
- [148] D. Scalapino, S.-C. Zhang, and W. Hanke, $SO(5)$ symmetric ladder, *Phys. Rev. B* **58**, 443 (1998).
- [149] H. Frahm and M. Stahlsmeier, Electronic ladders with $SO(5)$ symmetry: Phase diagrams and correlations at half filling, *Phys. Rev. B* **63**, 125109 (2001).
- [150] H.-H. Tu, G.-M. Zhang, and T. Xiang, Class of exactly solvable $SO(n)$ symmetric spin chains with matrix product ground states, *Phys. Rev. B* **78**, 094404 (2008).
- [151] M. Takahashi, *Thermodynamics of One-Dimensional Solvable Models* (Cambridge University Press, 1999).
- [152] V. E. Korepin, N. M. Bogoliubov, and A. G. Izergin, *Quantum Inverse Scattering Method and Correlation Functions*, Cambridge Monographs on Mathematical Physics (Cambridge University Press, 1993).
- [153] M. Grabowski and P. Mathieu, Structure of the conservation laws in quantum integrable spin chains with short range interactions, *Ann. Phys. (N. Y.)* **243**, 299 (1995).
- [154] K. Tamura and H. Katsura, Quantum many-body scars of spinless fermions with density-assisted hopping in higher dimensions, *Phys. Rev. B* **106**, 144306 (2022).
- [155] L.-H. Tang, N. O’Dea, and A. Chandran, Multimagnon quantum many-body scars from tensor operators, *Phys. Rev. Res.* **4**, 043006 (2022).
- [156] S. Moudgalya and O. I. Motrunich, Exhaustive Characterization of Quantum Many-Body Scars using Commutant Algebras (2023), [arXiv:2209.03377 \[cond-mat.str-el\]](https://arxiv.org/abs/2209.03377) .
- [157] F. Schindler, N. Regnault, and B. A. Bernevig, Exact quantum scars in the chiral nonlinear Luttinger liquid, *Phys. Rev. B* **105**, 035146 (2022).
- [158] I. Martin and K. A. Matveev, Scar states in a system of interacting chiral fermions, *Phys. Rev. B* **105**, 045119 (2022).
- [159] D. Liska, V. Gritsev, W. Vleeshouwers, and J. Minář, Holographic Quantum Scars, *SciPost Phys.* **15**, 106 (2023).

-
- [160] J. Cotler and A. Y. Wei, Quantum Scars in Quantum Field Theory, [*Phys. Rev. D* **107**, 125005 \(2023\)](#).
- [161] Y. Nozawa and K. Fukai, Explicit Construction of Local Conserved Quantities in the XYZ Spin-1/2 Chain, [*Phys. Rev. Lett.* **125**, 090602 \(2020\)](#).
- [162] K. Fukai, All Local Conserved Quantities of the One-Dimensional Hubbard Model, [*Phys. Rev. Lett.* **131**, 256704 \(2023\)](#).
- [163] L. Eck and P. Fendley, From the XXZ chain to the integrable Rydberg-blockade ladder via non-invertible duality defects (2023), [arXiv:2302.14081 \[cond-mat.stat-mech\]](#) .
- [164] F. Iemini, A. Russomanno, J. Keeling, M. Schirò, M. Dalmonte, and R. Fazio, Boundary time crystals, [*Phys. Rev. Lett.* **121**, 035301 \(2018\)](#).
- [165] B. Buča, J. Tindall, and D. Jaksch, Non-stationary coherent quantum many-body dynamics through dissipation, [*Nat. Commun.* **10**, 1730 \(2019\)](#).
- [166] S. Dutta and N. R. Cooper, Out-of-equilibrium steady states of a locally driven lossy qubit array, [*Phys. Rev. Res.* **3**, L012016 \(2021\)](#).
- [167] J. Tindall, F. Schlawin, M. A. Sentef, and D. Jaksch, Analytical solution for the steady states of the driven Hubbard model, [*Phys. Rev. B* **103**, 035146 \(2021\)](#).
- [168] B. Buča, C. Booker, and D. Jaksch, Algebraic theory of quantum synchronization and limit cycles under dissipation, [*SciPost Phys.* **12**, 097 \(2022\)](#).
- [169] N. Shibata and H. Katsura, Dissipative spin chain as a non-Hermitian Kitaev ladder, [*Phys. Rev. B* **99**, 174303 \(2019\)](#).
- [170] N. Shibata and H. Katsura, Dissipative quantum Ising chain as a non-Hermitian Ashkin-Teller model, [*Phys. Rev. B* **99**, 224432 \(2019\)](#).
- [171] A. A. Ziolkowska and F. Essler, Yang-Baxter integrable Lindblad equations, [*SciPost Phys.* **8**, 044 \(2020\)](#).
- [172] M. de Leeuw, C. Paletta, and B. Pozsgay, Constructing integrable Lindblad superoperators, [*Phys. Rev. Lett.* **126**, 240403 \(2021\)](#).
- [173] M. de Leeuw, C. Paletta, B. Pozsgay, and E. Vernier, Hidden quasi-local charges and Gibbs ensemble in a Lindblad system (2023), [arXiv:2305.01922 \[cond-mat.stat-mech\]](#) .
- [174] V. Gritsev and A. Polkovnikov, Integrable Floquet dynamics, [*SciPost Phys.* **2**, 021 \(2017\)](#).

- [175] M. Vanicat, L. Zadnik, and T. Prosen, Integrable Trotterization: Local Conservation Laws and Boundary Driving, [Phys. Rev. Lett. **121**, 030606 \(2018\)](#).
- [176] A. Lotkov, V. Gritsev, A. Fedorov, and D. Kurlov, Floquet integrability and long-range entanglement generation in the one-dimensional quantum Potts model, [Phys. Rev. B **105**, 144306 \(2022\)](#).
- [177] Y. Miao, V. Gritsev, and D. V. Kurlov, The Floquet Baxterisation (2022), [arXiv:2206.15142 \[math-ph\]](#) .
- [178] H. Georgi, *Lie algebras in particle physics: from isospin to unified theories* (Taylor & Francis, London, 2000).
- [179] R. J. Baxter, *Exactly solved models in statistical mechanics* (Elsevier, Amsterdam, 2016).
- [180] J. Cao, S. Cui, W.-L. Yang, K. Shi, and Y. Wang, Spin-1/2 XYZ model revisit: General solutions via off-diagonal Bethe ansatz, [Nucl. Phys. B **886**, 185 \(2014\)](#).
- [181] I. S. Gradshteyn and I. M. Ryzhik, *Table of integrals, series, and products* (Academic press, Cambridge, 2014).
- [182] T. Kimura and R.-D. Zhu, Bethe/gauge correspondence for SO/Sp gauge theories and open spin chains, [J. High Energ. Phys. **2021** \(3\), 227](#).